Journal Research of the National Bureau of Standards Vol. 49, No. 2, August 1952 Research Paper 2342

Heats of Hydration and Pozzolan Content of Portland-Pozzolan Cements

Edwin S. Newman and Lansing S. Wells

Methods are described for the measurement of the approximate heat of solution in acid of portland-cement–pozzolan mixtures. Examples are given of the estimation of the heat of hydration of portland-pozzolan cements. Determinations of the amount of material undissolved in the calorimeter, as well as the heats of solution, were applied to the problem of determining the composition of mixtures of portland cement and pozzolan. Data are presented for the calculation of the heat capacity of the vacuum–flask calorimeter with amounts of hydrofluoric acid other than the 8-milliliter quantity used in measuring the heat of hydration of portland cement by the standard method.

1. Introduction

In recent years pozzolans have been widely used with portland cement because of their favorable effects on many of the properties of concrete. Many methods of test of cement or of concrete are not affected by the presence of the pozzolan, which contains a large percentage of silica. The measurement of the heat of hardening [1, 2] [1] of a portland-pozzolan cement by the heat-of-solution procedure however, is less reliable than the measurement for ordinary portland cement because of the presence of material not readily soluble in acid. The heat-of-solution method depends on the measurement of the heats of solution in acid of a sample of dry cement and of a corresponding sample of hardened paste. The difference between the two heats of solution is the heat of hardening of the cement paste. A mixture of nitric and hydrofluoric acids, in which nearly all portland cements will dissolve rapidly and completely, is used. Considerable portions of many pozzolans, however, are not readily soluble, and for even approximately complete solution far more time would be required than is desirable in the usual procedure for portland cement. The Bureau has occasionally measured the approximate heat of solution or hydration of pozzolan cements in a variety of investigations scattered over a period of nearly two decades. This paper presents the results of tests made by methods devised to reduce the effect of the difficultly soluble material.

In addition to the problem of measuring the heat of hydration of portland-pozzolan cements, there also exists, perhaps more urgently, the problem of determining the pozzolan content of such blends. In the course of the calorimetric measurements, it was observed that part of each pozzolan was undissolved. It was also observed that the heats of solution of the cement-pozzolan mixtures, as well as the percentage of undissolved material, were related to the pozzolan content. So that these data might not be lost, they have been included in this paper, and their application to the measurement of the pozzolan content of portland-pozzolan cements is discussed.

[1] Figure in brackets indicate literature references at the end of this paper.

Two calorimeters were used for this work: (1) an isothermal-jacket precision-type calorimeter, and (2) the vacuum-flask calorimeter required by the ASTM and the Federal Specification Board for the routine determination of the heat of hydration of portland cement [1, 2]. The isothermal-jacket calorimeter is equipped with a controlled-temperature water bath, a platinum resistance thermometer, and electrical and time-measuring instruments for determining with high precision the temperature rise and the electrical energy of calibration. The vacuum-flask calorimeter consists only of a vacuum flask, a stirrer driven by a synchronous motor, and a Beckmann thermometer. No attempt is made to surround it with a constant-temperature environment, and it is subject to lags and errors arising from changes in the laboratory temperature. Consequently, although it is much less expensive and easier to operate than the isothermal-jacket calorimeter, the vacuum-flask calorimeter is considerably less precise. Because of the difference in the operation of these instruments and in the application of their characteristics to the problem, they will be discussed separately.

2. The Isothermal-Jacket Calorimeter

The isothermal-jacket calorimeter described in other publications [3, 4] is capable of measuring the heat of solution of a 3-g sample of a material completely soluble in 35 min with a precision (standard deviation of a single observation) of about 0.2 cal/g. However, the necessary corrections for thermal leakage, heats of stirring and evaporation, etc., increase progressively with the length of the solution period, and it is felt that 90 min is the longest solution period that should be used. For longer periods, the corrections become such a large portion of the measured temperature rise that they are applied with less confidence.

In the determination of a heat of solution, the apparatus is assembled, and the stirring motor is started and allowed to operate undisturbed until the temperature of the calorimeter is found to rise at a nearly uniform rate. The sample is introduced, and readings of the calorimeter temperature are taken until the rate of change has again become uniform.

212644—52——1

The two periods of constant rate are termed the initial and final rating periods, and the intervening time is known as the solution period. From observations of the temperature of the calorimeter and of the isothermal jacket during the rating periods, the thermal leakage constant and the heat of stirring and evaporation are calculated [5]. The corrections to be applied to the observed temperature change occuring during the solution period are calculated from these constants and from the calorimeter temperatures observed during that period.

If an experiment is performed with a completely soluble cement, and if observations are taken for an extended period, it will be found that soon after the introduction of the sample it is completely dissolved and that thereafter the calculated value of the heat of solution ceases to increase with longer solution periods. After the sample has dissolved completely, the calorimeter soon reaches a rate of temperature rise controlled by the heat of stirring and the thermal leakage to or from the surroundings. Corrections for these two factors during the solution period compensate for their effects, and, as a result, extending the solution period materially beyond the point at which solution is complete does not have any systematic effect upon the value obtained for the heat of solution of the sample. In fact, the best available criterion of the completion of the solution of the sample appears to be the repeated calculation of the heat of solution, using arbitrarily chosen solution periods of different lengths. In table 1 are listed heats of solution calculated in this manner for a sample of portland cement. It will be seen that the solution of the portland cement was completed in a relatively short time, since the calculated heat of solution became essentially constant after 30 min.

If a similar experiment is performed with a pozzolan cement, the calculated value of the heat of solution continues to increase with increasing solution period because the difficultly soluble material continues slowly to dissolve. This condition is illustrated by the values given in table 1 for the heat of solution of a pozzolan cement. The calculated value was still increasing after a solution period of 75 min. It is impracticable to determine the total heat of solution of a cement that is still incompletely dissolved after such a long time.

TABLE 1. *Heats of solution of portland and portland-pozzolan cements*

The heats of solution of 3-g samples (ignited weights) in 10 ml of 48-percent HF plus sufficient 2.00 *N* HNO_3 to make 647.5 g of total acid were measured in a precision-type isothermal-jacket calorimeter [4]. Only two heat-of-solution experiments are represented. For each solution period indicated, all prior readings of calorimeter temperature are included in the calculations, the subsequent 10-min period being taken as the final rating period.

Duration of solution period	Calculated heat of solution	
	Portland cement	Portland-pozzolan cement
min	*cal/g*	*cal/g*
10	588.6	------
11	589.4	------
12	590.3	------
13	591.1	------
14	592.0	------
15	592.6	------
20	594.8	------
25	596.4	------
30	597.6	------
35	598.1	549.3
40	598.0	550.7
45	598.2	552.1
55	597.9	554.5
65	------	556.5
75	------	558.1
80	------	[a] 558.8

[a] Undissolved at end of the experiment, 6.7 percent by weight.

2.1. Heats of Hydration of Portland-Pozzolan Cements

When a pozzolan cement is dissolved in the calorimeter, the greater part of the heat of solution is evolved in a relatively short time (see table 1). Since the hydrated pozzolan cement behaves similarly, an approximate value for the heat of hydration may be obtained without waiting for the complete solution of the sample. In table 2 are shown the heats of partial solution of several portland-pozzolan cements calculated for solution periods of increasing lengths. The values calculated for the hydrated pastes for similar periods are also shown. All these values are based on the total weight of the sample, without regard to the amount of material undissolved. The values in table 2 are (except for the last sample) each the average of two determinations. In no case did the two values differ by more than 4 cal/g, and in most cases the agreement was much better.

TABLE 2. *Heats of partial solution and heats of hydration of portland-pozzolan cements*

Heats of solution of 3-g samples (ignited weights) were determined in 10 ml of 48-percent HF plus sufficient 2.00 *N* HNO_3 to make 647.5 g of total acid in a precision-type isothermal-jacket calorimeter [4]. Each value is the average of 2 determinations differing by not more than 4 cal/g.

Cement	Solution period	Heats of solution			Heats of hydration	
		Dry cement	7-day paste	28-day paste	7-day	28-day
	min	*cal/g*	*cal/g*	*cal/g*	*cal/g*	*cal/g*
1	25	527.4	464.9	444.0	62	83
	30	528.3	465.9	445.0	62	83
	35	529.2	466.6	446.0	63	83
2	25	531.8	469.9	455.0	62	77
	30	533.8	471.7	457.0	62	77
	35	535.4	474.3	458.6	62	77
3	25	582.8	504.9	486.6	78	96
	30	584.6	506.4	488.4	78	96
	35	585.9	507.3	490.0	79	96
4	25	595.8	544.1	526.2	52	70
	30	596.0	------	526.1	------	70
	35	595.7	------	526.0	------	70
5	25	546.1	487.7	473.4	58	73
	30	548.0	489.4	475.0	59	73
	35	549.5	491.1	476.6	58	73
	45	552.3	493.8	477.0	58	75
	55	554.7	497.0	478.2	58	76
5	25	------	------	[a] 473.1	------	[a] 73
	30	------	------	[a] 474.8	------	[a] 73
	35	------	------	[a] 476.2	------	[a] 73
	45	------	------	[a] 479.0	------	[a] 73
	55	------	------	[a] 480.0	------	[a] 75

[a] Results of 1 determination only. Values obtained at 30, 35, 45, and 55 min were calculated from the same determinations as the 25-min values, using time-temperature data taken after 25 min.

In table 3 are given the amounts of material undissolved at the end of the calorimetric experiments of table 2. The finding of more undissolved material remaining from the hydrated pastes than from the dry cements was unexpected. The hydration

reactions would be expected to render soluble in the acid mixture some part of the previously insoluble portion of the pozzolan. Similar behavior has been noted in other cases, although some reversals have been observed.

In table 2 the heats of hydration are shown as the differences between the heats of partial solution of the dry cement and of the hydrated pastes. Although, except for sample 4, the heats of solution increase with increasing solution period, the heats of hydration do not so change. For these heats of hydration to be accurate, it is necessary to assume that any systematic errors are the same in the determinations of the heats of partial solution of the dry cements, and of the hydrates. Although this assumption may not be true from the standpoint of precise calorimetry, the error in the heat of hydration is probably small enough for the satisfactory testing of portland-pozzolan cement and must be accepted for the present in the absence of a more satisfactory method of test.

TABLE 3. *Material undissolved in the calorimeter*

Percentage of 3-g sample (ignited weight) of cement or cement paste undissolved in acid charge of 10 ml of HF plus sufficient 2.00 *N* HNO_3 to make 647.5 g of total acid. Each value is the average of 2 determinations.

Cement	Sample	Undissolved material	Time in contact with acid mixture
		Percent	*Min*
1	Dry	9.2	43
	7-day paste	[a] 9.5	43
	28-day paste	9.9	48
2	Dry	8.0	43
	7-day paste	8.3	51
	28-day paste	8.8	48
3	Dry	2.9	43
	7-day paste	3.0	40
	28-day paste	3.8	43
4	Dry	0.4	30
	7-day paste	.5	31
	28-day paste	.5	42
5	Dry	7.0	85
	7-day paste	7.8	65
	28-day paste	8.0	58

[a] One determination only.

The departure of the heat of partial solution of a portland-pozzolan cement from the value for complete solution arises from two sources, both caused by the difficulty of dissolving the pozzolan. The sample does not completely dissolve, and therefore the pozzolan does not contribute its entire heat of solution. (Portland cement is assumed to dissolve completely and usually does so.) The slow dissolving of the pozzolan during the final "rating period" continues to liberate heat, and thus slightly incorrect values are obtained for the heat of stirring and the coefficient of thermal leakage. If the pozzolan dissolves to the same extent and at the same rate for both the dry cement and the hydrated pastes, the systematic errors in the heats of partial solution disappear when the heat of hydration is calculated. Some idea of the possible effect of undissolved material may be obtained by noting that the maximum difference in undissolved material for dry cement and 28-day hydrated paste in table 2 is 1.0 percent. If it is assumed that the heat of partial solution of the paste is therefore 1.0 percent, or 4.8 calories, low, the resulting error in the heat of hydration would be 5 cal/g. It is doubtful if this large an error is caused because the heat of solution of undissolved pozzolan (see table 4) may be considerably less than the approximately 520 cal/g of a hydrated portland-cement paste.

2.2. Heats of Solution and Undissolved Residues of Cement-Pozzolan Mixtures

The heats of partial solution were determined for several finely ground pozzolans [2] and for blends of these with finely ground portland-cement clinker. The samples were prepared by placing weighed amounts of the finely ground components in a laboratory ball mill with a few wooden balls and mixing for 2 hr. After the determinations of the heat of partial solution, the calorimeter acid was filtered and the residue of insoluble material was ignited, and weighed.

The values of the heat of solution are given in table 4 and are plotted in figure 1. The undissolved residue in the calorimeter, expressed as the percentage by weight of the sample, is given in table 5 and plotted in figure 2. It will be seen that a relatively constant proportion of the pozzolan remained undissolved at the end of the experiments, although the ratios of pozzolan to calorimeter acid differed rather widely. The experimental points fall closely about

TABLE 4. *Heats of solution of portland-cement-pozzolan mixtures*

Heats of solution of 3-g samples (ignited weights) were determined in 10-ml of 48-percent HF plus sufficient 2.00 *N* HNO_3 to make 647.5 g of total acid in a precision-type isothermal-jacket calorimeter [4]. Time of contact, 30 min.

Pozzolan content of mixture	Pozzolan				
	A	B	C	D	E
Percent	*cal/g*	*cal/g*	*cal/g*	*cal/g*	*cal/g*
0	601.6	601.6	601.6	601.6	601.6
20	------	560.9	541.1	535.0	------
25	------	551.6	525.6	------	520.0
30	------	539.5	511.5	502.2	------
33	608.4	538.3	------	------	485.3
35	------	------	------	------	------
100	621.2	393.0	301.5	269.9	253.5

TABLE 5. *Solubility of portland-cement-pozzolan mixtures in acid*

Undissolved portion of portland-cement-pozzolan mixtures, shown in table 4, after 30-min contact with a mixture of 10 ml of 48-percent HF plus sufficient 2.00 *N* HNO_3 to make 647.5 g of total acid.

Pozzolan content of mixture	Pozzolan			
	A	B	C	D
Percent	*Percent*	*Percent*	*Percent*	*Percent*
0	0.00	0.00	0.00	0.00
20	------	4.33	6.12	8.27
25	------	4.71	7.30	10.30
30	------	6.28	9.21	12.39
33	.00	------	------	------
35	------	6.77	10.74	14.56
100	.00	23.62	29.70	40.60

[2] Details of the constitution and properties of the pozzolans unfortunately are not now obtainable. Sample A, tables 4 and 5 and figures 1 and 2, was a blast-furnace slag; B was a burned shale; C and D are identified as Pennsylvania pozzolans; and E as a California pozzolan. Before mixing, the clinker and the pozzolans were ground to finenesses now unknown but comparable to portland cement.

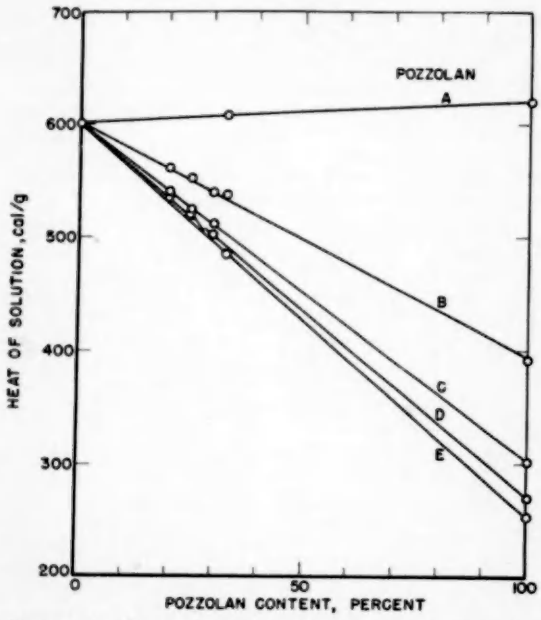

FIGURE 1. *Heats of solution of portland cement-pozzolan mixtures.*

The heats of solution were determined in a 647.5-g mixture of 10 ml of 48-percent HF and 2.00 *N* HNO_3 in a precision-type isothermal-jacket calorimeter. Time of contact with acid, 30 min.

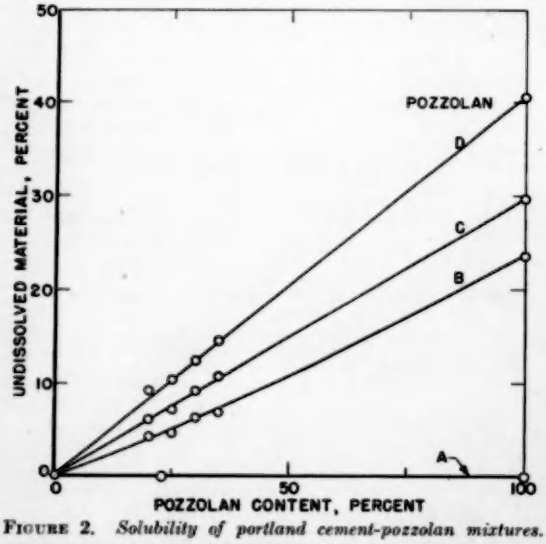

FIGURE 2. *Solubility of portland cement-pozzolan mixtures.*

Percentage of material undissolved by 30-minute contact of 3-g sample with 647.5-g mixtures of 10 ml of 48-percent HF and 2.00 *N* HNO_3.

the lines joining the heats of solution of the components of the mixtures and indicate that the experimental values of the heat of solution agree well with the values calculated from the proportions of cement and pozzolan.

3. The Vacuum-flask Calorimeter

To determine the heat of partial solution of a pozzolan cement with the vacuum-flask calorimeter, a modification of the standard [1, 2] procedure for portland cement is useful. The environment of the calorimeter is not sufficiently well defined, nor is its temperature measured with sufficient accuracy, to permit the use of long solution periods. However, by assuming that the temperature of the environment (the room temperature) remains constant, and that the thermal leakage remains at the average value determined during measurements made with portland cement, one of the two rating periods ordinarily necessary to calculate the corrected temperature rise can be eliminated. It is convenient in working with pozzolan cements to omit the final rating period. Then at some arbitrarily chosen time, such as 60 min after the introduction of the sample, the solution period can be considered ended and the determination stopped. It must be emphasized that even in the standard procedure [1, 2] the room temperature is assumed constant. The equation for the corrected temperature rise R [2, p. 51] becomes by this method

$$R=\theta_{60}-\theta_i-V_aT_x+K(\theta_xT_x-\theta_aT_x),$$

where

θ_i, θ_{60} = temperature of the calorimeter at the beginning and end, respectively, of the solution period.

V_a = the average temperature rise per 5-min interval during the initial rating period;

T_x = the number of 5-min intervals in the solution period, here arbitrarily taken 12;

θ_a = the average calorimeter temperature during the initial rating period;

θ_x = the average calorimeter temperature during the solution period, (θ_xT_x is the integral of the time-temperature curve during the solution period); and,

K = the thermal leakage coefficient, 0.0055 $(5\text{-min})^{-1}$ in the present work.

These symbols are the same as in the published specifications [1, 2]. The corrected temperature rise, R, is multiplied by the heat capacity of the calorimeter, and the product divided by the ignited weight of the sample is the heat of solution. To increase the precision of the determination of V_a, the initial rating period is extended over a 20-min period. This procedure is less precise than the normal determination of the heat of solution of a portland cement, but by its use an approximate value of the heat of partial solution of a pozzolan cement can be obtained.

3.1. Heat of Solution and Pozzolan Content of Cement-Pozzolan Mixtures

The work reported in the first part of this paper seemed to show linear relations between the heats of partial solution of cement-pozzolan mixtures and

the percentages of pozzolan present. From such a relation the composition of a mixture might be calculated from determinations of the heats of solution of the mixture and its two components. This calculation would be useful if the heats of solution of the two components were sufficiently different. To test the method, determinations were made of the heats of solution of a series of mixtures of cement and pozzolan. Two unknown mixtures were supplied by a cement manufacturer, together with samples of the cement and the pozzolan with which they had been prepared. Known mixtures were prepared at the Bureau and their heats of solution determined by means of the vacuum-flask calorimeter The heats of solution of the cement and of the pozzolan were also determined. The normal amount, 8 ml, of hydrofluoric acid was used, and each determination was arbitrarily ended 60 min after the introduction of the sample. The undissolved material remaining in the calorimeter at the end of each determination was recovered on a filter, ignited, and weighed. The heats of partial solution were calculated by the procedure already described.

The data obtained are given in table 6 and shown in figure 3. The relation between the percentage pozzolan and the heat of partial solution of the mixture is not linear. The equation of a line representing these data, chosen by the method of least squares, is

$$H = 607.8 - 0.939P - 0.00344P^2,$$

where P is the percentage of pozzolan, and H is the heat of partial solution of the mixture. From the equation and the average values of the heat of solution of the unknown samples of 592.5 and 581.3 cal/g, respectively, for samples 7 and 8, table 6, the amount of pozzolan in the two samples was calculated to be 15.2 and 25.8 percent, respectively. The precision of these data is such that the estimated value of the standard deviation is about ± 2.9 cal/g, which corresponds to about ± 3.1 percent of pozzolan in the cement-pozzolan mixture. The actual compositions of the two unknown mixtures were subsequently given by the manufacturer as 10.5 and 25.5 percent of pozzolan, respectively.

In view of the good agreement between the observed and calculated heats of solution of the known mixtures of cement and pozzolan, it was rather surprising to find such a wide difference between the value of 10.5 percent of pozzolan given for one mixture and the 15.2 ± 3.1 percent determined from the heat of solution. For the other unknown sample the agreement is excellent between the 25.5 percent given and the 25.8 ± 3.1 percent of pozzolan found.

TABLE 6. *Heats of solution of cement-pozzolan mixtures in acid*

The heats of solution were measured in a vacuum-flask calorimeter [1, 2]. Determinations were ended arbitrarily after 60-min contact between the mixture and the acid charge of 8 ml of 48-percent HF and sufficient 2.00 N HNO_3 to make a total weight of 425 g. Thermal leakage of calorimeter was taken as its average of 0.0055 (5-min)$^{-1}$, and the final rating period was omitted.

Sample	Pozzolan content	Heat of solution	Undissolved residue
	Percent	*cal/g*	*Percent*
11	0	607.4	0
	0	607.2	0
	0	612.4	0
	0	607.9	0
12	100	481.5	18.34
	100	475.0	20.56
	100	478.0	18.75
13	20	582.8	2.80
	20	587.2	3.11
14	40	564.4	5.99
	40	562.8	6.55
15	60	542.4	9.85
	60	537.8	10.19
16	80	510.5	13.91
	80	517.5	14.38
17 [a]	----------	592.3	1.55
		592.7	1.77
18 [b]	----------	569.8	3.51
		578.6	3.91
		580.0	3.88
		585.1	3.98
		581.4	3.83

[a] Stated by the manufacturer to contain 10.5 percent of pozzolan.
[b] Stated by the manufacturer to contain 25.5 percent of pozzolan.

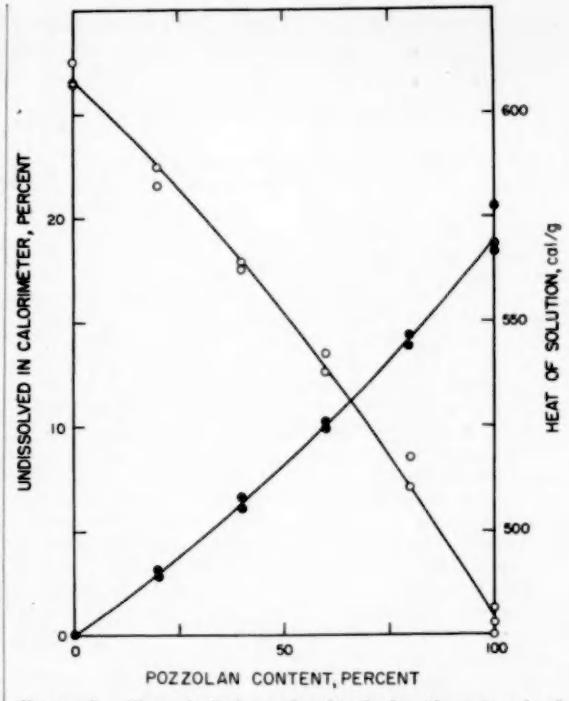

FIGURE 3. *Heats of solution and undissolved residues of portland cement-pozzolan mixtures in the vacuum-flask calorimeter.*

Determinations ended after 60-minute contact between 3-g samples and acid charges of 8 ml of 48-percent HF and sufficient 2.00 N HNO_3 to make a total weight of charge of 425 g. Open circles, heat of solution; closed circles, undissolved residue.

3.2. Undissolved Residues of Cement-Pozzolan Mixtures

The determination of the undissolved residue appeared to give a better and simpler method of determining the percentage of pozzolan in a cement-pozzolan mixture. The percentages of undissolved residue obtained in the experiments described above are

given in table 6 and are shown in figure 3. The equation of the line fitted to these data by the method of least squares is

$$U=0.108+0.1268P+0.000636P^2,$$

where P is the percentage pozzolan in the mixture, and U is the percentage undissolved material. Values of the pozzolan content of the two "unknown" samples calculated from the above equation were 11.6 ± 0.8 and 25.9 ± 1.0 percent, respectively. These values agree better with the given compositions of the unknown samples than do the values calculated from the heats of solution. The precision is better also, since the standard deviation of the percentage calculated from the heat of solution is three times that determined from the insoluble material.

The determination of undissolved material is much simpler than the determination of the heat of solution, as no calorimeter is needed. Plastic beakers can be used for reaction vessels with a stirring machine, such as is now commonly used in cement laboratories for the analytical determination of MgO with 8-hydroxyquinoline. The practicability of the determination of the pozzolan content of a mixture by either method depends on the percentage of the pozzolan dissolved by the acid in a given time interval. The rate of solution will vary with the surface area and with the type of pozzolan, and a curve must be determined for each variety of pozzolan and of cement. If solution is complete, the insoluble-material method cannot be used, but the heat-of-solution method will be improved in accuracy because of the improvement in the accuracy of the calorimetric determination.

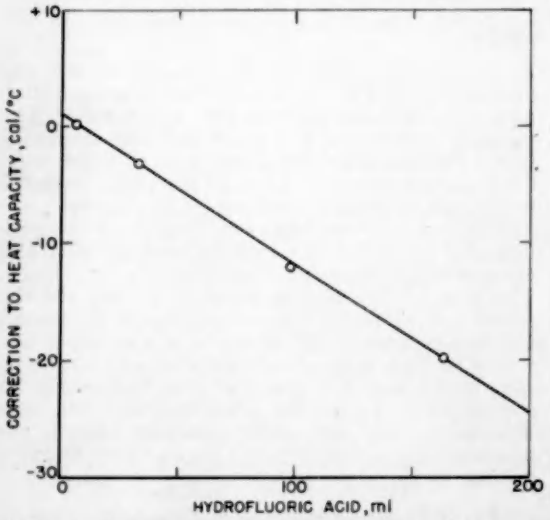

FIGURE 4. *Heat-capacity correction for vacuum-flask calorimeter*

Correction to be added to value obtained by the standard method with ZnO, using 8 ml of 48-percent HF and sufficient 2.00 N HNO_3 to make 425 g of acid. For use only with 425 g of total acid consisting of 2.00 N HNO_3 and indicated amount of hydrofluoric acid. The equation of the line is $C=1.02-0.127\ M$, where C is the correction to be added, and M is the number of milliliters of 48-percent HF in the 425-g acid charge.

3.3. Heat-Capacity Corrections

For some pozzolans it may be desirable to use more than 8 ml of hydrofluoric acid in the calorimeter in order to expedite the dissolving of the sample. Such a change will alter the heat capacity of the calorimeter. Normally, the heat capacity is determined by dissolving a standard substance, zinc oxide, in the 425-g charge of 2.00 N HNO_3 containing 8 ml of 48-percent HF. For this purpose the heat of solution of zinc oxide in such a mixture has been carefully determined, and the value has been published in the specifications. However, data are not available for other mixtures of nitric and hydrofluoric acid so that the heat capacity of the calorimeter containing other amounts of HF cannot be determined by the specification method. The heat capacity can be calculated, however, from the change in the heat capacity of the liquid contents of the calorimeter, since the heat capacity of the glass, plastic, and metal parts are not affected by a change in the concentration of hydrofluoric acid. From heat-capacity data obtained with the precision calorimeter, the correction to be made to the heat capacity determined with the solution containing 8 ml of HF was calculated over a range of concentration of HF from 0 to 0.47 ml of 48-percent HF solution per gram of total acid (HF+2.00 N HNO_3). The maximum concentration corresponds to the use of 200 ml of HF in the 425-g calorimeter charge. The correction to be applied can be estimated from figure 4 and may be calculated from the equation $C=1.02-0.127\ M$, where C is the correction in calories per degree Celsius (centigrade) and M is the milliliters of 48-percent HF in 425 g of total acid.

The authors acknowledge their indebtedness to J. Arthur Swenson, formerly of the National Bureau of Standards, who determined the heats of solution of the cement-pozzolan mixtures with the precision calorimeter.

4. References

[1] Federal Specification SS–C–158b for Cements, hydraulic; general specifications (Methods for sampling, inspection, and testing) (May 20, 1946).
[2] Standard Method of test for heat of hydration of portland cement. American Society for Testing Materials, Designation C–186–47. (October 15, 1947).
[3] Edwin S. Newman and Lansing S. Wells, Heats of hydration and transition of calcium sulfate. J. Research NBS **20**, 825 (1938) RP1107.
[4] Leo Shartsis and Edwin S. Newman, Some energy relations in the systems PbO–B_2O_3 and Pb–SiO_2. J. Research NBS **40**, 471 (1948) RP1893.
[5] Walter P. White, The modern calorimeter. (The Chemical Catalog Co., New York, N. Y., 1928).

WASHINGTON, April 7, 1952.

Journal of Research of the National Bureau of Standards Vol. 49, No. 2, August 1952 Research Paper 2343

Infrared Properties of Cesium Bromide Prisms

Earle K. Plyler and Nicolo Acquista

A prism of cesium bromide has been installed in a Perkins-Elmer spectrometer, and spectra have been observed in the region from 15 to 38 μ. This prism is of better optical quality than those of KRS–5, which makes it possible to obtain sharp images at the second slit of the spectrometer. Measurements have been made with this cesium bromide prism, which has a refracting angle of 55°, and the results have been compared with those obtained with a 26° KRS–5 prism. The dispersion of cesium bromide from 15 to 38 μ is about equal to KRS–5, but the effective resolution is about twice as great. A group of rotational lines of water vapor at 28.4 μ is now clearly resolved into three components, the two narrow ones being separated by 1.8 cm $^{-1}$. The long wavelength bands of carbon disulfide and chloroform have been measured in the vapor state, and it is possible, with the good definition available, to observe the *P*, *Q*, and *R* branches. In the spectral region beyond 33 μ, the stray radiation produces a considerable amount of the total deflection. The stray radiation was reduced to one-tenth of its value by the use of a roughened silver mirror located in the source box of the spectrometer.

1. Introduction

The extension of infrared measurements to wavelengths greater than 25 μ by the use of KRS–5 prisms has been of considerable value in measuring the low lying fundamental bands of molecules.[1] Although the KRS–5 prisms usually have poor optical quality, they have been used in many laboratories. The purpose of this investigation is to test another crystalline material, cesium bromide, for possible use in the infrared region between 25 and 40 μ. Previous measurements on crystals of this material grown at this Bureau showed that it was transparent to 40 μ for a window 6 mm in thickness.[2]

In recent months CsBr crystals of good optical quality have been grown in industrial laboratories. Prisms obtained from two companies have been tested in a Perkin-Elmer spectrometer. One prism had a fault in the crystal which increased the stray radiation, but there was very little diffusion of the image on the slit. On comparing spectra obtained by this prism with those measured by the one without apparent flaws, no appreciable difference was noted in the results.

A cesium bromide prism with a refracting angle of 55° was mounted in the Perkin-Elmer spectrometer, and it was placed at such an angle that the yellow lines of mercury could be brought on the exit slit when the drum of the spectrometer was set for large numbers. It was then possible to reach 40 μ before the drum was turned the full way to the zero. The prism was adjusted in the spectrometer by the use of the visible lines of mercury.

After the final adjustment of the instrument, some properties of the cesium bromide prism were determined. They are discussed in the following part of this paper.

2. Results

2.1. Transmittance

Transmittance of a cesium bromide prism with a 55° refracting angle is sufficient to allow measurements to be made to 38 μ. This limit is about 1.8 microns smaller than the cut-off of a 26° TlBr-I prism.

2.2. Resolution and Definition

The resolution of the cesium bromide prism is greater than that obtained with TlBr-I prisms. A practical test of resolution of the instrument, with a CsBr prism as the dispersing component, has been made. Figure 1 shows the resolution of the instrument in the region from 25 to 38 μ, the absorption bands being produced by water vapor in the air. Three closely spaced lines are resolved in the region of 28.4 μ, two of the lines resolved differing in wave number by only 1.8 cm^{-1}. These lines could not be resolved with the TlBr-I prism. The better resolution of the cesium bromide prism in the long wavelength region is made possible by its higher optical quality and its high dispersion, approximately equal to that of TlBr-I.

There is very little fuzziness or spreading out of the images of atomic spectral lines when they are focused on the second slit. This feature of the prism material makes it possible to follow rapid changes in absorption over small wavelength intervals. Many

[1] Earle K. Plyler, J. Chem. Phys. **17**, 218 (1949).
[2] Earle K. Plyler and Francis P. Phelps, J. Opt. Soc. Am. **41**, 209 (1951).

absorption bands of substances in the vapor state have P, Q, and R branches. In measurements with the TlBr-I prism, it is not possible to observe band shapes on account of the poor definition of the image, but with the CsBr prism the band shapes can be observed for many molecules. An example of the observation of band shapes can be seen in figure 2. The carbon disulfide band at 25.17μ is clearly resolved into P, Q, and R branches. The 27.2μ band of chloroform, which appeared as a single maximum when measured by the TlBr-I prism, is now resolved into four components. The dotted part of the curve is an approximation of the true absorption; interference caused by water vapor partially masks the absorption due to the chloroform. The good definition of the prism is also advantageous for measuring spectra in that narrow absorption bands or lines can be measured to their true depths rather than as shallow diffuse bands.

2.3. Dispersion

The indices of refraction of cesium bromide have not been measured, but a good idea of the dispersion of the prism can be obtained by measuring the number of microns scanned for one revolution of the spectrometer drum. The prism was set for minimum deviation in the visible region and was off from the minimum deviation by a few degrees in the region from 24 to 37μ. Figure 3 shows the number of microns included for one revolution of the drum. The results for eight measurements at intervals throughout the spectral range are well represented by the straight line in the figure. For comparison, a similar set of measurements for TlBr-I prism with a refracting angle of 26° are also shown. Since the deviations of the two prisms are in the ratio of 2 to 1, and the refracting angles are about in the same ratio, it appears that the dispersions of cesium bromide and TlBr-I are comparable in the region from 24 to 38μ.

2.4. Stray Radiation

The effect of stray radiation is large beyond 24μ, and becomes a serious problem in measuring spectra with the cesium bromide prism. The transmittance of TlBr-I is small in the near infrared region, and thus a filtering effect is produced; but there is no absorption by cesium bromide in the short wavelength region and hence no filtering effect is produced. When the instrument is set for the long wavelength regions, the ratio of the stray radiation to the measured energy increases and is about 80 percent of the total energy at 37μ. The amount of stray radiation present in an instrument is, in part, dependent on the accidental reflection from the interior of the spectrometer. Diaphragms of black paper were placed in various parts of the spectrometer, but with this shielding the stray radiation was reduced very little, which makes it appear that the stray radiation originates principally from the surfaces and interior of the prism. In order to cope with this situation, it is necessary to reduce the amount of the short wavelength energy which enters the spectrometer, since the stray radiation is primarily composed of the peak energy in the region from 1 to 5μ of the globar source.

Two types of filters, transmission and reflection, were tested for use in removing the stray radiation. It was found that satisfactory results were obtained by the use of a reflection filter which was made by roughening the surface of a polished silver mirror. The roughened silver mirror was placed in the source box of the spectrometer in place of the plane aluminum mirror. Figure 4 represents the percentage of the total energy contributed by the stray radiation at different wavelengths for the aluminum mirror, the rough and the very rough silver mirrors. The rough surface was produced by rubbing the polished mirror several times over 3/0–80 emery cloth, and the very rough mirror was produced by rubbing on 1/0–120 emery cloth. The very rough silver mirror reduces by a factor of ten the amount of stray radiation that is present with the aluminum mirror. The roughened mirrors do not reflect the long wavelength radiation quite as well as the polished mirrors, and it was found that the nonstray radiation was reduced to 85 percent of that obtained with the aluminum mirror. This reduction in effective energy was less than that found for transmission filters.

3. Conclusion

The higher optical homogeneity and the lower refractive index with approximately the same dispersion of the cesium bromide prism make it more suitable for measurements in the region from 24 to 38 μ than a TlBr-I prism. Also, from about 20 to 24 μ, the results obtained with a cesium bromide prism are comparable with those obtained with a potassium bromide prism. For measurements covering the region from 2 to 38 μ, fair resolution can be obtained by the use of two prisms, sodium chloride and cesium bromide. However, for the highest resolution, prisms of lithium fluoride, calcium fluoride, and potassium bromide must be employed in the appropriate regions. The use of different prisms to cover the greatest span may be somewhat changed when cesium iodide becomes available. Small cyrstals of high transparency have been grown at this Bureau and an estimate of probable transparencies suggests that this material will make possible the extension of prism spectrometry to wavelengths greater than 50 μ.

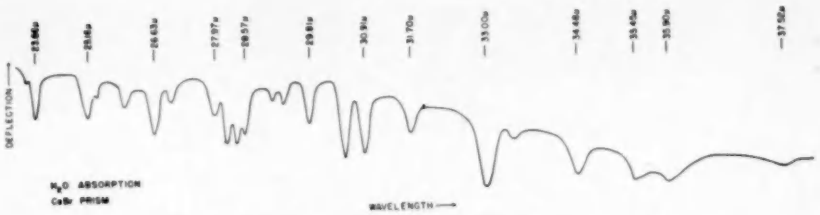

FIGURE 1. *Infrared spectrum of water vapor from 23.6 to 37.5 μ.*
H_2O absorption CsBr prism.

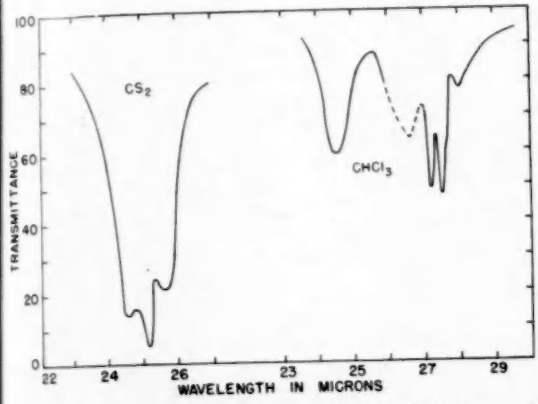

FIGURE 2. *Absorption bands of carbon disulfide at 25.2μ and those of chloroform at 28μ.*
CS_2 cell length, 10 cm; pressure, 19 cm; $CHCl_3$ cell length, 160 cm; saturated pressure.

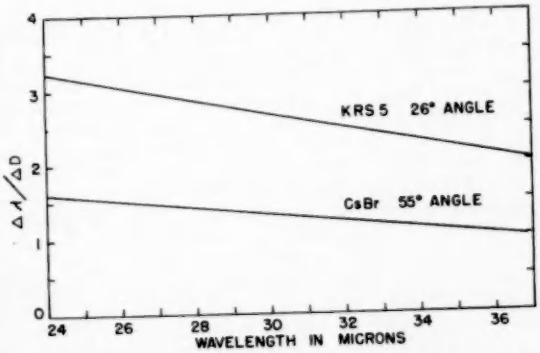

FIGURE 3. *Change in wavelength per revolution of spectrometer drum for prisms of KRS–5 and cesium bromide in the region from 24 to 37μ.*
KRS–5, 26° angle; CsBr, 55° angle.

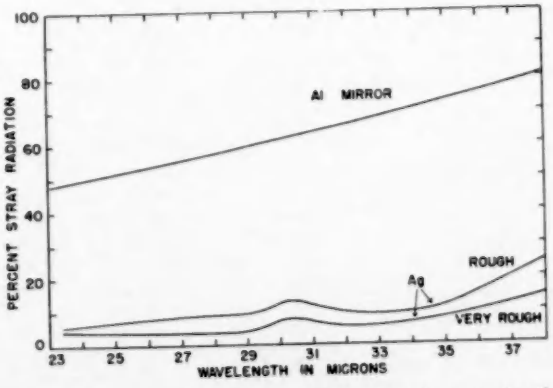

FIGURE 4. *Percentage of stray radiation in the long-wavelength region for different reflectors.*

WASHINGTON, April 8, 1952.

212644—52——2

Journal of Research of the National Bureau of Standards Vol. 49, No. 2, August 1952 Research Paper 2344

Titanium Dioxide Rectifiers

R. G. Breckenridge and W. R. Hosler

A new type of metal rectifier is described which utilizes a film of semiconducting titanium dioxide produced on titanium metal. These rectifiers, which have been prepared either by a two-step process involving a heating of the metal in oxygen followed by a reduction of the oxide in hydrogen or by a single heating of the metal in water vapor, are shown to have properties comparing favorably with existing types, particularly for high temperature applications. The properties of the units in regard to the nature of the counter electrode, and relation to theories of rectification are discussed.

1. Introduction*

The phenomenon of rectification at a metal-semiconductor contact has been of commercial as well as scientific importance since the first announcement of the cuprous oxide rectifier by Grondahl in 1926 [1].† Since this first practical rectifier was produced, a number of other somewhat similar types have appeared, the magnesium copper sulfide [2] and the selenium [2] rectifiers being widely used commercially. While the point contact types, such as the silicon and germanium rectifiers [3], are similar in principle, they are designed for handling small amounts of radiofrequency power instead of rather large amounts of low-frequency power.

There have been a great number of theories proposed to explain rectification, the most widely used probably being those of Mott [4] and Schottky [5]. Although these theories differ considerably in their details, both discuss a model consisting of an asymmetrical potential barrier such that charge carriers are transferred readily across the barrier in one direction and with difficulty in the other. It is in the nature of this barrier, e. g., chemical, physical, or both, and in the mathematical details describing the charge flow in the various possible situations that the differences arise. Unfortunately, the multiplicity of theories has not materially aided the search for new or improved rectifiers, and their discovery still seems almost fortuitous. The properties of the Cu-Cu_2O system are, however, at least suggestive of the properties needed for a practical rectifier of the oxide type. It is evident that the oxide must be readily produced as a thin, tightly adhering layer on the metal surface, the oxide composition must be controllable so that it may be made a semiconductor with a relatively high conductivity, and finally, there must be some means of producing an asymmetrical potential barrier in the system. In the Cu_2O rectifier there is some evidence [6] that the barrier is a layer of nearly stoichiometric Cu_2O at the Cu_2O-Cu interface.

Even a brief consideration of the first two rather obvious requirements serves to eliminate the great majority of the metal-oxide combinations, since there are very few oxides that are readily produced with conductivities great enough to be of interest (about 1 to $10\Omega^{-1}$ cm^{-1} at room temperature), let alone in the form of a thin adherent film.

Some observations on the oxidation of titanium metal [7] have shown, however, that a thin film satisfying the mechanical requirements is readily produced on the metal surface. Similarly, there have been a number of studies of the electrical properties of titanium dioxide semiconductors [8 to 12] showing that the oxide can be made an n-type semiconductor with a conductivity in the desired range by heating the oxide in hydrogen. It is then apparent that at least the possibility exists for a feasible rectifier unit, providing that in some way the asymmetrical potential barrier may be produced. The formation of this barrier seems not unlikely, since a concentration gradient similar to that in the Cu_2O rectifier might be formed at the metal-oxide interface or possibly at the oxide surface. A number of experiments on this system have been carried out, and two methods of producing such a rectifier have been developed. Although the unit is still in an early stage of development, the observed characteristics are comparable to those reported for commercially available types. It should be mentioned that, in common with other rectifier developments, it has proved difficult to obtain entirely consistent results, so the numerical values quoted later in the paper should be regarded as representative and not necessarily final values.

2. Titanium Oxide Films

The titanium metal used in these studies was obtained through the courtesy of the Allegheny-Ludlum Steel Co., Watervliet, N. Y. The sample was in the form of a sheet 0.015 in. thick of standard commercial grade Ti 75A, reported by the company to be about 99.5 percent pure, with 0.1 percent of Fe, 0.02 percent of N, a trace of O, C$<$0.04 percent, and variable amounts of W present as inclusions ranging from 0.05 to 0.5 percent. This metal was cut into ½-in. squares and ground with No. 400 alundum. A few trials were also made with the unpolished sheet, and no pronounced differences in the electrical results were noted. In the first series of studies, these squares, contained in a small porcelain boat, were placed in the furnace without protection. More consistent results were obtained if they were imbedded in Al_2O_3 powder, and this procedure was followed in most of the studies. The samples were

*The results of this work were first presented at the National Research Council's Conference on Electrical Insulation meeting in Washington, D. C., Oct. 29-31, 1951.

†Figures in brackets indicate the literature references at the end of this paper.

TABLE 1. *Properties of titanium oxide films*

Temperature	Time					
	25 min	1 hr	1½ hr	2 hr	2½ hr	9 hr
°C						
800	Smooth, thin, light-grey, tightly adhering coat.* Breakdown voltage: V+, 60 to 90; V−, 150.		Smooth, blue-grey, tightly adhering coat.* Breakdown voltage: V+, 120 to 150; V−, 150.	Smooth, tightly adhering, grey-yellow coat. Breakdown voltage: V+, 125, V−, 185.	Grey-yellow, badly chipped coat.* Breakdown voltage: V+, 120 to 150; V−, 140 to 150. Thickness ~0.0003 in.	Blue-grey, thick, tightly adhering coat.
820	Smooth, even, blue-grey, tightly adhering coat.* Breakdown voltage: V+, 60; V−, 70 to 90.	Smooth, even, blue-grey, partially chipped coat.* Breakdown voltage: V+, 60 to 90; V−, 120 to 150. Thickness <0.0001 in.	Grey-yellow, partially loose from surface coat.* Breakdown voltage: V+, 120; V−, 150. Thickness ~0.0001 in.	Grey, almost completely chipped off coat.* Breakdown voltage: V+, 120 to 150; V−, 150. Thickness ~0.0001 in.		
850	Yellow-grey, tightly bound coat. Breakdown voltage: V+, >320; V−, >320.	Greenish-yellow rough but tightly bound coat. Breakdown voltage: V+, >320; V−, >320.	Yellow, tightly bound coat. Breakdown voltage: V+, >320; V−, >320.	Yellow, partially chipped coat. Breakdown voltage: V+, >320; V−, >320.		
900	Yellow, loosely bound coat. Breakdown voltage: V+, >320; V−, >320.	Yellow, badly chipped coat. Breakdown voltage: V+, 450; V−, >500. Thickness 0.0008 in.	White-yellow coat, chipped at edges. Breakdown voltage: V+, >500; V−, >500. Thickness 0.002 in.			

then heated to the desired temperature in a tube furnace regulated to ±5 °C, while a stream of inert gas, in this case helium, was flowing through the tube. When the system was stabilized, the helium was swept out by oxygen dried by a liquid air trap and the samples kept in 1 atmosphere of oxygen for the desired time. At the end of this time, the oxygen was swept out with helium and the furnace allowed to cool to room temperature.

The physical and electrical properties of these samples were then examined in a number of ways. Because the oxide film must be thick enough to withstand appreciable voltages before breakdown, the breakdown strength was first explored. The oxide was ground off on one corner of the square so that electrical contact could be made to the titanium metal. Then a small metal point of copper, about 0.1 mm in diameter, was placed on the surface and the voltage raised to breakdown. This was done for both directions of current flow on about 10 spots on the surface.

The thickness of some of these films was determined with a simple optical system. The oxide was chipped off the metal at one point. Then, using a small tripod on which a mirror was mounted, the displacement of a light beam was measured when one of the tripod points rested on metal or oxide. The sensitivity of the setup was 3.5μ/mm of deflection on the scale.

The studies of the oxide films are reported in table 1, where the physical appearance, measured thickness and typical breakdown voltages are given for the various samples. The polarity of the point contact is indicated for V. The samples oxidized without the Al_2O_3 covering are indicated with an asterisk. In some of the higher temperature samples, the oxide film was so loosely adherent or flaky that no further studies were made. It is apparent, however, that samples produced at about 800° C for a variety of times, ranging from ½ to 9 hours, have very satisfactory electrical properties. An undesirable feature noted in the higher temperature samples was an embrittlement of the metal produced by a solution of the oxygen in the metal, as has been previously reported [13]. This embrittlement, while present, was not excessive in the 800° samples.

The kinetics of the oxidation of Ti metal has been studied by several authors [14, 15, 16] with conflicting results. It has not been clearly established whether the growth follows a parabolic, logarithmic, or linear law with time, and all authors find considerable deviations for times as short as those used in this investigation. The work reported here cannot resolve this difficulty because a wide scatter of the data was found. This scatter arises from the fact that precise measurements of thickness were not attempted, the difficulty of controlling the short-time treatments, and the possibility of oxygen dissolving in the metal rather than forming a surface oxide.

3. Reduced TiO_2 Rectifiers

The reduction of titanium dioxide by hydrogen has been studied in detail by Nasu [17], who concludes that the reaction product is Ti_2O_3. For the purposes of rendering the rutile semiconducting with a conductivity in the desired range, only a partial reduction is needed, corresponding to a formula of about $TiO_{1.95}$ [11], that is, with a 2.5-percent excess of titanium, which is presumably present as the trivalent ion. This amount of reduction was achieved in solid ceramic samples of rutile by treatment with hydrogen for 10 minutes at 1,350°C [11]. As it was anticipated that the speed of reduction would be much greater in the thin films, a series of trial runs was made, following a procedure similar to that for the oxidation process, at temperatures of 450° to 800° C and for times ranging from 5 to 60 minutes, using oxide films formed at 800° C for 9 hours. The samples were not imbedded in Al_2O_3 for the reduction in hydrogen. The most satisfactory properties resulted from a treatment at 500° C for 15 minutes, although this was not critical. For long reductions at temperatures much above 500° C, however, the oxide film was found to flake off, and for lower temperatures the process was very slow.

After reduction, the units were tested for rectification using a small spot of metallic indium for the counter electrode. This electrode material was chosen because other studies have shown [11, 12] that no anomalous electrical effects arise at the interface of this metal and titania semiconductors. This preliminary testing was done with a simple circuit to display the current-voltage curve on a cathode-ray oscilloscope [2]. If a reasonable evidence of rectification was found, a counter electrode was applied for more detailed measurements. This counter electrode was conveniently applied by plating with a-c for about 30 seconds so that the sensitive areas would be preferentially coated. Electrodes of a variety of metals have been used with effects to be discussed in detail later in this paper. However, silver was used for the major portion of the work because it is readily plated and the metal does not oxidize easily under heat treatment. The properties of the rectifiers formed in this fashion were then studied, using conventional voltmeter-ammeter measurements, both with point contacts to individual sensitive spots and with an 0.08—cm² copper plate pressed to the electroplated surface to make a large area contact.

In the rectifier tests some nonlinearity was observed in almost all cases, but in a number of samples good rectifying properties were found. The sense of the rectification is such that the direction of easy flow of electrons is from the *n*-type semiconductor to the counter electrode; that is, the counter electrode is positive. A typical measurement of such a point-contact rectifier formed by heating for 9 hours in O_2 at 800° C followed by 15 minutes in H_2 at 500° C is shown in figure 1, where the current in milliamperes is plotted as a function of voltage. A more revealing method of plotting these data is shown in figure 2, where the log of the current in milliamperes is plotted as a function of the voltage. The forward current as a function of voltage is described by an equation of the form

$$I_f = A_f[e^{\alpha_f(V - I_f r)} - 1] \qquad (1)$$

so that α_f, A_f, and r, the spreading resistance, may be determined from the data of figure 2. For this sample the values found are $A_f = 0.001$ ma, $\alpha_f = 9.4$ volts^{-1}, and $r = 21\Omega$. This value of r indicates a conductivity at room temperature of about $7.4\Omega^{-1}\text{cm}^{-1}$ and thus is in the desired range. As is typical for such measurements [2] the value of α_f is considerably smaller than the theoretical value of 40 volts^{-1} but is similar to those found for commercial units.

The reverse current for applied voltages greater than 0.5 may be described by an equation of the form

$$I_b = A_b\ (e^{\alpha_b V} - 1)$$

with values of $A_b = 0.38$ ma and $\alpha_b = 0.35$ volt^{-1}. These results are also similar to those found for other rectifier types. A similar study of a plated sample, using an 0.08-cm² contact area, is shown in figures 3 and 4. The forward and reverse currents are described by the same equations with constants $\alpha_f = 8.6$ volts^{-1}, $A_f = 0.0033$ ma, and $r = 12\Omega$ in the forward direction, and $\alpha_b = 0.39$ volt^{-1} and $A_b = 0.29$ ma for the reverse current.

While no highly specific conditional requirements were found for either the oxidation or reduction treatments, the general trend of the observations suggests an oxygen treatment of about 2 hours at

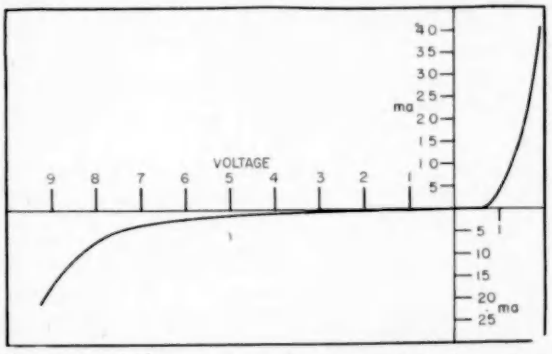

FIGURE 1. *Direct-current rectifier characteristics from silver point contact on titanium dioxide rectifier made by two-step process.*

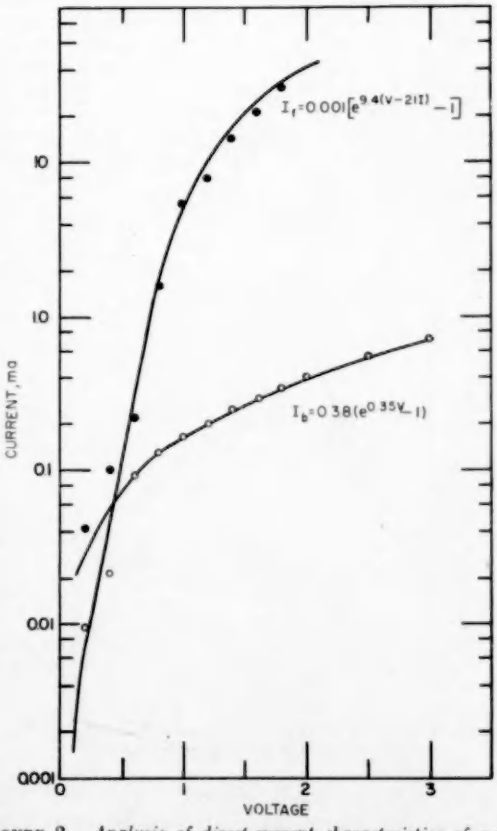

FIGURE 2. *Analysis of direct-current characteristics of point contact titanium dioxide rectifier.*

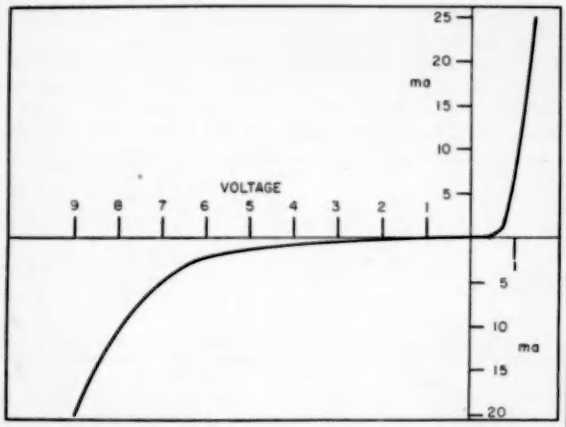

FIGURE 3. *Direct-current characteristics from large area silver counter electrode on titanium dioxide rectifier made by two-step process.*

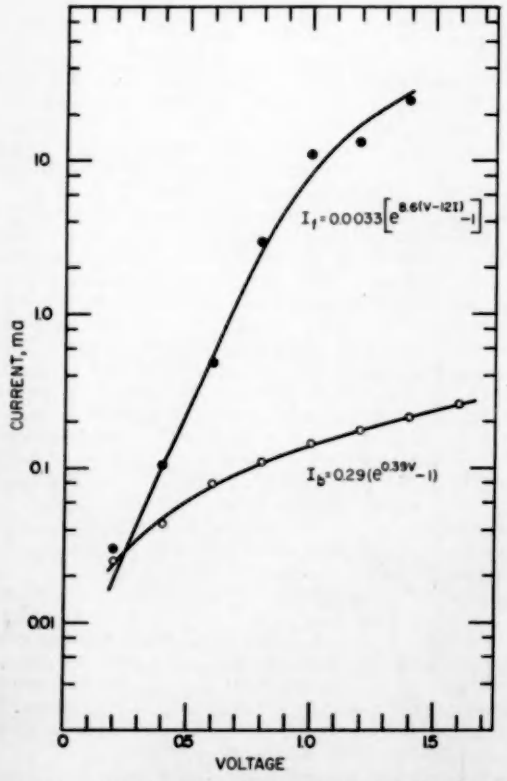

FIGURE 4. *Analysis of direct-current characteristics of large contact area titanium dioxide rectifier.*

800° C, followed by a reduction in hydrogen for about 15 minutes at 500° C for the production of a satisfactory rectifier.

However, some undesirable features of the units formed in this way were apparent. The results in general were rather erratic, indicating that in spite of the efforts made to control the conditions of reduction, the precautions were still insufficient. Similarly, a considerable lack of uniformity of the surface on a single sample was frequently noted. Finally, hydrogen is known to be rather soluble in titanium metal [15] and a great embrittlement of the metal results. This made the physical characteristics of the rectifiers rather undesirable for the fabrication of a practical device.

4. Steam Treated Rectifiers

The difficulties encountered in the control of the two-step process, coupled with the highly undesirable embrittlement of the titanium metal by both hydrogen and oxygen, led to a search for other possible reactions to produce the oxide layer. A thermodynamic calculation showed that a reaction of Ti metal with water vapor was possible and that either TiO_2 or Ti_2O_3 were possible products. A series of exploratory studies was made to investigate the feasibility of this procedure. The results are presented in table 2. Coats described as very thin were less than 0.0001 in., very thick, greater than 0.005 in.

From the results of these explorations it was evident that the rather low temperature reactions were producing in one step an oxide layer whose physical properties were satisfactory and which was already a semiconductor with a conductivity in the desired range. Similarly, tests for rectification showed that quite satisfactory rectifiers were obtained from these units. A second series of samples was made at 600° and 650° C for times ranging from 10 to 240 minutes. These samples were weighed before and after treatment to study the oxygen gain. While considerable scattering was found in the results for these rather short times, just as in the oxidation treatment, it seems that the results correspond roughly to a linear increase in $\Delta W/W$ with time up to about 3½ hours, the constants being 7×10^{-3}/hr for 600° C and 1×10^{-2}/hr for 650° C. The film thickness was also found to increase more or less linearly with time up to about 12μ, beyond which no reliable measurements could be made, probably because of flaking and chipping off of the oxide.

Studies were made of the rectification in these samples, using a silver-plated counter electrode and with an 0.08-cm² copper backing plate. Considerable rectification was found in all cases, although the reverse resistance was low in the short-time samples. Because it was apparent that the ability to withstand voltage in the reverse direction was the dominant factor, the breakdown voltage in the reverse direction was investigated, using the 0.08 cm² electrode area.

The breakdown voltages measured were quite erratic but show a rough dependence on the square root of the forming time up to a maximum of about 25 volts at 600° C and 16 volts at 650° C. The

TABLE 2. *Properties of titanium oxide film on steamed samples*

Temperature °C	Time: 10 min	15 min	20 min	40 min	1 hr	2 hr	3 hr
650					Dark-grey, very thin, tightly bound coat. Good conductivity.	Dark-blue grey coat, fairly thin, tightly bound to metal. Good conductivity.	Dark-grey, medium thin coat, tightly bound to metal. Good conductivity.
700					Grey, medium thin coat, chipped from the surface in sections. Fair conductivity. Sample badly warped.	Blue-grey, medium thin coat, chipped in spots. Fair conductivity. Sample warped.	Grey, medium thin coat, tightly bound. Fair conductivity.
800			Light-grey, thin coat, tightly bound. Fair conductivity.	Light-grey, thick, glassy coat, tightly bound to metal. Low conductivity. Sample slightly warped.	Light-grey layer, very thick, glassy, tightly bound to metal. Low conductivity. Sample badly warped.		
900	Light brownish grey layer, very thick, loosely bound to surface. Very low conductivity. Sample slightly warped.	Light brownish grey layer, very thick, loosely bound to metal. Very low conductivity. Sample warped.	Very thick layer resembling that of pure ceramic, loosely bound to metal. Good insulator. Sample warped.				

constant A in an expression $V=A\sqrt{t}$ has the value of 1.2 volts/min$^{\frac{1}{2}}$ for the 600° C run and 1.1 volts/min$^{\frac{1}{2}}$ for the 650° C series, with V in volts and t in minutes.

These measurements indicate that a forming treatment of about 3 hours in steam at 1 atmosphere and a temperature of 600° C produces a satisfactory rectifier.

The d-c properties of such a unit are shown in figures 5 and 6. The solid lines in figure 6 are drawn for the equations $I_f=0.018\ (e^{4.08\ V}-1)$ and $I_b=0.12\ (e^{0.47\ V}-1)$ for I in milliamperes and V in volts. An analysis of the results, as done for figure 2, shows a spreading resistance of 10Ω, indicating that the oxide layer produced in this way is almost identical with that formed in the two-step process.

A feature of great practical importance is the behavior of the rectifiers at elevated temperatures. The d-c characteristics at various temperatures were studied on a sample steam-treated for 3 hours at 600° C with silver counter electrodes. The results are shown in figure 7. It will be observed that the performance is actually improved by operation at temperatures up to about 140° C, since the forward current is increased while the reverse current is somewhat reduced. Rectification is still observed at 200° C, but the unit is damaged irreversibly by this treatment, the forward current being considerably reduced. An analysis of the data of figure 7 shows

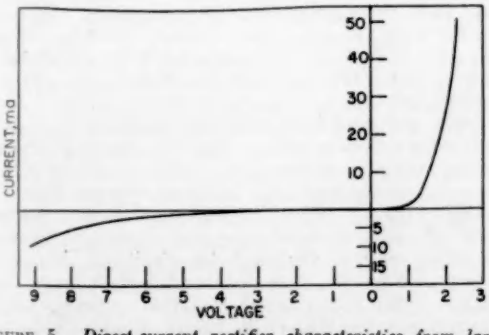

FIGURE 5. *Direct-current rectifier characteristics from large area silver counter electrode on titanium dioxide rectifier made by one-step process.*
Steam treated 3 hr, 20 min at 600° C, 0.08 cm² contact area, Ag plated electrode.

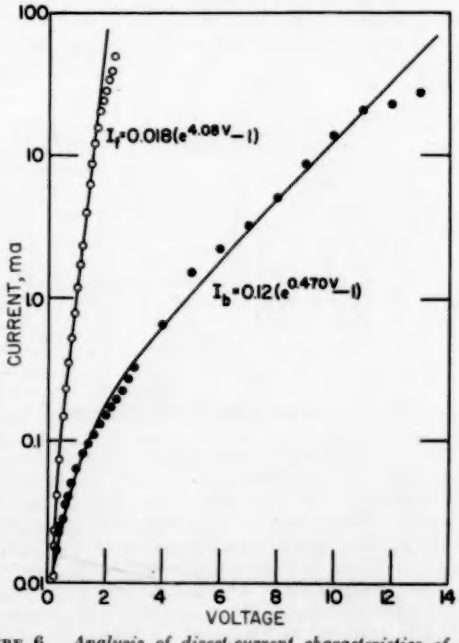

FIGURE 6. *Analysis of direct-current characteristics of large contact area titanium dioxide rectifier from one-step process.*
Steam treated 3 hr, 20 min at 600° C, 0.08 cm² contact area, Ag plated electrode

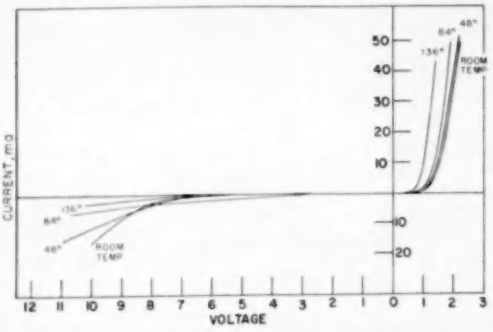

FIGURE 7. *Direct-current titanium dioxide rectifier characteristics at elevated temperature.*

Steam treated at 600° C for 3 hr, 20 min, 0.08-cm² contact area, Ag plated electrode.

that A, r, and α in eq 1 and 2 are a function of temperature for both forward and reverse currents. The values for these constants (for voltages ≥ 0.5 v) at the various temperatures are given in table 3. The effect of the thermal treatment on the barrier is clearly illustrated by the behavior of r. For temperatures up to 136° C, r in general is reduced presumably by the increase in number of charge carriers in the semiconducting layer. There is a sudden increase in r by an order of magnitude near 160° C and a further increase at 200° C probably brought about by a partial reoxidation of the semiconductor layer.

Detailed life studies have not yet been performed on the rectifiers, but one unit was maintained at 85° C with 10 volts applied in the reverse direction for a period of 28 days with an increase in current only from 1.65 to 3.1 ma.

TABLE 3. *Direct-current characteristics of samples measured at various temperatures*

$I_f = A_f(e^{\alpha_f(V-I_f r)}-1)$; $I_b = A_b(e^{\alpha_b V}-1)$

Temperature	α_f	A_f	r	α_b	A_b
°C	v^{-1}	ma	Ohms	v^{-1}	ma
25	6.42	0.001	11.8	0.793	0.009
48	7.71	.0003	13.3	.286	.019
84	8.82	.00037	11.7	.90	.03
136	12.0	.00012	9.0	.144	.69
160	7.12	.0031	95.0	.300	1.22
200	9.05	.0016	115.0	.254	.707

5. Counter Electrode Effects

While the current theories of rectification [4 and 5] suggest that the constant A_f in eq 1 is related to $e^{(e/kT)\phi_0}$, where ϕ_0 is the work function of the contact metal, this is not clearly observed in practice, although A_f does depend on the nature of the counter electrode. Such a dependance has also been observed in the titanium dioxide rectifiers. A series of measurements has been made on a duplicate set of samples treated in steam for 3 hours at 600° C. The counter electrodes were electrodeposited for 30 seconds using a-c deposition, and the samples were

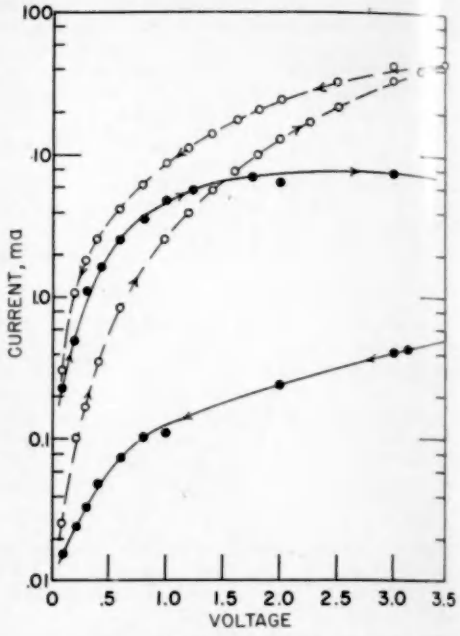

FIGURE 8. *Direct-current titanium dioxide rectifier characteristics for zinc counter electrode.*

Forward ○; reverse ●

then measured with 0.08-cm² copper contact plate. The counter electrode metals were Ag, Au, Sb, Cu, Ni, Zn, and Cd. Rectification is observed in all cases, but some rather striking differences are noted in the characteristics. The metals fall naturally into three groups: those metals low on the electromotive series and hence not readily oxidizable, for example, Ag, Au, and Sb; those forming n-type semiconducting oxides fairly readily, for example, Zn and Cd; and those metals forming p-type semiconducting oxides fairly readily, for example, Cu and Ni. The observed rectifier characteristics also fall into three groups. The inert metals give rectifiers with reasonably similar properties, although the Sb gives a somewhat smaller reverse current than the Au or Ag. Some hysteresis effects were noticed with these electrodes, but they are not conspicuous.

For a zinc counter electrode a striking change in properties was observed. The d-c forward current shown in figure 8 increases rather slowly with increasing voltage, although reaching normal values at about 3.0 volts. With decreasing voltages the forward current is noticeably greater than with increasing voltages, and for very low voltages is appreciably greater than that observed for the inert electrodes. The behavior of the d-c reverse current shown for low voltages in figure 8 and for higher voltages in figure 9 is even more striking. For voltages less than 1.5, the reverse current is considerably larger than the forward current for the same

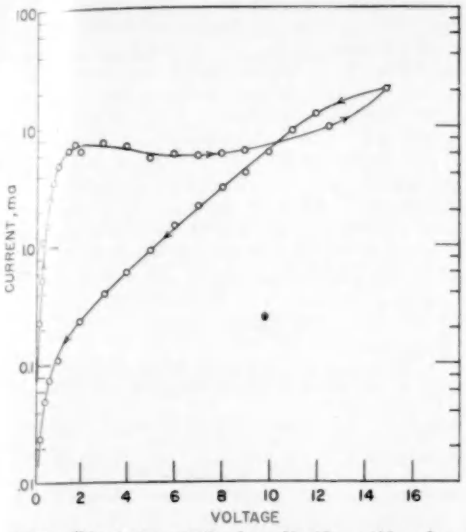

FIGURE 9. *Direct-current titanium dioxide rectifier characteristics for zinc counter electrode for large reverse voltages.*

voltage. The reverse current reaches a maximum near 2 volts and then remains relatively constant to about 10 volts, when it commences to increase slowly. As the voltage is lowered, the current at first is somewhat greater than with increasing voltages, but for voltages below about 10, the current is very much less than observed for increasing voltage. If a 60 c/s a-c test is made, and the characteristics are displayed on an oscilloscope, as described in the reference in footnote 2, the current-voltage characteristics show nonlinearity but very poor rectification. It is apparent that the blocking layer found in the d-c measurements is a polarization effect and, from some observations of the time of formation of the layer, which is of the order of seconds, can only be due to an ionic process.

With a Cd counter electrode an unusually large forward current was observed, the constants being A_f=0.049 ma and α_f=15.3 volts^{-1}; a somewhat larger than normal reverse current A_b=6.3 ma and α_b=0.19 volts^{-1}, but the hysteresis effects were small.

For the metals forming *p*-type oxides a somewhat different situation was observed. With copper a better than normal forward current was found, particularly at low voltages, and a small reverse current was also obtained. The effects were even more striking with a nickel counter electrode. Again, an increased forward current at low voltages was found and the reverse current was notably small. These d-c measurements show rather pronounced hysteresis effects, particularly in the reverse direction. When the rectification was observed on 60 c/s a-c test, the forward current behaves in a normal manner, but the reverse current is small only for low voltages and increases suddenly at about 4 volts reverse. This again indicates that the d-c properties are influenced by a slow polarization process.

TABLE 4. *Direct-current rectifier characteristics for various counter electrodes*

Metal	ϕ_0	A_f	α_f	A_b	α_b	
	ev	ma	v^{-1}	ma	v^{-1}	
Au	4.78	0.20	3.8	20	0.05	
Ag	4.6	.38	2.7	5.9	.10	
Sb	4.6	.40	3.2	0.04	.40	
Ni	5.0	.042	5.1	.032	.49	Increasing voltage.
Ni	5.0	.0059	13.8	.035	.84	Decreasing voltage.
Cu	4.1	.31	3.9	.22	.50	Increasing voltage.
Cu	.....	.....	.....	.31	.28	Decreasing voltage.
Cd	4.1	.049	15.3	6.3	.19	.....
Zn	3.3	2.0	1.3	.....	.....	Increasing voltage.
Ti	4.18	.....	.....	.....	.....	.....

It should be mentioned that no permanent "electroforming" effects have thus far been noted, although they would be anticipated in view of these counter electrode effects. The data for these d-c characteristics are summarized in table 4. The photoelectric work functions of the various metals are included [18]. The value for Ti is that given by Rentschler and Henry [19.]

It is apparent that the constant A is not directly related to $\exp(e\phi_0/kT)$, but that the counter electrode influences the properties of the unit in some other fashion. It should be stressed that too great reliance should not be placed on the individual values of A and α in table 4 because a considerable variation between samples has been noticed. Compare, for example, the data for a silver counter electrode in tables 3 and 4 and figure 4. The general properties mentioned have, however, been observed in all specimens tested.

6. Discussion

It seems evident that the rectifier described here has considerable possibilities, even though it has not yet been investigated in great detail. The ease of preparation of the units, particularly by the steam process, and the quality of their performance at such an early stage in their development are very encouraging, although a great deal of study will be needed to assess their practicality. Similarly, a much more intensive study of many of the properties will be needed to obtain a clear picture of the nature of the rectification process. The information obtained thus far does, however, give some grounds for preliminary speculation.

The nature and location of the asymmetric potential barrier is of great interest in any interpretation of the rectification mechanism. In all rectifier types thus far discovered the direction of easy flow of charge carriers over the barrier is from the semiconductor to the metal electrode. Because TiO_2 is an *n*-type semiconductor, the charge carriers are electrons; and since we have observed the forward direction to be that with the counter electrode positive, we must conclude that the barrier layer is located between the counter electrode and the semiconductor. This is suggested also by the observation of the counter electrode effects; if

the barrier were located between the oxide and the titanium base, the counter electrode would not be expected to have much influence on the rectifier characteristics.

It is possible that the barrier is a "physical" barrier of the Schottky type, but extensive measurements, particularly of the a-c characteristics, will be required to establish agreement with the predictions of the Schottky theory [2, 5, 6]. Such measurements are in progress. A "chemical" barrier of the Mott type [4] seems less likely to be present. Although it might be assumed that a film of nearly stoichiometric TiO_2 exists on the free surface during the steam treatment, the opposite situation would be normally expected in the reduction of the oxide film by hydrogen, and the free surface presumably would be the most strongly reduced. Another mechanism of rectification considered by Fan [20] may be possible in this situation. Fan showed that rectification was possible if a semiconducting film separates two metals with different work functions. This is supported by the striking behavior noted with the Zn counter electrode, since Zn was the only metal investigated whose work function is clearly lower than that reported for Ti. On the other hand, no direct dependence on the value of the work function for metals with $\phi_0 \geq 4.2$ is indicated in the values of the constants in table 4.

Possibly even more suggestive is the fact that unusual properties were noted with counter electrodes that might be rather reactive chemically. The observed excellent d-c characteristics for the metals forming *p*-type oxides might imply that the formation of a *p-n* junction layer was aiding the rectification; conversely, a Zn counter electrode which forms an *n*-type oxide impaired the rectification. These effects, of course, would not explain the good rectification observed with supposedly inert counter electrodes unless it was postulated that compound formation took place in the surface layer in all cases. Even this assumption would, however, not explain the "normal" behavior of the Cd counter electrode which is known to form an *n*-type oxide [21]. It seems likely, in fact, that several mechanisms for rectification are operating in the combination, and evidently a great deal of study will be needed to assess the relative importance of the various processes.

It would seem, in view of these counter electrode effects in which a transient barrier is formed in each half-cycle, that it should be possible to improve the existing units by the formation of a similar barrier of a permanent type. This possibility is being investigated, with some indications of success.

The particular feature of these rectifiers of greatest practical interest is probably the behavior at high temperatures. The difficulties encountered in most units currently available [22] have stressed the utility, particularly for military applications, of a power unit that could be operated at a temperature of about 150° C. The titania rectifiers apparently are quite effective in this range of temperature, and so merit serious consideration as power rectifiers.

7. References

[1] L. O. Grondahl, Phys. Rev. **27,** 813 (1926).
[2] e. g., H. K. Henisch, Metal rectifiers (Clarendon Press, Oxford, 1949).
[3] e. g., H. C. Torrey and C. A. Whitmer, Crystal rectifiers (McGraw-Hill Book Co., Inc., New York, N. Y., 1948).
[4] N. F. Mott, Proc. Roy. Soc. [A] **171,** 27 (1939).
[5] W. Schottky, Z. Physik **113,** 367 (1939).
[6] W. Schottky and F. Waibel, Naturwissenschaften **20,** 297 (1932).
[7] J. W. Hickman and E. A. Gulbransen, J. Anal. Chem. **20,** 158 (1948).
[8] W. Meyer, Physik. Z. **36,** 749 (1935).
[9] W. Meyer and H. Neldel, Physik. Z. **38,** 1014 (1937).
[10] M. Earle, Phys. Rev. **61,** 56 (1942).
[11] A. von Hippel, R. G. Breckenridge, A. P. de Bretteville, Jr., and J. M. Brownlow, N. D. R. C. Rept. 540, Lab. for Insulation Research M. I. T., Oct. 1945.
[12] R. G. Breckenridge and W. R. Hosler, unpublished data.
[13] Tech. Information on Ti Metal, Remington Arms Co., Bridgeport, Conn. (1949).
[14] W. A. Alexander and L. M. Pigeon, Canadian J. Research **B28,** 60 (1950).
[15] E. A. Gulbransen and K. F. Andrews, Trans. A. I. M. E. **185,** 741 (1949).
[16] M. H. Davies and C. E. Birchenall, Trans. A. I. M. E., J. Metals, 877 (1951).
[17] N. Nasu, Sci. Repts. Tôhoku Imp. Univ. **25,** 510 (1936).
[18] A. L. Hughes and L. A. duBridge, Photoelectric phenomena, McGraw-Hill Book Co., Inc., New York, N. Y., (1932).
[19] H. C. Rentschler and D. E. Henry, Trans. Electrochem. Soc. **87,** 289 (1945).
[20] H. Y. Fan, Phys. Rev. **74,** 1505 (1948).
[21] H. H. v. Baumbach and W. Wagner, Z. Physik, Chem. **B22,** 208 (1933).
[22] W. F. Bonner and F. J. Oliver, Elect. Mfg. **48,** No. 4, 128 (1951).

WASHINGTON, May 26, 1952.

Journal of Research of the National Bureau of Standards Vol. 49, No. 2, August 1952 Research Paper 2345

Infrared Spectra of Noble Gases (12000 to 19000 A)[1]

Curtis J. Humphreys and Henry J. Kostkowski

The first spectra of helium, neon, argon, krypton, and xenon, excited by discharges in Geissler tubes, operated by direct connection to a transformer, have been explored in the infrared (12000 to 19000 A). A high-resolution, automatically recording, infrared spectrometer, employing a 15000-lines-per-inch grating and lead-sulfide photoconducting detector, was used as the dispersing instrument. A new set of wavelength values is reported for all these spectra. New data include 18 previously unreported lines of neon and 36 of krypton, all of which have been classified. The descriptions of the spectra of argon, krypton, and xenon represent essentially a repetition of the observations of Sittner and Peck. Several previously missing classifications are supplied, also a few amended interpretations. The analysis of these spectra may be regarded as complete. Use of selected lines as wavelength standards is suggested.

1. Introduction

The essentially complete character of both the description and interpretation of the photographed spectra of the noble atmospheric gases makes it apparent that any reopening of the subject can be justified only on the basis of the availability of new sources of information, such as a new technique of observation permitting an extension of the observations into a previously unexplored region, leading to significant additions to the experimental material. Such a technique is the utilization of lead-sulfide photoconducting detectors in combination with high-resolution gratings for radiometric observation. The lead-sulfide cell extends the range of such high-resolution observations beyond the photographic limit to the limit of its sensitivity near 30000 A, and because it is also sensitive to the visible and ultraviolet as far as 3500 A, at least, use of higher order standard lines for comparison is possible.

Three of these spectra, argon, krypton, and xenon, have been observed by this radiometric technique by Sittner and Peck, whose reported observations and analysis [1][2] cover essentially the same region as those herein presented. These excellent observations appear to have been essentially complete, and the overwhelming majority of the classifications are correct. In the intervening period, however, sufficient new information has been accumulated to make it appear justifiable to prepare a new publication, which should complete these analyses as far as any reasonable effort will permit. Discussion of the specific points of difference between this analysis and that of Sittner and Peck, together with extensions to the analyses as reported in other earlier publications, will be included in the separate sections dealing with the respective spectra. In brief, these consist of inclusion of He I and Ne I, presentation of previously unreported data consisting mainly of 18 new lines in Ne I and 36 in Kr I, interpretation of nearly all reproducible previously unclassified lines, and amended classifications in a few instances.

Observations of Kr I and A I, obtained with a prism spectrometer, equipped with a glass prism and thermocouple detector were reported by Humphreys and Plyler [2]. These observations covered the same spectral region in which the data herein reported were obtained, but, because of well-known limitations affecting the precision of spectral data obtained by prism spectrometers with thermal detectors, may be considered as entirely superseded by the present work. The earlier paper may be referred to for a fairly extensive list of references on the first spectra of the noble gases, which will not be repeated in full here. It also reported two new levels, designated 4U and 4W, in Kr I, computed from photographic data by Meggers [3] but requiring confirmation by radiometric observation of infrared lines, arising from combinations of the same levels. The first, or neutral-atom, spectra of all the noble gases are very rich in infrared lines. Considerable portions of these infrared spectra lie in the photographically accessible region, and have been the subject of exhaustive investigations. Reference is made to a few of the more recent publications, which, in addition to those already mentioned, will serve as a background and introduction to the current work, and provide cross references to earlier work as required. A paper entitled "The Infrared Spectra of Neon, Argon, and Krypton", published by Meggers and Humphreys [4] in 1933 brought the analysis of these spectra essentially to completion. A separate paper by Humphreys and Meggers [5], and of similar scope, appearing a few months earlier, brought Xe I up to date. Shortly after this, plates incorporating new photosensitizing dyes, made available by the Eastman Kodak Co. [6], permitted photographic observation as far as 13000 A in favorable instances. With these new plates Meggers [3] reobserved all the noble gas spectra to the photographic limit and interpreted nearly all the new lines. In the intervening years no further extension of the range of photographic sensitivity has been accomplished, and no further observations of noble-gas spectra were made up to the time of the radiometric investigations at the National Bureau of Standards [2] and at Northwestern University [1].

2. Energy Levels of the Noble Gases

Although the analysis of the spectra of the noble gases may be regarded as essentially complete, in the sense that nearly all the levels predictable from the

[1] Presented, in part, at the meeting of the Optical Society of America, Buffalo, N. Y., Oct. 1949.
[2] Figures in brackets indicate the literature references at the end of this paper.

electron configurations have been found, and that, in most instances, long series have permitted highly precise calculation of absolute term values, these spectra are somewhat unusual in their structure in that they do not permit arrangement into regular multiplets with any reasonable conformity to rules regarding intervals or intensities. Paschen [7] adopted a special notation in reporting his analysis of Ne I. This notation has been retained in all subsequent publications on these spectra; evidently because it is not possible to describe the levels according to the currently accepted notation, which is actually meaningful only when vector coupling of *LS*-type is present. This inability to identify multiplets in rare-gas spectra points to the probable existence of a different type of coupling. This has generally been supposed to resemble the *jj*-case but evidence, principally from Zeeman effect, indicates that extreme *jj*-coupling is not realized, and that an intermediate type prevails. Considerable light was shed on the problem by a theoretical paper by Racah [8], who discussed an intermediate coupling scheme, designated *jl*, and discussed the conditions for its existence. It was pointed out that, whereas *ls*-coupling occurs when the spin-orbit interaction is weak compared to the electrostatic, and *jj*-coupling occurs when the electrostatic interaction is weaker, a third possibility, the *jl*-case, may be realized, according to which the electrostatic interaction is weak compared to the spin-orbit interaction of the parent ion, but is strong compared to the spin coupling of the external electron. The vectorial representation of this case is to combine the total angular moment j of the parent ion with the orbital moment l of the external electron to form a resultant K, known as the intermediate quantum number. Finally, K is combined with the spin of this electron to obtain the resultant J, which has the usual significance, namely, total angular moment of the resultant configuration.

Racah suggested a special notation for representing levels originating under the condition of *jl*-coupling. This notation has been selected for the appropriate sections, pertaining to noble-gas spectra, of "Atomic Energy Levels" [10]. This innovation has been followed in tabulating the descriptions of spectra listed in this paper, except for He I, which is described in conventional notation. The Racah notation has been abbreviated by omitting the description of the parent ion, $mp^5(^2\mathrm{P}^\circ_{1\frac{1}{2}})$ or $(^2\mathrm{P}^\circ_{0\frac{1}{2}})$, the omission or insertion of the prime with the letter indicating the running electron being sufficient to distinguish between the two respective possible cases. This usage is also borrowed from [10], which not only employes the prime in the manner indicated, but also supplies the complete parent ion description. Descriptions of the transitions, according to the Paschen notation, are also included along with the Racah notation in parallel columns in the tables pertaining to argon, krypton, and xenon. This is intended to permit ready comparison with earlier published analyses and to provide a basis for translating the old notation into the new. It is to be noted that every symbol in the new notation is physically significant. The number within the bracket is Racah's K or intermediate quantum number obtained by vectorial addition of the j-value of the parent ion to the l-value of the external electron. In the instance of the noble-gas configurations, where the parent ion has j-value$=1\frac{1}{2}$ (unprimed case), there can be a maximum of four K-values; and where the parent ion has j-value$=0\frac{1}{2}$ (primed case), no more than two values of K appear. For each K-value, by addition or subtraction of the spin moment S of the external electron, always$=0\frac{1}{2}$, two possible j-values appear for the resultant vector sum. We thus obtain a pair of levels for each K. A maximum total of twelve levels is possible for any rare-gas configuration where the external electron has l-value 2 or greater. As might be expected, this is the same total number and the same set of j-values that would be obtained with *LS*-coupling. Table 1 illustrates the development of the set of levels and appropriate quantum numbers associated with the binding of the *f*-electron in the configuration $mp^5\,nf$.

TABLE 1. *Development of notation for jl coupling, according to Racah, illustrated by f-type levels of noble gases*

Ion configuration	j_c	K			J
$p^5(^2\mathrm{P}^\circ)$	$1\frac{1}{2}$	$+l=3$	$[4\frac{1}{2}]$	$+s=0\frac{1}{2}$	5, 4
			$[3\frac{1}{2}]$		4, 3
			$[2\frac{1}{2}]$		3, 2
			$[1\frac{1}{2}]$		2, 1
$p^5(^2\mathrm{P}^\circ)$	$0\frac{1}{2}$	$+l=3$	$[3\frac{1}{2}]$	$+s=0\frac{1}{2}$	4, 3
			$[2\frac{1}{2}]$		3, 2

The pair structure resulting from the *jl*-coupling scheme was pointed out by Shortley and Fried [9]. This structure is quite apparent in the level schemes of the four noble-gas-atomic spectra, Ne I, A I, Kr I, and Xe I, up to and including the levels based on the configurations $p^5\,nd$. In the instance of the pair arrays from $p^5\,nf$ these features are much less obvious. They are developed in three out of four possible cases in Xe I, and show diminishing separations for the gases of smaller atomic number, until in Ne I these *f*-type pairs of levels merge into single levels even with the high resolving power now employed in presently available techniques. Lack of knowledge regarding these *f*-type levels has constituted the most conspicuous gap in the analysis of these spectra, and a considerable part of the information supplied by this investigation is concerned with these structures. Details for the respective spectra are given under the appropriate headings.

The numerical values of the levels used in obtaining the calculated wave numbers of emission lines that appear in the tables that follow, pertaining to A I, Kr I, and Xe I are those that are currently

appearing in [10]. The levels reported in that publication for Ne I, A I, Kr I and Xe I, are taken from unpublished manuscript by Edlén. These values represent a revision, together with reassignments in a few instances, of the tables of levels listed in two publications already quoted [4, 5], and are based on the same data. A small number of missing levels, required to complete the arrays and predicted from series calculations, have been confirmed by observed transitions.

3. Experiments

The high-resolution grating spectrometer used for these observations has been described briefly in an earlier publication [11]. It is of conventional design incorporating a 15000-lines-per-inch Johns Hopkins grating, 1-meter focus off-axis paraboloidal collimating mirror, ground and figured in the Optical Instrument Shop of the National Bureau of Standards. The cone-bearing, grating-mounting, worm-gear assembly, and simultaneously movable bilateral slits were constructed in the Instrument Shops of the Department of Physics, University of Michigan. The slits conformed essentially to the design of Roemer and Oetjen [12]. Figure 1 shows the instrument with the cover and baffles removed. The amplifier shown on the table beneath the spectrometer was constructed by W. R. Wilson, and is of the same design as that used for similar purposes at Northwestern University [13]. The electronic components visible in the picture also serve to establish the scale of relative sizes of parts. It may be noted that the mirrors are 7 inches in diameter, and that the grating is ruled on a 9-inch blank, with segments cut off to adapt it to the ruling machine.

The data reported were obtained in most instances by using Geissler tubes as radiation sources. In instances where higher-order comparison standards from the same spectrum were employed, the source was simply imaged on the entrance slit by means of a quartz lens. Where lines of a different spectrum were used as standards an arrangement similar to that illustrated in the paper by the senior author on Ca I [14] was employed. In this system the quartz lens was left in position and a concave mirror was also set up on the optic axis in such a position that it formed an image of the source in the position of the conjugate focus of the lens with respect to the slit. When the comparison source included a tube of fairly large bore, it was set up with its axis coincident with the image of the first source, so that both could be imaged on the slit simultaneously. In other cases, the comparison source was moved into or out of the described position, but the comparison lines were always introduced under the condition of continuous scanning.

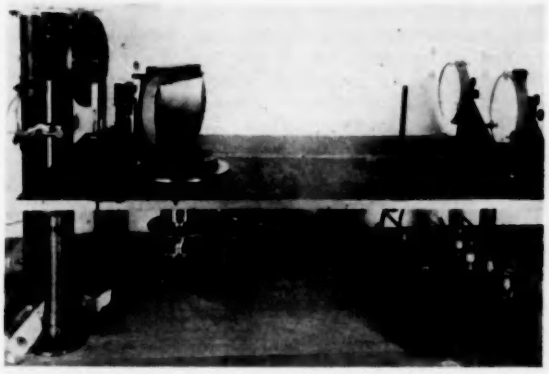

FIGURE 1. *National Bureau of Standards infrared grating spectrometer with the cover and baffles removed.*

4. Characteristic Features of Noble Gas Spectra

4.1. Helium

The observation of the helium spectrum was for the purpose of improving the wavelength data, because there was no reasonable prospect of finding new level combinations of appreciable intensity in this thoroughly analyzed spectrum. The results are given in table 2 and comprise data on six lines. The first two lines listed, $3\,^3D - 5\,^3F°$, and $3\,^1D - 5\,^1F°$ were the lines of greatest wavelength reported by Meggers [3] and were evidently at the limit of photographic sensitivity. The wavelengths of the others are known only from the early radiometric measurements of Paschen [15]. Because of a radiometric application utilizing some of these lines, special care was taken to evaluate the relative intensities precisely. It is believed that the apparent relative in-

TABLE 2. *Description of* He I *in the infrared region*

Observed wavelength in air	Observed intensity	Term combination	Wave number		Difference (calc.−obs.)
			Observed	Calculated	
A			cm^{-1}	cm^{-1}	
12784.79	10	$3d\,^3D - 5f\,^3F°$	7819.66	7819.89	0.23
12790.27	1	$3d\,^1D - 5f\,^1F°$	7816.31	7815.09	−1.22
17003.11	20	$^a3p\,^3P° - 4d\,^3D$	5879.67	5879.73	0.06
18685.12	70	$3d\,^3D - 4f\,^3F°$	5350.39	5350.71	.32
18697.00	10	$3d\,^1D - 4f\,^1F°$	5346.99	5348.02	1.03
20580.9	5000	$2s\,^1S - 2p\,^1P°$	4857.55	4857.45	−0.10

[a] Triple level unresolved in these experiments.

tensities are correctly evaluated, bearing in mind that no correction has been made for spectral sensitivity of the detector, or effect of the properties of the grating, on apparent spectral distribution of energy. The calculated values of wave numbers are based on the values of the levels quoted in [10]. The wavelengths of the various lines of the fundamental series have been evaluated by bracketing them between fairly close third-order neon lines. There is no possibility of an experimental error nearly as large as the difference between observed and calculated wave numbers indicated for the singlets, particularly since the relative precision of the determination of the singlet and triplet transitions for a given series member is high. It is suggested, therefore, that reevaluation of the first two members of the *f*-series is in order. The following values would bring the levels into agreement with the reported wavelength measurements:

$4f\ ^1\mathrm{F}^\circ$, *191446.21*

$4f\ ^3\mathrm{F}^\circ$, *191446.29*

$5f\ ^1\mathrm{F}^\circ$, *193915.53*

$5f\ ^3\mathrm{F}^\circ$, *193915.56*

The indicated extremely close proximity of the singlet and triplet F-terms of given order number is in accord with their relative positions for the higher series members. The difference between the observed and calculated wave numbers for $2s\ ^1\mathrm{S} - 2p\ ^1\mathrm{P}^\circ$, namely, 0.10 cm $^{-1}$, is close to the expected experimental error. The line at 17003 A arises from a transition between multiple levels, unresolved by available techniques. No revision of accepted level values based on the measured wavelengths of these two lines appears to be required.

4.2. Neon

The observations on Ne I have been confined to the limited wavelength region, 18035 to 18625 A, in which the electron transitions of the type $3d - 4f$ occur. The only previous data pertaining to this region consist of a few lines reported by Hardy [16] that could not be resolved or measured by methods then available with sufficient precision to improve the existing set of level values. The new data are listed in table 3 and comprise 18 lines. A reproduction of a typical record is shown in figure 2. The wavelengths have been evaluated by interpolation between third-order neon lines included in the well-known group of red neon lines, which are accepted international standards. The calculated wave numbers are based on a set of adjusted values of *f*-levels determined from these observations rather than upon the values currently published [10]. These revised *f*-levels are compared with the current set in table 4. The bracketed values quoted are, of course, predictions, which are now confirmed by the present set of observations.

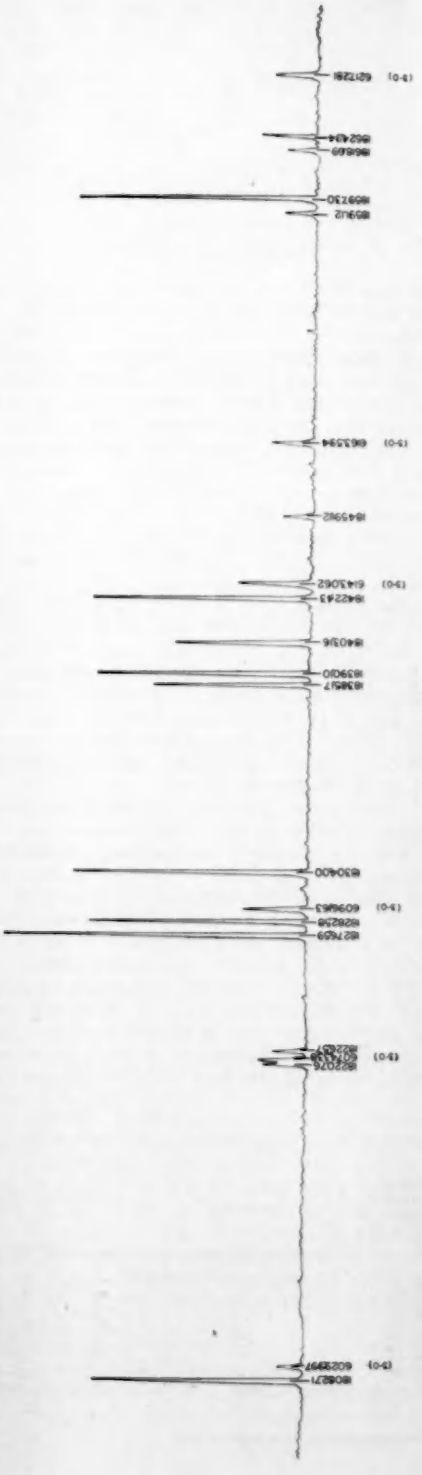

FIGURE 2. *Reproduction of tracing of chart record of infrared spectrum of neon, 18000 to 18700 A, including third-order standards.*

TABLE 3. *Newly observed and classified lines of* Ne I

Observed wavelength in air	Observed intensity	Term combination	Wave number		Difference (calc.—obs.)
			Observed	Calculated	
A			cm^{-1}	cm^{-1}	
18035.49	22	$3d\ [0\frac{1}{2}]^0_1 - 4f\ [1\frac{1}{2}]_{1,2}$	5543.11	5543.11	0.00
18082.71	130	$3d\ [0\frac{1}{2}]^0_1 - 4f\ [1\frac{1}{2}]_{1,2}$	5528.63	5528.57	−.06
18220.76	15	$3d\ [3\frac{1}{2}]^0_2 - 4f\ [3\frac{1}{2}]_{3,4}$	5486.74	5486.75	.01
18226.57	11	$3d\ [3\frac{1}{2}]^0_3 - 4f\ [3\frac{1}{2}]_{3,4}$	5485.00	5484.98	−.02
18276.59	260	$3d\ [3\frac{1}{2}]^0_3 - 4f\ [4\frac{1}{2}]_{4,5}$	5469.98	5469.97	−.01
18282.58	200	$3d\ [3\frac{1}{2}]^0_3 - 4f\ [4\frac{1}{2}]_{4,5}$	5468.19	5468.20	.01
18304.00	140	$3d\ [1\frac{1}{2}]^0_2 - 4f\ [2\frac{1}{2}]_{2,3}$	5461.79	5461.81	.02
18359.21	6	$3d\ [1\frac{1}{2}]^0_2 - 4f\ [1\frac{1}{2}]_{1,2}$	5445.37	5445.48	.11
18385.17	160	$3d'[2\frac{1}{2}]^0_2 - 4f'[3\frac{1}{2}]_{3,4}$	5437.68	5437.71	.03
18390.10	180	$3d'[2\frac{1}{2}]^0_3 - 4f'[3\frac{1}{2}]_{3,4}$	5436.22	5436.19	−.03
18403.16	65	$3d\ [1\frac{1}{2}]^0_1 - 4f\ [2\frac{1}{2}]_{2,3}$	5432.36	5432.45	.09
18422.43	110	$3d'[1\frac{1}{2}]^0_2 - 4f'[2\frac{1}{2}]_{2,3}$	5426.68	5426.68	.00
18458.58	10	$3d\ [1\frac{1}{2}]^0_1 - 4f\ [1\frac{1}{2}]_{1,2}$	5416.05	5416.12	.07
18475.79	3	$3d'[1\frac{1}{2}]^0_1 - 4f'[2\frac{1}{2}]_{2,3}$	5411.01	5410.98	−.03
18591.12	25	$3d\ [2\frac{1}{2}]^0_2 - 4f\ [3\frac{1}{2}]_{3,4}$	5377.44	5377.44	.00
18597.30	120	$3d\ [2\frac{1}{2}]^0_3 - 4f\ [3\frac{1}{2}]_{3,4}$	5375.65	5375.65	.00
18618.69	15	$3d\ [2\frac{1}{2}]^0_2 - 4f\ [2\frac{1}{2}]_{2,3}$	5369.48	5369.41	−.07
18624.94	22	$3d\ [2\frac{1}{2}]^0_3 - 4f\ [2\frac{1}{2}]_{2,3}$	5367.67	5367.62	−.05

TABLE 4. *Revision of f-type levels in* Ne I

Proposed values	Atomic Energy Levels [10]	Racah notation
167054.70	167054.59	$2p^5(^2P^0_{1\frac{1}{2}})4f\ [1\frac{1}{2}]_{1,2}$
167062.28	[167062.5]	$4f\ [4\frac{1}{2}]_{4,5}$
167071.03	167071.08	$4f\ [2\frac{1}{2}]_{2,3}$
167079.06	[167079.1]	$4f\ [3\frac{1}{2}]_{3,4}$
167848.33		$2p^5(^2P^0_{0\frac{1}{2}})4f'[3\frac{1}{2}]_{3,4}$
167848.62	167848.67	$4f'[2\frac{1}{2}]_{2,3}$

It is to be noted that a total of only six of these *f*-levels have been found, two primed and four unprimed. This represents the complete development of the level system, but with the Racah pairs either coalesced or so close together that they cannot be distinguished in cases where there is a possible combination of both members of a pair with a given *d*-level, producing a close doublet. Such close levels might also be distinguished on the basis of a small difference in numerical value based on determinations from strictly single transitions according to selection rules, but here again the attainable precision appears inadequate for the *f*-levels of Ne I.

4.3. Argon

The observations on A I extend from approximately 12000 to 17000 A, covering essentially the region explored by Sittner and Peck [1], but slightly less extended in the directions of both shorter and longer wavelengths. There appeared to be no advantage in overlapping the region observed photographically by Meggers [3] below about 12000 A where the photographic emulsions were sufficiently sensitive to permit essentially complete recording of the spectrum. The principal reason for reobserving A I was that a considerable number of the lines beginning with 13273 A and lying in the region of greater wavelengths were either left unclassified by Sittner and Peck or had been assigned to transitions that appeared improbable. Part of Sittner and Peck's observations were made with flash tubes. The differences in excitation are responsible for considerable variation in the intensities of some level combinations, when Geissler tube and flash tube excitations are compared. In general, the effect of the flash tube excitation is to increase the intensities of combinations of levels where one or both the levels belong to the family converging to the higher level of the inverted doublet constituting the ion limit, namely, $^2P^0_{\frac{1}{2}}$. A few of the weak lines observed by Sittner and Peck do not appear on our records and, vice versa. We have observed a small number not included in their list. These few weak lines remain unclassified, and there may be some doubt of their origin in A I. Table 5 contains the pertinent information regarding 66 lines included in the current set of observations. All but three of these lines are classified. The wave numbers observed by Sittner and Peck and by Meggers for the overlapping region are listed for comparison. A slight majority of the observed wave numbers show better agreement with the calculated values than those of Sittner and Peck, but the precision of observation is not regarded as being significantly improved. The observations on argon were not expected to give precise evaluations of intensities. The same remark also applies to the sections on krypton and xenon. Because of the

TABLE 5. *Description of* A I *in the infrared region*

Observed wavelength in air, Humphreys and Kostkowski	Observed intensity	Wave number observed			Term combination		Wave number [corrected, Moore 10]
		Humphreys and Kostkowski	Sittner and Peck	Meggers	Paschen notation	Racah notation	
A		cm^{-1}	cm^{-1}	cm^{-1}			
12112.20	300	8253.87	8254.06	8253.81	$2p_5 - 3d'_2$	$4p\,[2\frac{1}{2}]_3 - 3d\,[2\frac{1}{2}]\frac{5}{2}$	8253.81
12139.79	100	8235.11	8235.22	8235.16	$2p_4 - 3s'_1$	$4p'[1\frac{1}{2}]_1 - 3d'[1\frac{1}{2}]\frac{3}{2}$	8235.14
12151.57	15	8227.13	8227.33	8227.32	$3d'_1 - 4W$	$3d\,[2\frac{1}{2}]\frac{3}{2} - 4f'\,[3\frac{1}{2}]_{3,4}$	8227.35
12343.72	150	8099.06	8099.40	8099.30	$2p_8 - 3d'_2$	$4p\,[2\frac{1}{2}]_2 - 3d\,[2\frac{1}{2}]\frac{3}{2}$	8099.29
12356.82	100	8090.48	8090.87	8090.86	$3d_3 - 4Y$	$3d\,[1\frac{1}{2}]\frac{3}{2} - 4f\,[2\frac{1}{2}]_3$	8090.83
12402.88	400	8060.43	8060.44	8060.47	$2p_7 - 3d_2$	$4p\,[1\frac{1}{2}]_1 - 3d\,[1\frac{1}{2}]\frac{1}{2}$	8060.45
12419.39	20	8049.71	8049.95	8049.74	$3d_3 - 4X$	$3d\,[1\frac{1}{2}]\frac{3}{2} - 4f\,[1\frac{1}{2}]_2$	8049.68
12439.19	500	8036.90	8037.02	8036.81	$2p_{10} - 3d_3$	$4p\,[0\frac{1}{2}]_1 - 3d\,[1\frac{1}{2}]\frac{3}{2}$	8036.84
12456.05	400	8026.02	8025.83	8025.98	$2p_8 - 2s_4$	$4p\,[2\frac{1}{2}]_2 - 5s\,[1\frac{1}{2}]\frac{1}{2}$	8025.95
12487.63	700	8005.72	8005.68	8005.71	$2p_9 - 2s_5$	$4p\,[2\frac{1}{2}]_3 - 5s\,[1\frac{1}{2}]\frac{3}{2}$	8005.75
12554.44	5	7963.12	7962.87	7963.43	$2p_9 - 3d''_1$	$4p\,[2\frac{1}{2}]_3 - 3d\,[2\frac{1}{2}]\frac{5}{2}$	7963.25
12596.27	5	7936.68	7936.60	-------	$3d'_1 - 4W$	$3d\,[2\frac{1}{2}]\frac{5}{2} - 4f'\,[3\frac{1}{2}]_{3,4}$	7936.79
12621.82	6	7920.61	7920.09	7920.78	$2p_5 - 2s_2$	$4p\,[0\frac{1}{2}]_0 - 5s'\,[0\frac{1}{2}]\frac{1}{2}$	7920.75
12639.01	2	7909.84	7909.21	-------	$2p_8 - 3d_2$	$4p\,[1\frac{1}{2}]_2 - 3d\,[1\frac{1}{2}]\frac{1}{2}$	7910.15
12651.14	2	7902.26	-------	-------	----------	----------	-------
12702.39	150	7870.37	7870.46	7870.46	$2p_2 - 3s'_1$	$4p'[0\frac{1}{2}]_1 - 3d'[1\frac{1}{2}]\frac{1}{2}$	7870.44
12733.59	75	7851.09	7850.91	7851.22	$2p_8 - 2s_5$	$4p\,[2\frac{1}{2}]_2 - 5s\,[1\frac{1}{2}]\frac{3}{2}$	7851.23
12746.31	40	7843.25	7843.09	7843.38	$2p_4 - 2s_2$	$4p'[0\frac{1}{2}]_1 - 5s'\,[0\frac{1}{2}]\frac{1}{2}$	7843.31
*12802	300	-------	7808.75	7808.73	$2p_8 - 3d''_1$	$4p\,[2\frac{1}{2}]_2 - 3d\,[2\frac{1}{2}]\frac{5}{2}$	7808.73
12912.26	4	7742.45	-------	-------	----------	----------	-------
12933.33	60	7729.84	7729.26	7729.99	$2p_4 - 2s_2$	$4p'[1\frac{1}{2}]_1 - 5s'\,[0\frac{1}{2}]\frac{1}{2}$	7729.91
12956.59	250	7715.96	7715.92	7715.94	$2p_{10} - 3d_3$	$4p\,[0\frac{1}{2}]_1 - 3d\,[0\frac{1}{2}]\frac{1}{2}$	7715.95
13008.47	200	7685.19	7684.99	7685.39	$2p_3 - 2s_2$	$4p'[1\frac{1}{2}]_2 - 5s'\,[0\frac{1}{2}]\frac{1}{2}$	7685.32
13028.27	5	7673.51	7673.28	-------	$2p_4 - 3s''_1$	$4p'[1\frac{1}{2}]_1 - 3d'[1\frac{1}{2}]\frac{3}{2}$	7673.42
13214.70	150	7565.25	7565.11	-------	$2p_{10} - 3d_5$	$4p\,[0\frac{1}{2}]_1 - 3d\,[0\frac{1}{2}]\frac{3}{2}$	7565.73
13228.49	200	7557.37	7557.49	-------	$2p_9 - 3d_4$	$4p\,[2\frac{1}{2}]\frac{5}{2} - 3d\,[3\frac{1}{2}]\frac{5}{2}$	7557.59
13231.37	120	7555.72	7555.78	-------	$2p_7 - 2s_4$	$4p\,[1\frac{1}{2}]_1 - 5s\,[1\frac{1}{2}]\frac{1}{2}$	7555.96
13273.05	750	7532.00	7532.27	-------	$2p_3 - 3s'''_1$	$4p'[1\frac{1}{2}]_2 - 3d'[2\frac{1}{2}]\frac{5}{2}$	7532.24
13302.37	3	7515.39	7515.34	-------	$2p_3 - 3s''_1$	$4p'[1\frac{1}{2}]_2 - 3d'[1\frac{1}{2}]\frac{3}{2}$	7515.43
13313.39	600	7509.17	7509.41	-------	$2p_4 - 3s''''_1$	$4p'[1\frac{1}{2}]_1 - 3d'[2\frac{1}{2}]\frac{3}{2}$	7509.28
13330.32	7	7499.64	7499.67	-------	$3d'_4 - 4U$	$3d\,[3\frac{1}{2}]\frac{7}{2} - 4f\,[3\frac{1}{2}]_{3,4}$	7499.93
13367.38	800	7478.84	7479.06	-------	$2p_8 - 3d'_3$	$4p\,[1\frac{1}{2}]_2 - 3d\,[2\frac{1}{2}]\frac{5}{2}$	7479.01
13406.57	250	7456.98	7456.92	-------	$3d'_4 - 4V$	$3d\,[3\frac{1}{2}]\frac{7}{2} - 4f\,[4\frac{1}{2}]_5$	7457.10
13499.24	50	7405.79	7405.45	-------	$2p_6 - 2s_4$	$4p\,[1\frac{1}{2}]_2 - 5s\,[1\frac{1}{2}]\frac{1}{2}$	7405.66
13503.99	850	7403.18	7403.21	-------	$2p_9 - 3d_4$	$4p\,[2\frac{1}{2}]_2 - 3d\,[3\frac{1}{2}]\frac{5}{2}$	7403.07
13543.75	15	7481.45	7380.74	-------	$2p_7 - 2s_5$	$4p\,[1\frac{1}{2}]_1 - 5s\,[1\frac{1}{2}]\frac{3}{2}$	7381.25
13573.60	25	7365.22	7364.47	-------	$2p_2 - 2s_3$	$4p'[0\frac{1}{2}]_1 - 5s'\,[0\frac{1}{2}]\frac{3}{2}$	7365.21
13599.18	55	7351.36	7351.02	-------	$2p_3 - 3s''''_1$	$4p'[1\frac{1}{2}]_2 - 3d'\,[2\frac{1}{2}]\frac{3}{2}$	7351.29
13622.38	500	7338.84	7338.74	-------	$2p_7 - 3d''_1$	$4p\,[1\frac{1}{2}]_1 - 3d\,[2\frac{1}{2}]\frac{3}{2}$	7338.75
13678.53	300	7308.72	7308.83	-------	$2p_2 - 3s''_1$	$4p'[0\frac{1}{2}]_1 - 3d'\,[1\frac{1}{2}]\frac{3}{2}$	7308.72
13718.77	1000	7287.28	7287.54	-------	$2p_9 - 3d'_4$	$4p\,[2\frac{1}{2}]_3 - 3d\,[3\frac{1}{2}]\frac{7}{2}$	7287.42
13825.99	30	7230.76	-------	-------	$2p_6 - 2s^5$	$4p\,[1\frac{1}{2}]_2 - 5s\,[1\frac{1}{2}]\frac{3}{2}$	7230.95
13828.79	20	7229.30	7229.85	-------	$3d_4 - 4U$	$3d\,[3\frac{1}{2}]\frac{7}{2} - 4f\,[3\frac{1}{2}]_{3,4}$	7229.76
13907.41	12	7188.44	-------	-------	$2p_5 - 3d''_2$	$4p\,[1\frac{1}{2}]_2 - 3d\,[2\frac{1}{2}]\frac{5}{2}$	7188.45
13910.83	150	7186.67	7187.34	-------	$3d_4 - 4V$	$3d\,[3\frac{1}{2}]\frac{7}{2} - 4f\,[4\frac{1}{2}]_4$	7187.38
14093.61	120	7093.46	7093.33	-------	$2p_5 - 3d_2$	$4p\,[0\frac{1}{2}]_0 - 3d\,[1\frac{1}{2}]\frac{1}{2}$	7093.43
14249.93	7	7015.65	7015.82	-------	$2p_4 - 3d_2$	$4p'[1\frac{1}{2}]_1 - 3d\,[1\frac{1}{2}]\frac{1}{2}$	7016.00
14257.46	50	7011.94	7012.16	-------	$3s''''_1 - 4W$	$3d'[2\frac{1}{2}]\frac{5}{2} - 4f'\,[3\frac{1}{2}]_{3,4}$	7012.36
14596.27	40	6849.18	6849.14	-------	$3s''_1 - 4Z$	$3d'[1\frac{1}{2}]\frac{3}{2} - 4f'\,[2\frac{1}{2}]_3$	6849.14
14634.11	80	6831.47	6831.49	-------	$3s'''_1 - 4W$	$3d'[2\frac{1}{2}]\frac{5}{2} - 4f'\,[3\frac{1}{2}]_{3,4}$	6831.41
14649.97	60	6824.07	6823.98	-------	$3d''_1 - 4U$	$3d\,[2\frac{1}{2}]\frac{5}{2} - 4f\,[3\frac{1}{2}]_{3,4}$	6824.10
14692.39	5	6804.37	6803.73	-------	$3d''_1 - 4Y$	$3d\,[2\frac{1}{2}]\frac{5}{2} - 4f\,[2\frac{1}{2}]_{2,3}$	6804.02 6803.76
14739.11	3	6782.80	6782.65	-------	$2p_8 - 3d_4$	$4p\,[1\frac{1}{2}]_2 - 3d\,[3\frac{1}{2}]\frac{5}{2}$	6782.79
14786.29	2	6761.16	6760.89	-------	$2s_5 - 4Y$	$5s\,[1\frac{1}{2}]\frac{3}{2} - 4f\,[2\frac{1}{2}]_3$	6761.26
15046.42	70	6644.27	6644.31	-------	$2p_1 - 3s'_1$	$4p'[0\frac{1}{2}]_0 - 3d'[1\frac{1}{2}]\frac{1}{2}$	6644.23

* Confused with S. O. Ne λ6402.

TABLE 5. *Description of* A I *in the infrared region*—Continued

Observed wavelength in A, Humphreys and Kostkowski	Observed intensity	Wave number observed			Term combination		Wave number calculated, Moore [10]
		Humphreys and Kostkowski	Sittner and Peck	Meggers	Paschen notation	Racah notation	
A		cm^{-1}	cm^{-1}	cm^{-1}			
15172.33	22	6589.13	6588.82	------	$2p_5 - 2s_4$	$4p\ [0\frac{1}{2}]_0 - 5s\ [1\frac{1}{2}]_1^0$	6588.94
15229.92	1	6564.21	------	------	------	------	------
15302.26	75	6533.18	6533.62	------	$3d'_1 - 4U$	$3d\ [2\frac{1}{2}]_1^0 - 4f\ [3\frac{1}{2}]_{3,4}$	6533.54
15329.56	5	6521.54	6521.73	------	$2p_8 - 3d_3$	$4p\ [2\frac{1}{2}]_2 - 3d\ [1\frac{1}{2}]_2^0$	6521.66
15349.52	10	6513.06	6513.24	------	$3d'_1 - 4Y$	$3d\ [2\frac{1}{2}]_2^0 - 4f\ [2\frac{1}{2}]_3$	6513.20
15353.51	2	6511.37	6511.51	------	$2p_4 - 2s_4$	$4p'[1\frac{1}{2}]_1 - 5s\ [1\frac{1}{2}]_1^0$	6511.51
15402.58	10	6490.63	6490.84	------	$3d'_1 - 4V$	$3d\ [2\frac{1}{2}]_2^0 - 4f\ [4\frac{1}{2}]_4$	6491.16
15899.93	20	6287.60	6288.42	------	$3s'_1 - 4Z$	$3d'[1\frac{1}{2}]_1^0 - 4f'\ [2\frac{1}{2}]_2$	6287.68
15989.34	20	6252.44	6252.32	------	$2p_1 - 2s_2$	$4p'[0\frac{1}{2}]_0 - 5s'[0\frac{1}{2}]_1^0$	6252.40
16436.92	18	6082.18	6082.33	------	$3d_2 - 4Y$	$3d\ [1\frac{1}{2}]_1^0 - 4f\ [2\frac{1}{2}]_2$	6082.32
16520.14	9	6051.55	6052.55	------	$2p_7 - 3d_3$	$4p\ [1\frac{1}{2}]_1 - 3d\ [1\frac{1}{2}]_2^0$	6051.68
16549.81	6	6040.70	6041.06	------	$3d_2 - 4X$	$3d\ [1\frac{1}{2}]_1^0 - 4f\ [1\frac{1}{2}]_{1,2}$	6040.59 6040.91
16739.84	5	5972.12	5971.86	------	$2p_2 - 2s_3$	$4p'[0\frac{1}{2}]_1 - 5s\ [1\frac{1}{2}]_2^0$	5972.09
16940.39	100	5901.42	5901.59	------	$2p_8 - 3d_3$	$4p\ [1\frac{1}{2}]_2 - 3d\ [1\frac{1}{2}]_2^0$	5901.38

essentially linear character of the dependence of detector response upon incident energy, these records do, nevertheless, provide an excellent means of intensity evaluation. Because of the limited scale range of the recorder, it is necessary to make a large number of records with different amounts of energy incident on the entrance slit or with different slit widths, or else to introduce controlled attenuation into the amplifier output in order to reveal the range of intensities between the strongest and weakest lines. Both devices have been used to a limited extent. The relative intensities may be considered reasonably good estimates over moderate ranges, but are subject to the limitations mentioned in the section on helium. The nonuniformity in spectral distribution associated with use of a grating with a pronounced "blaze" angle is probably the most important of these limitations. It seems fairly certain that the most intense line included among those originating in transitions of the classes studied is $2p_9 - 3d'_4$. The newly classified lines originate in most instances in combinations involving four newly discovered levels which are the first members of the old V, U, and W series previously known only in higher members. In the Racah or pair-coupling notation, these levels are $4f[4\frac{1}{2}]_5$, $4f[4\frac{1}{2}]_4$, $4f[3\frac{1}{2}]_{3,4}$, and $4f'[3\frac{1}{2}]_{3,4}$. It is to be noted that in the last two instances the separation of the pairs has not been directly observed, or inferred, from existing data. These newly interpreted levels were actually identified from the data in the Sittner and Peck publication, previous to the observations herein reported, and communicated to Dr. Moore for inclusion in the first volume of [10], as noted in the section on argon. The following are the wave numbers of lines for which no classification has been published previously: 7673.51, 7532.00, 7515.39, 7456.98, 7381.45, 7011.94, 6824.07, 6533.18, and 6490.63 cm^{-1}. New classifications are proposed for 7499.64, and 6831.47 cm^{-1}. Each of the lines of wave number 7229.85 and 7187.34 cm^{-1}, as listed by Sittner and Peck, has a close resolved companion. The companion line in each instance should have the classification listed by those authors, and new interpretations are proposed for the lines in the positions first reported.

4.4. Krypton

Considerably more effort has been devoted to the observation and interpretation of Kr I than to any other part of this study. The principal reason for this emphasis is that, of these noble-gas spectra, Kr I has the greatest population of fairly uniformly distributed lines in the region between 10000 and 20000 A, and, as such, shows considerable promise as a source of standard wavelengths. The wavelengths have been determined by use of second-order krypton, neon, and argon lines as comparison standards, and in some instances third-order lines of Fe I excited in an arc. A few first-order krypton lines originating in transitions of the type $1s - 2p$, the wavelengths of which can be computed with great accuracy from known levels, were also used in regions where available. Actually, the relative scarcity of good standards was the principal impediment to the most satisfactory wavelength determinations. One of the sources used was a Geissler tube, imported several years ago from the firm of Robert Götze in Leipzig, and kindly loaned for this work by Wm. F. Meggers. This tube contained krypton of exceptional purity, and its operation under optimum conditions probably

TABLE 6. *Description of* Kr I *in the infrared region*

Observed wavelength in air, Humphreys and Kostkowski	Observed intensity	Wave number observed			Term combination		Wave number calculated Edlén levels
		Humphreys and Kostkowski	Sittner and Peck	Meggers	Paschen notation	Racah notation	
A		cm^{-1}	cm^{-1}	cm^{-1}			cm^{-1}
11792.25	120	8477.82	.....	8477.67	$2p_{10}-3d_2$	$5p\,[0\frac{1}{2}]_1-4d\,[1\frac{1}{2}]_1^0$	8477.71
11819.43	2000	8458.33	.....	8458.33	$2p_{10}-2s_5$	$5p\,[0\frac{1}{2}]_1-6s\,[1\frac{1}{2}]_1^0$	8458.36
11996.00	25	8333.82	.....	.....	$3d_3-4Y$	$4d\,[1\frac{1}{2}]_2^2-4f\,[2\frac{1}{2}]_2^3$	8333.84
11997.08	480	8333.07	.....	8333.03	$3d_2-4T$	$4d\,[1\frac{1}{2}]_1^2-4f\,[2\frac{1}{2}]_2^3$	8333.08
12077.42	115	8277.64	8277.96	8277.79	$3d_3-4Z$	$4d\,[1\frac{1}{2}]_2^2-4f\,[1\frac{1}{2}]_2^3$	8277.80
12117.81	100	8250.05	8250.09	8250.06	$3d'_4-4W$	$4d\,[3\frac{1}{2}]_4^3-4f\,[3\frac{1}{2}]_{3,4}^4$	8250.04
*12123.47	40	.....	8245.82	8246.15	$1s_2-2p_5$	$5s'\,[0\frac{1}{2}]_1^1-5p\,[0\frac{1}{2}]_0^1$	8246.16
12156.97	2	8223.48	.....	.....	$3d'_4-4T$	$4d\,[3\frac{1}{2}]_4^3-4f\,[2\frac{1}{2}]_3^3$	8223.51
12204.39	700	8191.52	8191.13	8191.43	$3d'_4-4U$	$4d\,[3\frac{1}{2}]_4^3-4f\,[4\frac{1}{2}]_5^4$	8191.43
12229.23	4	8174.89	.....	.....	$2p_4-3s_4$	$5p'\,[1\frac{1}{2}]_1-7s\,[1\frac{1}{2}]_1^0$	8174.78
12240.81	2	8167.15	.....	.....	$3d'_4-4p_8$	$4d\,[2\frac{1}{2}]_3^3-7p\,[1\frac{1}{2}]_2^2$	8167.31
12321.48	9	8113.68	8113.83	.....	$3s''_1-1534.60$	$4d''\,[1\frac{1}{2}]_2^3-4f''\,[2\frac{1}{2}]_3^3$	8113.98
12598.19	15	7935.47	.....	.....	$3s'_1{}'''-1536.49_2$	$4d''\,[2\frac{1}{2}]_3^3-4f''\,[3\frac{1}{2}]_4^3$	7935.75
12782.39	100	7821.11	8721.12	.....	$3d_4-4W$	$4d\,[3\frac{1}{2}]_4^3-4f\,[3\frac{1}{2}]_{3,4}^4$	7821.11
12825.08	5	7795.10	7794.70	.....	$3d_4-4T$	$4d\,[3\frac{1}{2}]_4^3-4f\,[2\frac{1}{2}]_3^3$	7794.58
					$3d_4-4Y$	$4d\,[3\frac{1}{2}]_3^3-4f\,[2\frac{1}{2}]_2^3$	7795.34
*12861.89	55	.....	7772.41	.....	$1s_3-2p_7$	$5s'\,[0\frac{1}{2}]_0^1-5p\,[1\frac{1}{2}]_1^1$	7772.78
12879.00	500	7762.46	7762.56	.....	$3d_4-4U$	$4d\,[3\frac{1}{2}]_4^3-4f\,[4\frac{1}{2}]_4^4$	7762.70
12934.48	1	7729.15	.....	.....	$2p_3-4d_2$	$5p'\,[0\frac{1}{2}]_1^1-5d\,[1\frac{1}{2}]_1^2$	7729.30
12977.98	2	7703.24	.....	.....	$2p_2-4d_2$	$5p'\,[1\frac{1}{2}]_2^1-5d\,[1\frac{1}{2}]_1^2$	7703.28
12985.08	12	7699.04	7698.32	.....	$2p_{10}-3d''_1$	$5p\,[0\frac{1}{2}]_1-4d\,[2\frac{1}{2}]_2^3$	7698.91
13022.05	15	7677.18	7676.47	.....	$3s'''_1-1536.49_2$	$4d'\,[2\frac{1}{2}]_3^3-4f'\,[3\frac{1}{2}]_{3,4}^4$	7676.97
13177.38	850	7586.70	7586.66	.....	$2p_8-2s_5$	$5p\,[2\frac{1}{2}]_2-6s\,[1\frac{1}{2}]_1^0$	7586.65
13210.56	10	7567.63	7566.35	.....	$2p_4-4d''_1$	$5p'\,[1\frac{1}{2}]_1-5d\,[2\frac{1}{2}]_2^3$	7567.58
13240.52	75	7550.51	7549.90	.....	$2p_4-2s_2$	$5p'\,[1\frac{1}{2}]_1-6s'\,[0\frac{1}{2}]_1^1$	7550.41
13304.30	5	7514.31	.....	.....	$2s_5-4p_9$	$6s\,[1\frac{1}{2}]_2^2-7p\,[2\frac{1}{2}]_3^3$	7514.31
13337.52	55	7495.59	7494.87	.....	$2p_4-2s_3$	$5p'\,[1\frac{1}{2}]_1-6s'\,[0\frac{1}{2}]_1^1$	7495.42
13622.28	800	7338.91	.....	.....	$2p_5-3d_2$	$5p\,[2\frac{1}{2}]_2-4d\,[1\frac{1}{2}]_1^2$	7338.84
13634.22	1700	7332.48	.....	.....	$2p_9-2s_5$	$2p\,[2\frac{1}{2}]_3-6s\,[1\frac{1}{2}]_1^0$	7332.47
13658.38	360	7319.51	.....	.....	$2p_8-2s_3$	$5p\,[2\frac{1}{2}]_2-6s\,[1\frac{1}{2}]_1^0$	7319.49
13711.23	100	7291.30	.....	.....	$2p_4-3s'_1$	$5p'\,[1\frac{1}{2}]_1-4d'\,[1\frac{1}{2}]_1^1$	7291.40
*13738.86	400	.....	.....	.....	$1s_2-2p_8$	$5s'\,[0\frac{1}{2}]_1^1-5p\,[1\frac{1}{2}]_2^2$	7276.64
13763.72	6	7263.49	.....	.....	$2p_2-4d_1{}'$	$5p'\,[1\frac{1}{2}]_2^1-5d\,[2\frac{1}{2}]_3^3$	7263.31
13800.03	3	7244.37	.....	.....	$2p_3-4d_1{}''$	$5p'\,[0\frac{1}{2}]_1^1-5d\,[2\frac{1}{2}]_2^3$	7244.35
13832.57	50	7227.33	.....	.....	$2p_3-2s_2$	$5p'\,[0\frac{1}{2}]_1^1-6s'\,[0\frac{1}{2}]_1^1$	7227.18
13882.64	240	7201.26	.....	.....	$2p_2-2s_2$	$5p'\,[1\frac{1}{2}]_2^1-6s'\,[0\frac{1}{2}]_1^1$	7201.16
13924.00	270	7179.87	.....	.....	$3d_1{}'^*-4W$	$4d\,[2\frac{1}{2}]_3^3-4f\,[3\frac{1}{2}]_3^3$	7179.97
13939.13	85	7172.08	.....	.....	$2p_3-2s_3$	$5p'\,[0\frac{1}{2}]_1^1-6s'\,[0\frac{1}{2}]_1^1$	7172.19
13974.15	70	7154.10	7154.11	.....	$3d_1{}''-4Y$	$4d\,[2\frac{1}{2}]_2^3-4f\,[2\frac{1}{2}]_2^3$	7154.20
14104.27	40	7088.10	.....	.....	$2p_3-4d_3$	$5p'\,[0\frac{1}{2}]_1^1-5d\,[1\frac{1}{2}]_2^2$	7088.10
14156.62	15	7061.89	.....	.....	$2p_2-4d_3$	$5p'\,[1\frac{1}{2}]_2^1-5d\,[1\frac{1}{2}]_2^2$	7062.08
14341.25	9	6970.97	.....	.....	$2p_2-4d_4$	$5p'\,[1\frac{1}{2}]_2^1-5d\,[2\frac{1}{2}]_3^3$	6971.31
14347.82	400	6967.78	6968.53	.....	$3d'_4-4W$	$4d\,[2\frac{1}{2}]_3^3-4f\,[3\frac{1}{2}]_{3,4}^4$	6968.00
.....	.....	.....	.....	.....	$2p_3-3s'_1$	$5p'\,[0\frac{1}{2}]_1^1-4d'\,[1\frac{1}{2}]_1^1$	6968.16
.....	.....	.....	6941.89	.....	$2p_2-3s'_1$	$5p'\,[1\frac{1}{2}]_2^1-4d'\,[1\frac{1}{2}]_1^1$	6942.14
14402.58	80	6941.29	.....	.....	$3d'_4-4Y$	$4d\,[2\frac{1}{2}]_3^3-4f\,[2\frac{1}{2}]_2^3$	6942.23
					$3d'_4-4T$	$4d\,[2\frac{1}{2}]_2^3-4f\,[2\frac{1}{2}]_3^3$	6941.47
14426.93	1100	6929.57	6929.97	.....	$2p_7-2s_4$	$5p\,[1\frac{1}{2}]_1-6s\,[1\frac{1}{2}]_1^0$	6929.64
14469.33	30	6909.27	6909.74	.....	$3d'_4-4U$	$4d\,[2\frac{1}{2}]_3^3-4f\,[4\frac{1}{2}]_4^4$	6909.59
14715.55	2	6973.66	.....	.....	$2p_1-4d_2$	$5p'\,[0\frac{1}{2}]_0^1-5d\,[1\frac{1}{2}]_1^2$	6973.38
14734.46	900	6784.95	.....	.....	$2p_9-3d'_1$	$5p\,[2\frac{1}{2}]_3-4d\,[2\frac{1}{2}]_3^3$	6784.99
14762.83	250	6771.90	6772.03	.....	$2p_8-3d'_1$	$5p\,[2\frac{1}{2}]_2-4d\,[2\frac{1}{2}]_2^3$	6772.01
14765.64	230	6770.62	6770.39	.....	$2p_6-2s_4$	$5p\,[1\frac{1}{2}]_2-6s\,[1\frac{1}{2}]_1^0$	6770.69
14961.76	110	6681.86	6681.56	.....	$2p_7-3d_2$	$5p\,[1\frac{1}{2}]_1-4d\,[1\frac{1}{2}]_1^2$	6681.83
14973.74	8	6676.52	.....	.....	$3d_5-3p_5$	$4d\,[0\frac{1}{2}]_1^1-6p\,[0\frac{1}{2}]_0^1$	6676.45
15005.57	25	6662.36	6661.74	.....	$2p_7-2s_3$	$5p\,[1\frac{1}{2}]_1-6s\,[1\frac{1}{2}]_1^0$	6662.48
15209.52	42	6573.02	6573.35	.....	$2p_9-3d''_1$	$5p\,[2\frac{1}{2}]_3-4d\,[2\frac{1}{2}]_3^3$	6573.02

See footnote at end of table.

TABLE 6. *Description of* Kr I *in the infrared region*—Continued

Observed wavelength in A Humphreys and Kostkowski	Observed intensity	Wave number observed			Term combination		Wave number calculated, Edlén levels
		Humphreys and Kostkowski	Sittner and Peck	Meggers	Paschen notation	Racah notation	
		cm^{-1}	cm^{-1}	cm^{-1}			cm^{-1}
15239.85	900	6559.94	6560.05	.....	$2p_8 - 3d_1''$	$5p\ [2\frac{1}{2}]_2 - 4d\ [2\frac{1}{2}]_3^3$	6560.04
15326.87	35	6522.69	6522.53	.....	$2p_6 - 3d_2$	$5p\ [1\frac{1}{2}]_2 - 4d\ [1\frac{1}{2}]_1^2$	6522.88
15335.29	850	6519.11	6519.19	.....	$2p_{10} - 3d_3$	$5p\ [0\frac{1}{2}]_1 - 4d\ [1\frac{1}{2}]_2^2$	6519.27
15371.89	350	6503.58	6503.09	.....	$2p_6 - 2s_5$	$5p\ [1\frac{1}{2}]_2 - 6s\ [1\frac{1}{2}]_1^2$	6503.53
15433.63	4	6477.57	.....	.....	$2p_4 - 4d_6$	$5p'[1\frac{1}{2}]_1 - 5d\ [0\frac{1}{2}]_0^1$	6477.56
*15474.02	65	.....	6460.84	.....	$1s_2 - 2p_8$	$5s\ [0\frac{1}{2}]_1^0 - 5p\ [2\frac{1}{2}]_2$	6460.68
15634.98	7	6394.15	6394.20	.....	$2s_5 - 4T$	$6s\ [1\frac{1}{2}]_2^2 - 4f\ [2\frac{1}{2}]_3$	6393.99
15680.94	75	6375.41	6375.59	.....	$3d_2 - 4Y$	$4d\ [1\frac{1}{2}]_1^0 - 4f\ [2\frac{1}{2}]_2$	6375.40
15771.44	1	6338.83	.....	.....	$2s_5 - 4Z$	$6s\ [1\frac{1}{2}]_2^2 - 4f\ [1\frac{1}{2}]_2$	6338.71
15820.10	35	6319.33	6319.40	.....	$3d_2 - 4Z$	$4d\ [1\frac{1}{2}]_1^0 - 4f\ [1\frac{1}{2}]_2$	6319.36
15823.40	2	6318.01	.....	.....	$3d_2 - 4X$	$4d\ [1\frac{1}{2}]_1^0 - 4f\ [1\frac{1}{2}]_1$	6318.24
15890.52	25	6291.32	6290.53	.....	$2p_1 - 2s_2$	$5p'[0\frac{1}{2}]_0 - 6s'[0\frac{1}{2}]_1^0$	6291.26
15925.64	6	6277.45	.....	.....	$3d_5 - 3p_8$	$4d\ [0\frac{1}{2}]_1^0 - 6p\ [1\frac{1}{2}]_2$	6277.42
16052.31	2	6227.91	6227.31	.....	$3d_5 - 3p_7$	$4d\ [0\frac{1}{2}]_1^0 - 6p\ [1\frac{1}{2}]_1$	6228.28
16109.46	3	6205.82	.....	.....	$2p_4 - 4d_5$	$5p'[1\frac{1}{2}]_1 - 5d\ [0\frac{1}{2}]_1^0$	6205.88
16315.58	12	6127.42	6127.23	.....	$2s_4 - 4Y$	$6s\ [1\frac{1}{2}]_1^0 - 4f\ [2\frac{1}{2}]_2$	6127.59
16347.31	5	6115.53	.....	.....	$3d_6 - 3p_{10}$	$4d\ [0\frac{1}{2}]_0^0 - 6p\ [0\frac{1}{2}]_1$	6115.69
16465.29	15	6071.70	.....	.....	$2s_4 - 4Z$	$6s\ [1\frac{1}{2}]_1^0 - 4f\ [1\frac{1}{2}]_2$	6071.55
16573.10	16	6032.21	6032.59	.....	$2p_1 - 3s_1'$	$5p'[0\frac{1}{2}]_0 - 4d'[1\frac{1}{2}]_1^0$	6032.24
*16726.48	70	.....	5976.46	.....	$1s_3 - 2p_{10}$	$5s'[0\frac{1}{2}]_0^0 - 5p\ [0\frac{1}{2}]_1$	5976.90
16784.65	950	5956.18	5956.05	.....	$2p_6 - 3d_1''$	$5p\ [1\frac{1}{2}]_2 - 4d\ [2\frac{1}{2}]_3^3$	5956.05
16853.45	480	5931.86	5931.86	.....	$2p_9 - 3d_4$	$5p\ [2\frac{1}{2}]_3 - 4d\ [3\frac{1}{2}]_4^3$	5931.88
16890.40	1000	5918.89	5918.95	.....	$2p_8 - 3d_4$	$5p\ [2\frac{1}{2}]_2 - 4d\ [3\frac{1}{2}]_3^3$	5918.90
16896.58	700	5916.72	5916.75	.....	$2p_{10} - 3d_3$	$5p\ [0\frac{1}{2}]_1 - 4d\ [0\frac{1}{2}]_1^2$	5916.69
16935.71	800	5903.05	5903.06	.....	$2p_7 - 3d_1''$	$5p\ [1\frac{1}{2}]_1 - 4d\ [2\frac{1}{2}]_2^3$	5903.03
16994.36	10	5882.68	.....	.....	$2p_3 - 4d_5$	$5p'[0\frac{1}{2}]_1 - 5d\ [0\frac{1}{2}]_1^2$	5882.65
17070.04	10	5856.60	.....	.....	$2p_2 - 4d_5$	$5p'[1\frac{1}{2}]_2 - 5d\ [0\frac{1}{2}]_1^2$	5856.63
17098.76	300	5846.76	5846.91	.....	$2p_4 - 3s_1'''$	$5p'[1\frac{1}{2}]_1 - 4d'[2\frac{1}{2}]_2^3$	5846.74
17230.21	10	5802.15	.....	.....	$3d_5 - 3p_{10}$	$4d\ [0\frac{1}{2}]_1^0 - 6p\ [0\frac{1}{2}]_1$	5802.00
17367.98	360	5756.13	5756.36	.....	$2p_2 - 3s_1'''$	$5p'[1\frac{1}{2}]_2 - 4d'[2\frac{1}{2}]_3^3$	5756.27
17404.67	32	5743.99	5744.15	.....	$2p_8 - 3d_1'$	$5p\ [1\frac{1}{2}]_2 - 4d'[1\frac{1}{2}]_2^2$	5744.08
17616.57	37	5674.90	5674.22	.....	$3d_3 - 3p_6$	$4d\ [1\frac{1}{2}]_2^3 - 6p\ [1\frac{1}{2}]_2$	5674.84
17630.44	4	5670.44	.....	.....	$2p_4 - 3s_1''$	$5p'[1\frac{1}{2}]_1 - 4d'[1\frac{1}{2}]_2^3$	5670.40
17770.21	4	5625.84	.....	.....	$3d_3 - 3p_7$	$4d\ [1\frac{1}{2}]_2^3 - 6p\ [1\frac{1}{2}]_1$	5625.70
17842.70	270	5602.98	5602.97	.....	$2p_{10} - 3d_6$	$5p\ [0\frac{1}{2}]_1 - 4d\ [0\frac{1}{2}]_0^1$	5603.00
18001.71	400	5553.49	5553.34	.....	$2p_5 - 3d_2$	$5p\ [0\frac{1}{2}]_0 - 4d\ [1\frac{1}{2}]_1^2$	5553.36
18098.46	10	5523.80	5523.50	.....	$2p_3 - 3s_1''$	$5p'[0\frac{1}{2}]_1 - 4d'[2\frac{1}{2}]_2^2$	5523.51
18167.12	1500	5502.92	5502.93	.....	$2p_9 - 3d_4$	$5p\ [2\frac{1}{2}]_3 - 4d[3\frac{1}{2}]_4^3$	5502.95
18184.43	15	5497.69	5497.57	.....	$2p_2 - 3s_1'''$	$5p'[1\frac{1}{2}]_2 - 4d'[2\frac{1}{2}]_3^3$	5497.49
18418.82	4	5427.72	.....	.....	$3d_3 - 3p_9$	$4d\ [1\frac{1}{2}]_2^3 - 6p\ [2\frac{1}{2}]_3$	5427.87
18581.19	30	5380.29	5380.45	.....	$2p_8 - 3d_3$	$5p\ [2\frac{1}{2}]_2 - 4d\ [1\frac{1}{2}]_2^3$	5380.40
18695.91	62	5347.28	5346.76	.....	$2p_3 - 3s_1''$	$5p'[0\frac{1}{2}]_1 - 4d'[1\frac{1}{2}]_2^2$	5347.17
18785.45	37	5321.79	5321.61	.....	$1s_2 - 2p_{10}$	$5s'[0\frac{1}{2}]_1^0 - 5p\ [0\frac{1}{2}]_1$	5321.81
18787.73	10	5321.15	.....	.....	$2p_2 - 3s_1''$	$5p'[1\frac{1}{2}]_2 - 4d'[1\frac{1}{2}]_2^2$	5321.15
18797.59	40	5318.36	5317.88	.....	$3d_4' - 3p_9$	$4d\ [3\frac{1}{2}]_4^4 - 6p[2\frac{1}{2}]_3$	5318.30

*Calculated wavelength used as a comparison standard.

revealed all of the krypton spectrum that can be excited in this type of source. The description and interpretation of the observed krypton spectrum in the region investigated is displayed in table 6, which presents the data on 98 krypton lines, all of which are classified. Included in this number are 36 lines not reported by Sittner and Peck. About three-fourths of these are weak lines scattered throughout the region, but nine lines between 13600 and 14000 A are among the most intense in the infrared krypton spectrum and may have been omitted inadvertently from the description by Sittner and Peck. A portion of a record showing this group of lines is displayed in figure 3. This was a survey record run with relatively wide slits in order to reveal as many of the faint lines as possible. The peaks of many of the intense lines

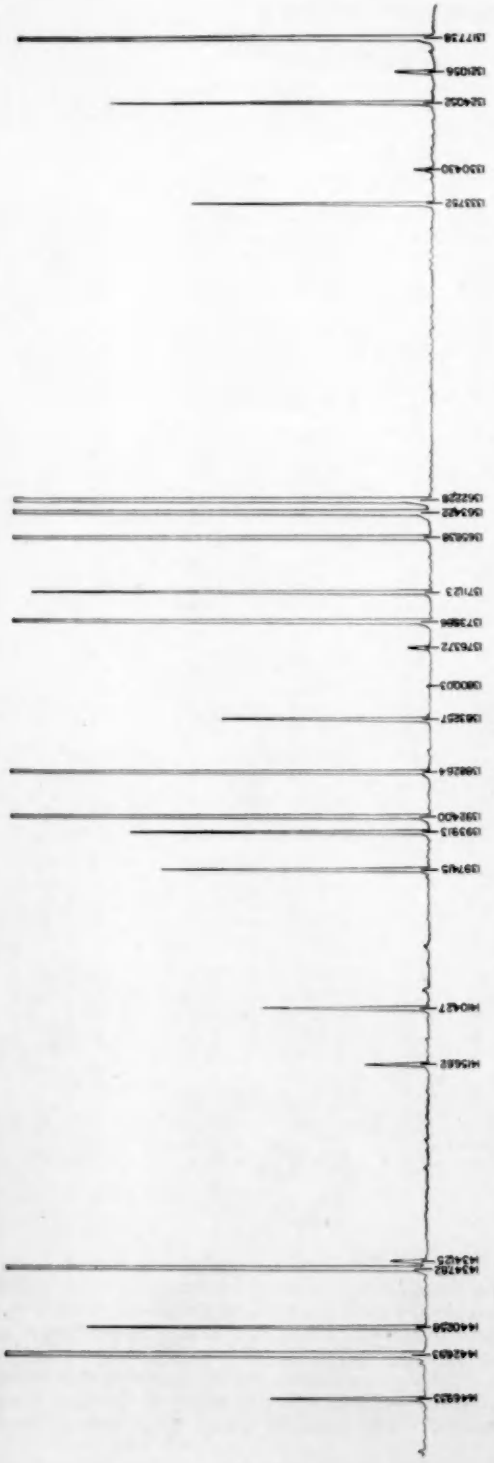

FIGURE 3. *Reproduction of tracing of chart record of infrared spectrum of krypton, 13100 to 14500 A.*

are cut off, because the deflections are off the scale of the recorder.

Edlén's revisions of the table of levels by Meggers and Humphreys [4] and listing of additional levels are the basis of the entries on Kr I in [10]. These changes are relatively few in number, emphasizing the fact that this analysis has long been regarded as essentially complete. The levels to which the designations $2s_2$ and $3s_1'$ were formerly assigned have been interchanged. A similar switch has been made with $3s_1''$ and $3s_1''''$. These changes should be taken into account in comparing Sittner and Peck's classifications with ours. The Edlén manuscript also supplied a complete set of values of the levels representing the first members of the various series originating in the $4f$ configuration, except that the doublet structure of the level designated 4W or $4f[3\frac{1}{2}]_{3,4}$ remained unresolved; a computed value only was proposed for one component of the 4U doublet, namely $4f[4\frac{1}{2}]_4$; and only three of the four possible $4f$-levels converging to the higher ion limit $p^5(^2P^\circ_{0\frac{1}{2}})$ were proposed. The experimental confirmation of the 4U and 4W by Humphreys and Plyler [2], has been mentioned. The new compilation of levels of Kr I also includes the previously missing $2s_2$. Edlén listed two choices, but it was noted that one of Sittner and Peck's intense unclassified lines, ν=7494.87 cm^{-1}, could be interpreted as $2p_4-2s_2$, if the level of absolute value 7823.56 were adopted as $2s_2$. Further confirmation is found in the classification of the moderately intense line, ν=7172.08 cm^{-1}, as $2p_3-2s_3$. Two of the remaining intense lines reported without classification by Sittner and Peck are assigned to transitions involving $4f$-levels of the family converging to the higher limit. These are ν, 8113.83 cm^{-1}, classified in pair-coupling notation $4d'[1\frac{1}{2}]^\circ_2-4f'[2\frac{1}{2}]_3$, and ν, 7676.47 cm^{-1}, classified $4d'[2\frac{1}{2}]^\circ_3-4f'[3\frac{1}{2}]_{3,4}$. Sittner and Peck listed two other intense krypton lines without classification, ν, 7578.37 cm^{-1}, which we have been unable to reproduce with our sources, and ν, 5982.33 cm^{-1}, which seems almost certainly to be the third order of the intense visible line, λ, 5570.29 A. Of the two values of the pair 4U, or $4f[4\frac{1}{2}]_{4,5}$ proposed by Edlén, the one with J-value 4 was bracketed indicating a predicted value. The pair separation is given as 0.20 cm^{-1}. The only possibility of a combination of both levels of the pair with a common level is that involving the level $3d_4'$ or $4d[3\frac{1}{2}]^\circ_4$ yielding the line, ν, 8191.52 cm^{-1}. No structure has been observed, but a resolving power of over 40000 would be required to split this doublet, something beyond what we have obtained in any clearly demonstrable case. It is probable that most of the energy in this line is accounted for by the transition $4d[3\frac{1}{2}]^\circ_4-4f[4\frac{1}{2}]_5$. All other combinations of this 4U pair involve the level J=4, uniquely owing to the ΔJ selection rule.

Evidence, principally from the measured wavelength of the intense line representing the combination, $4d[3\frac{1}{2}]^\circ_3-4f[4\frac{1}{2}]_4$, for which we give λ12879.00, indicates that Edlén's estimated absolute value for $4f[4\frac{1}{2}]_4$, namely, 6925.92 cm^{-1}, is too small. The observed value, obtained by averaging our measured result with that of Sittner and Peck, is 6926.10,

making the level indistinguishable from $4f[4\frac{1}{2}]_5$. As represented in [10], with the ground level=0, this level would become 105989.60 cm^{-1}. The Racah pair of closest separation that we have actually observed in combinations with a common level is $4f[1\frac{1}{2}]_2^o - 4f[2\frac{1}{2}]_{2,3}$, represented by the wave numbers 8333.82, and 8333.07 cm^{-1}. The observed separation is 0.75 cm^{-1} as compared with the calculated, 0.768. The actual observation of this pair is extremely difficult on account of the great disparity in intensities of the components. The pair of widest separation in this $4f$ group, 4X and 4Z or $4f[1\frac{1}{2}]_{1,2}$ occurs in easily observable combinations with a common level. The best example is the pair of wave numbers 8879.23 and 8880.35 reported by Meggers and Humphreys [3,4] and also demonstrable by radiometric techniques. So far there is no clue to the magnitude of the splitting of 4W, and the missing level $4f'[3\frac{1}{2}]_4$ has not been found unless it is unresolved with respect to $4f'[3\frac{1}{2}]_3$. Otherwise, the level structure of Kr I may be considered complete.

4.5. Xenon

The observations on xenon were less extensive than on any of the other four noble gases because both preliminary recordings and study of the level scheme had revealed that there was little possibility of adding significantly to the existing observational material. A small number of records were made in order that some material on all the noble gas spectra might be included in the current survey. The results are presented in table 7, which is organized in the same fashion as the corresponding tables 5 and 6 for argon and krypton. These observations cover the same region as those of Sittner and Peck, and their classifications are repeated without revision for lines common to both lists.

The principal reason for the relative paucity of xenon lines in the 1.2— to 1.8—micron region is that the $2p$ and $3d$ levels fall in much the same range of numerical values, with the result that the $2p-3d$ combinations, that are responsible for many of the intense analogous lines in argon and krypton, represent wavelengths much deeper in the infrared and out of range of observation with lead-sulfide detectors. For instance, the position of the expected most intense combination in this group, $2p_8-3d'_4$, is predicted at 1793.6 cm^{-1}. Most of the possible $3d-4f$ combinations have been observed photographically. Of the f-type levels, only those of the family converging to the $^2P^o_{1\frac{1}{2}}$ ion limit have been found. Owing to the extremely wide separation of the series limits, the first members of the f-series converging to $^2P^o_{0\frac{1}{2}}$ are above the first ionization limit.

The only noteworthy changes in the Xe I level scheme made by Edlén since the last publication of this array [5] have been to change the designation of the level at 4215.65 from $2s_2$ to $3s'_1$, to supply level values for $2s_2$ and $2s_3$, and to separate the series formerly designated W, into two according to the Racah scheme. The first pair of this series $4f[3\frac{1}{2}]_{3,4}$ has a separation of 0.10 cm^{-1} on the basis of previously existing photographic data. Discrimination

TABLE 7. *Description of* Xe I *in the infrared region*

Observed wave length in air, Humphreys and Kostkowski	Observed intensity	Wave number observed			Term combination		Wave number calculated, Edlén levels
		Humphreys and Kostkowski	Sittner and Peck	Meggers	Paschen notation	Racah notation	
A		*cm*$^{-1}$	*cm*$^{-1}$	*cm*$^{-1}$			
11742.01	90	8514.09	8514.77	8513.92	$3d'_4-4W$	$5d[2\frac{1}{2}]_3^o-4f\ [3\frac{1}{2}]_4$	8513.83
11793.04	40	8477.25	8476.84	8476.89	$3d'_1-4U$	$5d[2\frac{1}{2}]_2^o-4f\ [2\frac{1}{2}]_3$	8476.89
11857.00	30	8431.52	8431.47	8431.31	$3d'_1-4Z$	$5d[2\frac{1}{2}]_2^o-4f\ [4\frac{1}{2}]_4$	8431.31
11911.44	3	8392.99	8392.50	8392.53	$3d_3-2p_4$	$5d[0\frac{1}{2}]_1-6p'[1\frac{1}{2}]_1$	8392.49
11952.57	10	8364.10	8363.26	8363.81	$3d_3-3p_8$	$5d[1\frac{1}{2}]_2^o-7p\ [1\frac{1}{2}]_2$	8363.74
12084.82	20	8272.58	8272.59	8272.60	$3d'_4-3p_3$	$5d[3\frac{1}{2}]_4^o-7p\ [2\frac{1}{2}]_3$	8272.57
12235.14	80	8170.93	8170.88	8170.88	$2p_{10}-2s_4$	$6p[0\frac{1}{2}]_1-7s\ [1\frac{1}{2}]_1^o$	8170.88
12258.10	6	8155.63	8155.85	8155.83	$3d_5-3p_{10}$	$5d[0\frac{1}{2}]_0^o-7p\ [0\frac{1}{2}]_1$	8155.85
12451.21	2	8029.14	8028.32	.....	$3d_3-3p_9$	$5d[1\frac{1}{2}]_2^o-7p\ [2\frac{1}{2}]_2$	8028.92
12590.00	26	7940.63	7940.70	.....	$3d_5-3p_{10}$	$5d[0\frac{1}{2}]_1^o-7p\ [0\frac{1}{2}]_1$	7940.49
12623.32	300	7919.67	7919.30	7919.63	$2p_{10}-2s_5$	$6p[0\frac{1}{2}]_1-7s\ [1\frac{1}{2}]_2^o$	7919.66
13543.16	5	7381.77	.....	.....	$3d_4-3p_9$	$5d[3\frac{1}{2}]_3^o-7p\ [2\frac{1}{2}]_2$	7381.27
13656.48	150	7320.52	7320.19	.....	$2p_9-2s_4$	$6p[2\frac{1}{2}]_2-7s\ [1\frac{1}{2}]_1^o$	7320.23
14142.09	80	7069.15	7068.95	.....	$2p_9-2s_5$	$6p[2\frac{1}{2}]_2-7s\ [1\frac{1}{2}]_2^o$	7069.01
14241.39	40	7019.85	7020.18	.....	$3d_2-4V$	$5d[1\frac{1}{2}]_1^o-4f\ [2\frac{1}{2}]_2$	7020.11
14364.90	20	6959.50	6959.46	.....	$3d_2-4Y$	$5d[1\frac{1}{2}]_1^o-4f\ [1\frac{1}{2}]_2$	6959.50
14659.84	5	6819.42	6819.02	.....	$3d''_1-3p_7$	$5d[2\frac{1}{2}]_2^o-7p\ [1\frac{1}{2}]_1$	6819.04
14732.38	200	6785.90	6785.70	.....	$2p_3-2s_3$	$6p[2\frac{1}{2}]_3-7s\ [1\frac{1}{2}]_2^o$	6785.75
15418.01	110	6484.13	6484.16	.....	$2p_7-2s_4$	$6p[1\frac{1}{2}]_1-7s\ [1\frac{1}{2}]_1^o$	6483.99
16052.02	50	6228.03	6227.44	.....	$2p_8-2s_4$	$6p[1\frac{1}{2}]_2-7s\ [1\frac{1}{2}]_1^o$	6227.56
16727.52	50	5976.52	5976.05	.....	$2p_6-2s_5$	$6p[1\frac{1}{2}]_2-7s\ [1\frac{1}{2}]_2^o$	5976.34

between levels this close is beyond the precision of the current observations.

The complete status of the level scheme of Xe I makes it unnecessary to consider further observations in order to improve the analysis. Future availability of photoconductors sensitive to energy of greater wavelengths, possibly as far as 7 microns would still make Xe I an attractive subject for study owing to the existence of several predicted lines of probable high intensity that might be useful as wavelength standards.

5. Conclusion

Observation and interpretation of the noble gas spectra over a period of over thirty years have led to the essentially complete analysis of the spectra of these gases. One of the most interesting features of this work is that it has been made possible largely by the development of techniques for observing in the infrared region by either photographic or radiometric methods. The noble gases have provided some of the best sources of standard wavelengths. The possibility of extending the range of highly precise observations farther into the infrared region by combining interferometric with radiometric methods still constitutes an attractive challenge.

Several members of the staff of the Bureau's Radiometry Laboratory, have given valuable assistance in bringing this work to completion. In particular, Arthur J. Cussen and Joseph J. Ball contributed to the operation and maintenance of the electronic instruments used with the photoconductive detectors. Marshall E. Anderson assisted in obtaining and reducing the records. It is a pleasure to express to each of them appreciation for his contribution to the work.

6. References

[1] W. R. Sittner and E. R. Peck, J. Opt. Soc. Am. **39,** 47 (1949).
[2] C. J. Humphreys and E. K. Plyler, J. Research NBS **38,** 499 (1947) RP1790.
[3] W. F. Meggers, Zeeman Verhandelingen, p. 190 629 (Martinus Nijhoff, the Hague, 1935); J. Research NBS **14,** 487 (1935) RP781.
[4] W. F. Meggers and C. J. Humphreys, BS J. Research **10,** 427 (1933) RP540.
[5] C. J. Humphreys and W. F. Meggers, BS J. Research **10,** 139 (1933) RP521.
[6] C. E. K. Mees, J. Opt. Soc. Am. **25,** 80 (1935).
[7] F. Paschen, Ann. Physik [4] **60,** 405 (1919).
[8] G. Racah, Phys. Rev. **61,** 537 (L) (1942).
[9] G. H. Shortley and B. Fried, Phys. Rev. **54,** 749 (1938).
[10] Charlotte E. Moore, Atomic Energy Levels, NBS Circular 467, **I** (1949).
[11] E. K. Plyler and M. A. Lamb, J. Research NBS **45,** 202 (1950) RP2125.
[12] H. Roemer and R. A. Oetjen, J. Opt. Soc. Am. **36,** 47 (1946).
[13] R. C. Nelson and W. R. Wilson, Proc. Nat. Electronics Conference **3,** 579 (1947).
[14] C. J. Humphreys, J. Research NBS **47,** 262 (1951) RP2252.
[15] F. Paschen and R. Götze, Seriengesetze der Linienspektren (Springer, Berlin, 1922).
[16] J. D. Hardy, Phys. Rev. **38,** 2162 (1931).

Corona, Calif., February 15, 1952.

Journal of Research of the National Bureau of Standards Vol. 49, No. 2, August 1952 Research Paper 2346

A Viscometric Study of the Micelles of Sodium Dodecyl Sulfate in Dilute Solutions

Lawrence M. Kushner, Blanton C. Duncan, and James I. Hoffman

The viscosities of solutions of sodium dodecyl sulfate of concentrations up to 0.8 percent in distilled water and in 0.01- to 0.12-*M* sodium chloride have been measured. By introducing the concept of a monomer saturation concentration it is possible to determine the intrinsic viscosity of the micelles at each concentration of sodium chloride. A method for the experimental determination of the monomer saturation concentration is presented. The dependence of the intrinsic viscosity on the salt concentration is discussed in terms of electroviscous and hydration effects. The data indicate the presence of spherical micelles in the solutions investigated.

1. Introduction

Since the early experiments of Krafft [1][1] and McBain [2] on soap solutions, and the subsequent interpretation of their results in terms of the existence of micelles in such solutions, many researches [3, 4] have been undertaken to investigate the size and shape of these particles. It is now generally assumed that there are at least two types of micelles. In the concentration range between the onset of micelle formation (about 0.1 to 0.25 percent by weight) and about 1 to 2 percent, a small, highly charged and highly conducting micelle is thought to exist. This type of micelle has been discussed at some length by Hartley [5, 6]. He considered them as spheres, but there has been no general agreement on their shape. A large micelle, having a structure discernible by X-ray diffraction, exists at higher concentrations (about 10 percent or greater). They have been discussed and investigated by McBain [2], Hess [7], Philippoff [8], and others [9]. Harkins [10] and his coworkers interpret their later X-ray diffraction data for concentrated solutions in terms of cylindrical micelles. Brady [11], however, utilizing a treatment considered by Corrin [12], interprets his data for concentrated sodium dodecyl sulfate solutions in terms of a radial distribution of spherical micelles. Recent light-scattering investigations by Debye [13] indicate that in the presence of high concentrations of electrolyte, the micelles of hexadecyl trimethyl ammonium bromide are rod-like.

The purpose of this research was to investigate the viscometric behavior of dilute solutions of a pure, well-defined detergent, sodium dodecyl sulfate. Detergent concentrations up to 0.8 percent by weight were used. Distilled water and 0.01 to 0.12 M sodium chloride solutions were used as solvents.

2. Materials

The sodium dodecyl sulfate was synthesized, as described by Shedlovsky [14], from a vacuum-distilled sample of *n*-dodecyl alcohol. The chlorosulfonic acid used in the synthesis was distilled immediately before use. All other reagents used in the synthesis and subsequent purification conformed with American Chemical Society specifications. Prior to making up solutions for the measurements, the detergent was extracted with diethyl ether for about 8 hr in a Soxhlet extractor.

After a measurement, the detergent was recovered from solution in the following manner: The solution was evaporated to dryness and the residue taken up in ethyl alcohol. The alcohol solution was filtered and evaporated to dryness. This residue was then taken up in water and crystallized. Finally, the crystals were extracted with ether.

[1] Figures in brackets indicate literature references at the end of this paper.

3. Experimental Details

3.1. Viscosity

a. Efflux Times

The efflux times of all solutions were determined in modified Ostwald viscometers, which gave flow times of approximately 200 sec for water at 23° C. Absolute viscosities were calculated by means of the standard two-constant equation

$$\eta = A\rho t_c + \frac{B\rho}{t_c}. \tag{1}$$

The constants A and B were determined from experiments with distilled water at three temperatures. The absolute viscosity of water at 20° C was taken to be 1.002 centipoise [15]. ρ is the density of the solution. t_c is the efflux time corrected for surface-tension effects and for variations in the filling temperature. The surface-tension correction, arising from the difference of shape of the meniscus of the solution in the upper and lower bulbs of the viscometer, is treated as a time-averaged head correction. The filling-temperature correction is also treated as a head correction. The equation for t_c then takes the form

$$t_c = t_o\left(1+\frac{\Delta h_\gamma}{h}+\frac{\Delta h_f}{h}\right),$$

where t_o is the observed efflux time. Δh_γ and Δh_f represent the change in the effective head arising from surface tension effects and variations in filling temperature respectively. h is the mean

head during a run in the absence of such corrections. In the viscometers used $\Delta h_\gamma/h$ is about 1.4 percent for a liquid of $\gamma=70$ dynes/cm. $\Delta h_f/h$ exceeds 1 part per 10 thousand only when the difference between the filling and measuring temperatures is 5 deg or more. The calibration of capillary viscometers has been discussed fully by Barr [16].

A water bath whose temperature was maintained at 23.00° C was used for all measurements of efflux time and density. The reproducibility of the temperature setting of the bath from day to day was well within 0.003° C. During the course of any single measurement the mean temperature of the bath did not vary by more than 0.0015° C.

Timing was accomplished manually with a 60-cycle synchronous clock powered by an amplified constant-frequency 60-cycle signal. The average deviation from the mean of five determinations on the same solution was rarely more than 0.03 sec.

b. Surface Tension

The surface tension of each solution was determined with a conventional ring-type interfacial tensiometer. An accuracy of 1 dyne/cm was sufficient for the purposes of this research.

c. Density

All density measurements were made in picnometers similar to those described by Wright and Tartar [17]. The modified picnometers used by the authors held approximately 50 g of solution, thus making it a simple task to obtain densities with a precision of 2 parts per 100 thousand. Examination of these data shows that the densities of the solutions as a function of concentration above the region of micelle formation are best represented by straight lines of equal slopes. Below this region, not enough data were obtained to define the shape of the curve.

Table 1 lists the experimentally determined viscosities and densities.

3.2 Determination of the Monomer Saturation Concentration

Modern treatments of the problem of the viscosity of suspensions of large particles lead to an expression of the following type

$$\frac{(\eta_{rel}-1)}{\varphi}=K+D\varphi. \tag{2}$$

K is a constant related to the shape of the particles. It is equal to 2.5 for spheres. D is a constant related to those interactions in the suspension that give rise to disturbing hydrodynamic effects. φ is the volume fraction of the suspended particles, and η_{rel} is the viscosity of the solution relative to the viscosity of the suspending medium. It is usually more convenient to express the concentration of suspended particles in grams per deciliter of solution rather than in volume fractions. In this case

$$\frac{(\eta_{rel}-1)}{c}=[\eta]+D'c, \tag{3}$$

where $[\eta]$ is the intrinsic viscosity and has the units deciliters per gram. It is related to K by the expression

$$[\eta]=\frac{K}{100d}. \tag{4}$$

d is the density of the suspended particles.

If one wishes to apply eq 3 to the viscosity of detergent solutions with the hope of determining the intrinsic viscosity of the micelles, two problems must be considered. The first is that c must refer to the concentration of micelles, rather than to total detergent in solution. Second, η_{rel} is then the viscosity of the micelle solution relative to that of some arbitrary concentration of detergent, above which

TABLE 1. *Viscosity of sodium dodecyl sulfate in water and sodium chloride solutions (23°C)*

c	Density	η^1_{raw}	η^2_{corr}	c^3_m	η^4_{rel}	$\frac{\eta_{rel}-1}{cm}$
Water						
g/100 ml	*g/cm³*	*cp*	*cp*	*g/100 ml*		
0.00	0.99754	0.9323	------	------	------	------
.10	.99773	.9388	------	------	------	------
.20	.99790	.9398	------	------	------	------
.281* [5]	------	------	0.9434	0.00	1.0000	[0.065] [6]
.30	.99808	.9442	.9446	.019	1.0013	.068
.40	.99821	.9520	.9514	.119	1.0085	.071
.50	.99835	.9594	.9568	.219	1.0174	.079
.60	.99849	.9669	.9690	.319	1.0271	.085
0.01 *N* NaCl						
0.00	0.99799	0.9323	------	------	------	------
.05	.99809	.9350	------	------	------	------
.10	.99818	.9351	------	------	------	------
.20	.99834	.9394	------	------	------	------
.204*	------	------	0.9395	0.00	1.0000	[0.048]
.30	.99846	.9441	.9441	.096	1.0049	.051
.40	.99858	.9503	.9495	.196	1.0106	.054
.50	.99872	.9552	.9554	.296	1.0169	.057
.60	.99888	.9614	.9619	.396	1.0238	.060
.70	.99901	.9691	.9687	.496	1.0311	.063
0.02 *N* NaCl						
0.00	0.99838	0.9329	------	------	------	------
.05	.99847	.9360	------	------	------	------
.10	.99854	.9357	------	------	------	------
.15	.99862	.9385	------	------	------	------
.161*	------	------	0.9391	0.00	1.0000	[0.045]
.20	.99868	.9400	.9408	.039	1.0018	.046
.25	.99880	.9427	.9431	.089	1.0043	.048
.30	.99883	.9457	.9453	.139	1.0066	.047
.40	.99897	.9505	.9500	.239	1.0116	.049
.50	.99912	.9550	.9549	.339	1.0168	.050
.60	.99924	.9601	.9603	.439	1.0226	.051
.80	.99955	.9728	.9722	.639	1.0352	.055
0.03 *N* NaCl						
0.00	0.99880	0.9339	------	------	------	------
.05	.99891	.9362	------	------	------	------
.10	.99900	.9370	------	------	------	------
.136*	------	------	0.9386	0.00	1.0000	[0.041]
.15	.99905	.9385	.9392	.014	1.0006	.043
.20	.99911	.9416	.9411	.064	1.0027	.042
.25	.99920	.9451	.9432	.114	1.0049	.043
.30	.99924	.9452	.9452	.164	1.0070	.043
.40	.99942	.9498	.9496	.264	1.0117	.044
.50	.99954	.9539	.9542	.364	1.0166	.045
.60	.99965	.9589	.9590	.464	1.0217	.047
.80	.99999	.9692	.9692	.664	1.0326	.049

See footnotes at end of table.

TABLE 1. *Viscosity of sodium dodecyl sulfate in water and sodium chloride solutions (23°C)*—Continued

c	Density	η_{raw}[1]	η_{curve}[2]	c_m[3]	η_{rel}[4]	$\frac{\eta_{rel}-1}{cm}$
0.04 *N* NaCl						
0.00	0.99921	0.9349	------	------	------	------
.05	.99932	.9360	------	------	------	------
.10	.99938	.9376	------	------	------	------
.119*	------	------	0.9384	0.00	1.0000	[0.039]
.15	.99947	.9389	.9395	.031	1.0012	.039
.20	.99953	.9415	.9414	.081	1.0032	.040
.25	.99961	.9433	.9433	.131	1.0052	.040
.30	.99967	.9452	.9453	.181	1.0074	.041
.40	.99980	.9502	.9494	.281	1.0117	.042
.50	.99993	.9541	.9539	.381	1.0165	.043
.60	1.00008	.9579	.9585	.481	1.0214	.044
.80	1.00037	.9683	.9683	.681	1.0319	.047
0.05 *N* NaCl						
0.00	0.99963	0.9357	------	------	------	------
.05	.99969	.9371	------	------	------	------
.10	.99979	.9381	------	------	------	------
.109*	------	------	0.9386	0.00	1.0000	[0.038]
.15	.99989	.9400	.9401	.044	1.0016	.036
.20	1.00000	.9422	.9420	.094	1.0036	.038
.25	1.00005	.9438	.9439	.144	1.0056	.039
.30	1.00011	.9456	.9459	.194	1.0078	.040
.40	1.00024	.9504	.9500	.294	1.0121	.041
.50	1.00049	.9545	.9542	.394	1.0166	.042
.60	1.00053	.9586	.9586	.494	1.0213	.043
.80	1.00083	.9673	.9674	.694	1.0307	.044
0.08 *N* NaCl						
0.00	1.00084	0.9380	------	------	------	------
.05	1.00094	.9391	------	------	------	------
.083*	------	------	0.9408	0.00	1.0000	[0.037]
.10	1.00102	.9405	.9414	.017	1.0006	.035
.15	1.00110	.9439	.9432	.067	1.0026	.039
.20	1.00114	.9451	.9450	.117	1.0045	.038
.25	1.00124	.9473	.9469	.167	1.0065	.039
.30	1.00129	.9497	.9488	.217	1.0085	.039
.40	1.00142	.9532	.9527	.317	1.0126	.040
.50	1.00159	.9568	.9567	.417	1.0169	.041
.60	1.00170	.9607	.9609	.517	1.0214	.041
.80	1.00198	.9695	.9695	.717	1.0305	.043
0.12 *N* NaCl						
0.00	1.00245	0.9407	------	------	------	------
.095*	------	------	0.9422	0.00	1.0000	[0.035]
.10	1.00259	.9433	.9433	.035	1.0012	.034
.15	1.00268	.9467	.9450	.085	1.0030	.035
.20	1.00279	.9466	.9468	.135	1.0049	.036
.40	1.00306	.9553	.9541	.335	1.0126	.038
.60	1.00328	.9620	.9620	.535	1.0210	.039
.80	1.00355	.9701	.9701	.735	1.0296	.040

[1] η raw=experimental viscosity, in centipoise.
[2] η curve=viscosity taken from best smooth curve representing the dependence of η raw on concentration.
[3] c_m=(total concentration of detergent)−(monomer saturation concentration).
[4] η_{rel}=viscosity of solution/viscosity at monomer saturation concentration, both values being obtained from a smooth curve (see footnote 2).
[5] * indicates monomer saturation concentration.
[6] [ ] denotes the intrinsic viscosity in deciliters per gram.

it can be safely assumed that essentially all added detergent becomes micelles. This concentration shall be referred to as the monomer saturation concentration and is given the symbol c_s. The concentration of detergent present as micelles c_m, at a total detergent concentration c, is then very nearly $c-c_s$.

Consideration of the equilibrium between detergent molecules or ions and their micelles [3, 18] shows that the concentration range in which the fraction of added detergent going into micelles changes from 0 to 1 depends on n, the number of detergent molecules per micelle. For n less than 100, as previous investigations [18] have indicated for sodium dodecyl

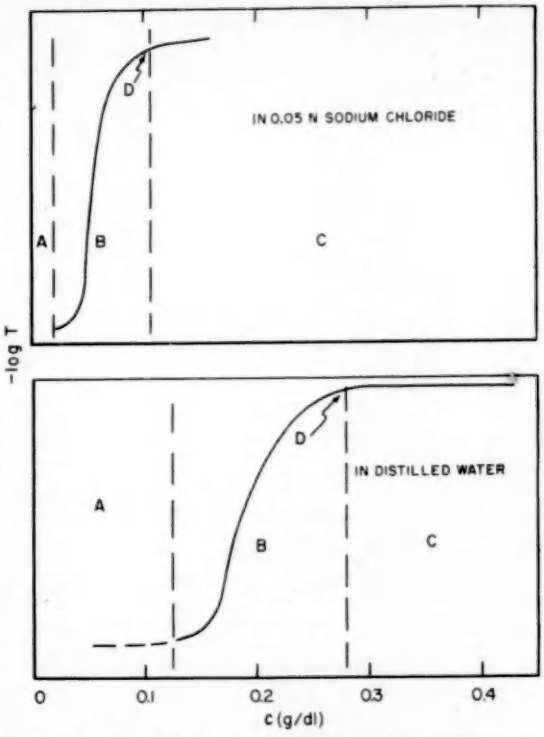

FIGURE 1. *Typical plots of the absorbance (−log T) versus concentration of sodium dodecyl sulfate.*

The concentration of toluidene blue is 0.001 g/dl. The point D occurs at the monomer saturation concentration.

sulfate, the monomer saturation concentration cannot be identified with the critical micelle concentration as defined by Debye [18]. Further, as a number of the published experimental methods for the determination of the critical micelle concentration yield results indicative of the concentration at which micelles begin to form (that is, even below Debye's critical micelle concentration), this identification would be less justified.

The method devised for estimating the monomer saturation concentration is based on the experiments of Corrin and Harkins [20] and Michaelis [19]. Michaelis observed that the absorption of toluidene blue at 630 mμ is markedly affected by the presence of colloidal materials, among these being the micelles of sodium oleate and Aerosol 22. Typical plots of absorbance (− log T), at constant concentration of toluidene blue, as a function of concentration of sodium dodecyl sulfate are shown in figure 1. The absorbance in region A, in which no micelles are present, is sensibly a constant. In region B, the absorbance undergoes a marked change. In region C, in which micelles are known to be present, the absorbance is once more almost constant.

That region B is the region of micelle formation is evident from the following considerations. Let N_0 be the number of dye molecules per unit volume of

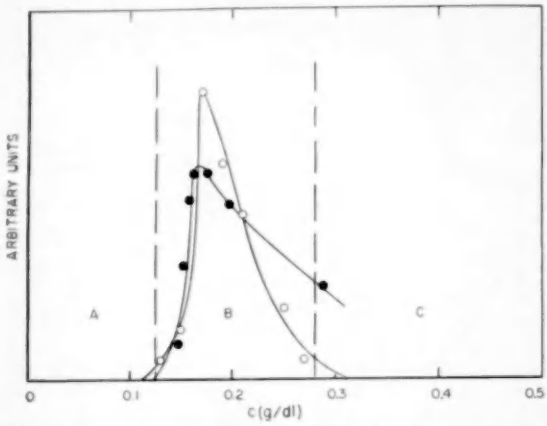

FIGURE 2. *$\Delta(c_m/c)/\Delta c$ versus c as obtained from calculations of Debye for the case $n=65$, and the observed $\Delta(-\log T)/\Delta c$ versus c.*

Hollow circles represent $\Delta(-\log T)/\Delta c$ versus concentration of sodium dodecyl sulfate in distilled water. Black circles indicate $\Delta(c_m/c)/\Delta c$ versus c.

solution, N_m/N_0 the fraction of dye molecules associated with micelles, and N_1/N_0 the fraction not associated with micelles. Assuming that an equilibrium exists between dye molecules associated with micelles and those not, N_m/N_0 should be a function of c_m/c. The observed behavior of the absorbance during a dilution, at constant dye concentration, can then be represented by an equation of the form

$$-\log T = k\frac{N_1}{N_0} + k'\frac{N_m}{N_0}. \qquad (5)$$

When $N_m/N_0=0$, $-\log T=k$ (region A). When $N_m/N_0=1$, $-\log T=k'$ (region C). Region B is then that in which N_m/N_0 goes from 0 to 1, this change arising from the rapid change of c_m/c in the region of micelle formation.

Figure 2 shows a plot of $\Delta(c_m/c)/\Delta c$ versus c as obtained from calculations of Debye [18] for the case $n=65$, and the observed $\Delta(-\log T)/\Delta c$ versus c. The similarity in the general nature of the curves strongly indicates that a close relationship exists between the observed absorbance and c_m/c.

All of the transmission data were obtained with a Coleman model No. 2 Universal Spectrophotometer set at 630 mμ. A known volume of detergent solution of concentration about twice the critical micelle concentration, and containing 0.001 g/dl of toluidene blue was placed in a Nessler tube, which fit into the cell carriage of the spectrophotometer. Dilutions were made by adding known volumes of distilled water or the appropriate sodium chloride solution; they too contained 0.001 g/dl of toluidene blue. After each addition of diluent the solution was stirred and a transmission measurement made.

The identification of the concentration at point D of figure 1 with the monomer saturation concentration would appear to be justified in the light of the following qualitative considerations. As dilution occurs in region C, the absorbance decreases slightly, indicating a slight decrease in the ratio N_m/N_0. This is associated with the decrease in c_m/c that occurs simply as a dilution effect in the region well above micelle formation. However, at point D, c_m/c begins to decrease much faster than can be attributed to dilution only. This must then correspond to the upper limit of the region of micelle formation. If the region of micelle formation is defined as being that in which the fraction of added detergent going into micelles goes from 0 to 1, then it is apparent that D is at the monomer saturation concentration. The point D, at each sodium chloride concentration, was visually estimated from a plot similar to those shown in figure 1. It was taken as that concentration at which, on dilution, the curve begins to deviate from linearity. Choosing a monomer saturation concentration significantly lower than D results in reduced specific viscosity, $(\eta_{rel}-1)/c$), versus concentration of micelle curves that deviate markedly from linearity at low concentrations. Choosing a monomer saturation concentration moderately higher than D causes a negligible change in the intrinsic viscosity. The critical micelle concentrations of sodium dodecyl sulfate as obtained by Corrin and Harkins [20] at various sodium chloride concentrations fall approximately in the center of the regions of micelle formation as determined by this method. The estimated monomer saturation concentrations C_s are indicated in table 1.

4. Discussion

The viscosities of sodium dodecyl sulfate solutions relative to the monomer saturation concentration (η_{rel}) are shown graphically in figure 3. It is to be observed that, at least up to 0.12 N, the presence of added neutral electrolyte lowers the relative viscosity curve, the effect becoming smaller with each addition. The reduced specific viscosities, $\eta_{rel}-1/C_s$, are shown in figure 4. The intrinsic viscosity of the micelles in water is 0.065 dl/g. However, in solvents of increasing salt concentration, it decreases to a limiting value of slightly less than 0.035 dl/g. This trend is shown in figure 5.

The existence of a charge on the kinetic units in these solutions eliminates the possibility of interpreting these data solely as a decrease in the axial ratio of the micelles. The viscosity of dilute solutions of charged spheres has been treated by Smoluchowski [21] and Krasny-Ergen [22]. Both arrived at substantially the same equation, which predicts that the electroviscous effect can be made vanishingly small by the addition of neutral electrolyte to the solution. The contribution of the electroviscous effect is such as to increase the relative viscosity of the solutions, thus resulting in a larger intrinsic viscosity than would be measured in the absence of any charge effects. Figures 3, 4, and 5 can be satisfactorily interpreted from this point of view, the limiting value of the intrinsic viscosity being that for the micelle when the electroviscous effect has become negligibly small.

It is also possible to interpret such data, at least qualitatively, from the point of view of a desolvation

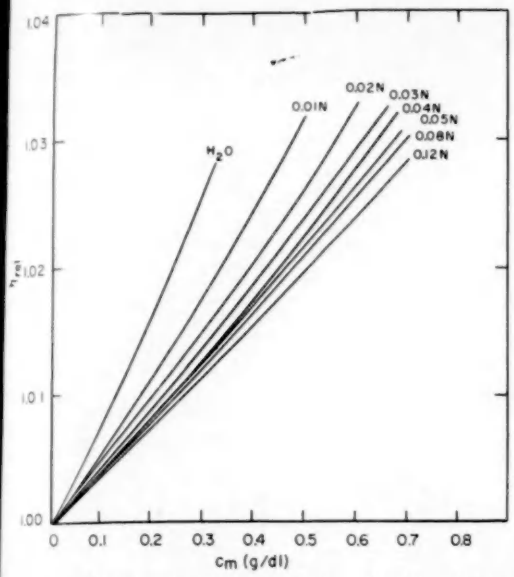

FIGURE 3. *Relative viscosities of solutions of sodium dodecyl sulfate in distilled water and aqueous sodium chloride as a function of c_m.*

In each solvent, the viscosities are relative to the monomer saturation concentration.

process [23]. Such an approach is particularly appropriate to the consideration of aqueous solutions of micelles that have a lyophilic surface. Experiments of McBain [24] have shown that potassium laurate molecules are hydrated to the extent of about 10 molecules of water per soap molecule. Presumably then the micelle, too, could be hydrated. If the micelle is hydrated, thus increasing its kinetic volume and intrinsic viscosity, then the addition of neutral electrolyte would tend to dehydrate the micelle until some limiting volume is reached corresponding to a dehydrated micelle.

From either the charge or solvation considerations, the limiting value of the intrinsic viscosity, as the electrolyte concentration is increased, should be determined by the nature of the micelle exclusive of such effects. It remains to consider the significance of a limiting value of the intrinsic viscosity of slightly less than 0.035 dl/g.

From eq 4, it is seen that the intrinsic viscosity of rigid, noninteracting spheres whose density is unity, is equal to 0.025 dl/g. Since most of the volume of any shape of micelle proposed for sodium dodecyl sulfate is occupied by dodecyl chains in a liquid-like array, it is reasonable to assume that the density of the micelle should be fairly close to that of liquid dodecane, approximately 0.75 at 20° C. Substitution of this value for d in eq 4 gives $[\eta]=0.033$ dl/g for spherical micelles. This is to be compared with the limiting value of 0.035 dl/g that has been obtained in these experiments.

Admittedly this close agreement between the observed and theoretical intrinsic viscosity rests on

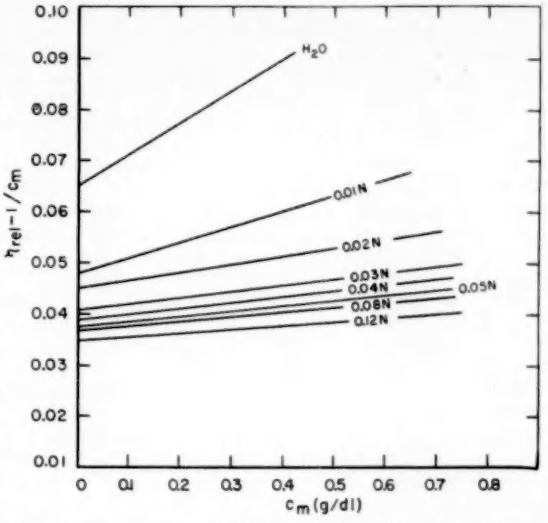

FIGURE 4. *Reduced specific viscosities of sodium dodecyl sulfate solutions as a function of c_m.*

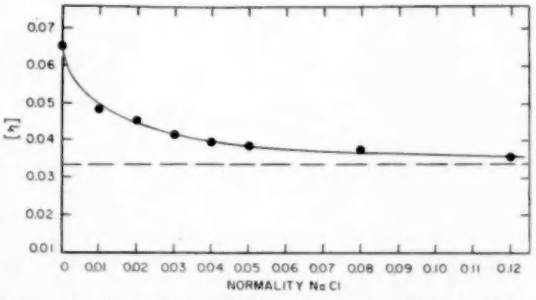

FIGURE 5. *Dependence of the intrinsic viscosity of sodium dodecyl sulfate micelles on concentration of sodium chloride.*

The broken line represents the calculated limiting value for spherical micelles, 0.033 dl/g.

the assumption that the density of the micelles is 0.75. However, additional evidence for the existence of spherical micelles in these solutions is to be obtained from the data. Previous work [18, 13] has indicated that as electrolyte is added to micellar solutions, not only does the region of micelle formation shift to lower concentrations, but the molecular weight of the micelles increases. If this actually occurs, and the micelles herein considered are rods or cylinders having a constant thickness as has been proposed for other detergents, then the axial ratio of the micelles must increase with increasing salt concentration. Such behavior would be evidenced by a corresponding increase in the intrinsic viscosity. This has not been observed.

In conclusion, it is necessary to point out that the assignment of spherical shape to the micelles of sodium dodecyl sulfate has been made on the basis of viscometric data. It is possible that other experimental techniques may favor a different inter-

pretation. Further, the interpretation presented here does not imply the micelles of all detergents are spherical. The molecules of sodium dodecyl sulfate have a very simple structure and shape. However, different detergent molecules may find it sterically or energetically impossible to agglomerate into spherical clusters. It must also be remembered that the data considered in this paper were all obtained from solutions no more concentrated than 0.8 percent in detergent and 0.12 *N* in sodium chloride. An extension of these results to systems having significantly higher concentrations of either would probably be unjustified. Factors other than those considered here would surely come into play. It might, for instance, be energetically more favorable for a large number of small, spherical micelles, close enough for their gegenion clouds to overlap, to coalesce with the formation of a few larger micelles which would probably not be spherical. However, Brady [11] is able to interpret his X-ray diffraction data for 14.71 and 29.42 percent sodium dodecyl sulfate solutions by utilizing the concept of small, spherical micelles.

5. References

[1] F. Krafft, Ber. dent. Chem. Ges. **29,** 1328 (1896).
[2] J. W. McBain, in Colloid Chemistry, edited by J. Alexander, **5,** p. 102 (Reinhold Publishing Corp., New York, N. Y., 1944).
[3] A. E. Alexander and P. Johnson, Colloid Science, **II,** p. 669 (Oxford University Press, London, 1949).
[4] J. W. McBain, Colloid Science, p. 255 (D. C. Heath & Co., Boston, 1950).
[5] G. S. Hartley, Aqueous Solutions of Paraffin-Chain Salts, (Hermann et Cie, Paris, 1936).
[6] G. S. Hartley, B. Collie, and C. S. Somis, Trans. Faraday Soc. **32,** 795 (1936).
[7] K. Hess, Fette u. Seifen, **49,** 81 (1942); K. Hess and J. Gundermann, Ber. deut. Chem. Ges. **70,** 1800 (1937).
[8] W. Philippoff, Kolloid-Z. **96,** 255 (1941); J. Colloid Sci. **5,** 169 (1950).
[9] H. Kiessig, Kolloid-Z. **96,** 252 (1941); J. Stauff, Kolloid-Z. **89,** 224 (1939); **96,** 244 (1941); S. S. Marsden and J. W. McBain, J. Phys. & Colloid Chem. **52,** 1100 (1948); W. D. Harkins, R. W. Mattoon, and M. L. Corrin, J. Am. Chem. Soc. **68,** 220 (1946).
[10] W. D. Harkins, J. Chem. Phys. **16,** 156 (1948); R. W. Mattoon, R. S. Stearns, and W. D. Harkins, J. Chem. Phys. **16,** 644 (1948).
[11] G. W. Brady, J. Chem. Phys. **19,** 1547 (1951).
[12] M. L. Corrin, J. Chem. Phys. **16,** 844 (1948).
[13] P. Debye and E. W. Anacker, J. Phys. & Colloid Chem. **55,** 644 (1951).
[14] L. Shedlovsky, Ann. N. Y. Acad. Sci. **46,** Art. 6, 427 (1946).
[15] J. F. Swindells, J. R. Coe and T. B. Godfrey, J. Research NBS **48,** 1 (1952) RP2279.
[16] G. Barr. A Monograph of Viscometry (Oxford University Press, London, 1931).
[17] K. A. Wright and H. V. Tartar, J. Am. Chem. Soc. **61,** 544 (1939).
[18] P. Debye, Ann. N. Y. Acad. Sci. **51,** Art. 4, 575 (1949).
[19] L. Michaelis, J. Phys. & Colloid Chem. **54,** 1 (1950).
[20] M. L. Corrin and W. D. Harkins, J. Am. Chem. Soc. **69,** 683 (1947).
[21] M. von Smoluchowski, Kolloid-Z. **18,** 194 (1916).
[22] W. Krasny-Ergen, Kolloid-Z. **74,** 172 (1936).
[23] H. R. Kruyt, Colloid Science, **II,** p. 209, (Elsevier Publishing Co., New York, N. Y., 1949).
[24] J. W. McBain, J. Kawakami, and H. P. Luca, J. Am. Chem. Soc. **55,** 2762, 2763 (1933).

WASHINGTON, D. C., April 22, 1952.

Journal of Research of the National Bureau of Standards Vol. 49, No. 2, August 1952 Research Paper 2347

Absorption Spectrum of Water Vapor Between 4.5 and 13 Microns [1]

W. S. Benedict,[2] H. H. Claassen,[3] and J. H. Shaw[4]

The absorption spectrum of water vapor has been measured from 4.5 to 13 microns with a 3,600 line per inch replica echelette grating as the dispersing element. Various absorbing path lengths and concentrations of water vapor at atmospheric pressure were used up to 8 meters of steam near 110° C. Almost all of the previously unreported lines that have been found are also present in the solar spectrum. A rotational analysis shows that most of the lines can be assigned either to rotational transitions or to rotation-vibration transitions of the ν_2 fundamental of the water-vapor molecule. In addition, a few lines have also been assigned to the transitions $(2\nu_2-\nu_2)$, $(\nu_1-\nu_2)$, and $(\nu_3-\nu_2)$.

1. Introduction

Investigations of the infrared spectrum of sunlight between 7 and 13 μ have shown that essentially all the structure is due to absorption by polyatomic gases that are in the earth's atmosphere. In addition to the known bands of ozone, carbon dioxide, water vapor, nitrous oxide, and methane that have been identified in this region, there is also a large number of irregularly spaced absorption lines. Some of these lines are very strong. In solar spectra taken at Columbus, it has been observed that most of their intensities are dependent on the amount of water vapor in the atmosphere. One of us (W.S.B.) had previously found that many of these lines observed in the grating map of the solar spectrum published by Adel [1][5] could be predicted from the known energy levels of the water-vapor molecule. To obtain a positive identification of these lines, it was thought desirable to observe them in a laboratory spectrum. If these lines are due to water vapor, most of them must originate from the higher rotational energy levels of the molecule, which have a low population at room temperature. Thus, in order to observe them in the laboratory, an absorbing layer giving an optical path length approaching that of the water vapor in the atmosphere is required. In this work a long path length was obtained by using a multiple-reflection cell similar to that described by J. U. White [2]. From this laboratory spectrum it has been possible to identify many lines in the solar spectrum with water-vapor lines and also to evaluate rotational energy levels of the ν_2 band and of the pure-rotation band, which are in good agreement with levels derived from other observations.

2. Apparatus and Experimental Procedure

The absorption cell used in this investigation is shown schematically in figure 1. It consists of a large cast-aluminum tank wound with heating coils and covered with a layer of asbestos for insulation. One end is held in place by bolts and can be completely removed for adjusting the optical system. Three spherical mirrors, each of 100-cm radius of curvature, are used in the optical system. Mirror M_3 is fixed, but an external control is provided for varying the inclination of the optic axes of mirrors M_1 and M_2. By means of this adjustment the path length of radiation passing through the cell can be changed in steps of 4 m. Figure 1 shows the arrangement for a path length of 8 m.

Rocksalt windows could not be used in this investigation, and it was found that silver-chloride windows reduced the energy very considerably. Satisfactory results were obtained by placing the Nernst filament, used as a source, inside the cell near mirror M_3 and leaving the exit window open. Radiation was reflected out of the cell and through this window by a small plane mirror.

Before introducing the steam, the cell was heated to 110° C to prevent condensation on the mirrors. The cell was filled with steam by displacement. When running spectra, a continuous stream of vapor from a gently boiling flask of distilled water entered at one end and escaped through the exit window.

For mapping regions of high absorption, air was allowed to enter the cell until a suitable concentration of water vapor was obtained. Near the center of the ν_2 fundamental the atmospheric water vapor in the spectrometer alone was sufficient to produce very intense absorptions. The region from 5.7 to 6.7 μ has been previously mapped by H. H. Nielsen [3] with very high resolution and with small amounts of water vapor. The present workers were unable to improve upon these results, and this region has not been remeasured. In the solar spectrum no energy is observed between 5.5 and 7.5 μ at Columbus during most of the year.

The spectrometer with which these measurements were made has already been described [4]. For this work a 3,600 line/in replica echelette grating (width 5.5 in., height 3.5 in.) was used, together with a Perkin-Elmer thermocouple (rated sensitivity 8 v/w) detector and their 13 c/s chopping system and amplifier. All spectra were recorded in the first order of the grating. Portions of the spectrum at short wavelengths were also scanned in the second

[1] The research reported in this paper was supported in part by the ONR, and in part by contract AF 19 (122)-65 between the U. S. Air Force and the Ohio State University Research Foundation through sponsorship of the Geophysics Research Division of the U. S. Air Force Cambridge Research Center.
[2] Present address, The Johns Hopkins University, Baltimore, Md.
[3] Department of Physics, University of Oklahoma, Norman, Okla.
[4] The Ohio State University, Columbus, Ohio.
[5] Figures in brackets indicate the literature references at the end of this paper.

FIGURE 1. *Multiple reflection cell.*

order, but no improvement in the resolution was found.

After the spectrum of the 8-m path of water vapor had been obtained, the entire region was scanned by using the atmospheric path in the spectrometer alone. In this background spectrum, a line was found at 791 cm^{-1}, which agrees in position with the Q-branch of a band of carbon dioxide. It is very weak in the laboratory spectrum and is probably caused by the carbon dioxide in the air path of the spectrometer.

To obtain the spectrum, small portions, corresponding to the rotation through 1 deg of the grating circle, were scanned. The rocksalt foreprism was adjusted for maximum energy in the middle of each degree, which was then run at least twice in each direction. Fiduciary marks were made on the chart paper by a mechanical trigger device operated by an observer viewing coincidences of the grating circle markings with a graduated scale in the eyepiece of a microscope. The "central image" corresponding to the position of the grating for zero-order diffraction was measured during each day's work, in both directions. It was found to vary a few seconds of arc from day to day.

Frequencies were calculated by using the formula

$$\nu = nK/\sin\theta,$$

where n is the spectral order, ν the frequency, K is a constant, and θ is the angular displacement from the central image. K was determined from measurements of the 0.546073-, 0.576960-, and 0.579066-μ mercury lines in the orders from 10 to 16 using a low-pressure (H-2) mercury arc as a source and a 931A photomultiplier tube as detector. These measurements gave an average value for K of 722.506 ± 0.025 cm^{-1}.

The four or more frequency measurements obtained for each line, including scannings in both directions, were averaged. These frequencies were then corrected to vacuum by assuming the laboratory air had an average refractive index of 1.0002565, corresponding to a barometric pressure of about 740 mm Hg and a temperature of 25° C.

3. Results

A map of the water-vapor spectrum from 4.5 to 13 μ is shown in figures 2 to 6, with the exception of a short interval from 5.7 to 6.6 μ, where water-vapor absorption is very intense. To reach the longest wavelengths, the grating had to be used at extreme angles to the incident radiation, and very little energy was obtained even with the widest slits permissible. This accounts for the small deflection shown in figure 2 beyond 12 μ. As short portions of the spectrum were run individually, the total energy varied slightly, giving the segments shown in the figures. The approximate amounts of water vapor in the path for each region are given in the captions of the figures, as well as the temperature of the cell or spectrometer. It should be noted that when a temperature of 110° C is indicated, this refers to the temperature of the absorption cell. There was always some water vapor in the spectrograph at about 25° C, also contributing to the absorption. This contribution is quite negligible when the cell contains steam at atmospheric pressure. The regions near the center of the 6.3-μ band were run with only the air path in the spectrometer. Although spectra were recorded on a cold, dry day in February, many lines were still more intense than was desired.

The effective slit widths used varied from 0.22 cm^{-1} at 13 μ to 0.83 cm^{-1} at 5 μ. These slit widths were approximately the same as those used in the investigation of the solar spectrum. Under these conditions the lines in the laboratory spectrum were wider than corresponding lines in the solar spectrum. Consequently, some lines clearly separated in the solar spectrum are blended in the laboratory spectrum. The increased line width observed in the spectrum of steam is caused both by the higher temperature and the much higher concentration of water vapor, giving a marked self pressure broadening effect. Approximately the same deflections were obtained in windows between absorption lines whether the cell was full of steam or air, indicating that there was little continuous absorption by water vapor in these windows. Thus the wings of water-vapor lines lying outside the region investigated played an insignificant part in the absorption observed.

The lines have been numbered in order of increasing frequency in the figures as an aid to their identification in table 1. The line number is given in the first column of this table and the observed frequency, corrected to vacuum, in the second.

It is believed that the absolute values for the frequencies of well-defined lines are correct to better than 0.2 cm^{-1} at short wavelengths and to 0.1 cm^{-1} elsewhere. Most line frequencies have been given to 0.01 cm^{-1}, but some of the very weak lines that are difficult to measure accurately are listed to the nearest 0.1 cm^{-1}. A number of absorptions can be seen to consist of more than one line, and here the frequency of the position of the maximum absorption is listed to the nearest 0.1 cm^{-1}. Scattered radiation did not amount to more than 10 percent of the total deflection anywhere in the region measured and would not give rise to any spurious lines.

When the solar spectrum is compared with the laboratory spectrum, it is found that the relative intensities of some of the lines are very different.

This is to be expected because the amount of water vapor in the atmospheric path traversed by the solar radiation varies between 1,000 to 10,000 atm-cm and is at an average temperature of about 14° C, whereas the laboratory path was only 800 atm-cm but at a temperature of 110° C. The higher temperature of the laboratory sample gave intensities comparable with those in the solar spectrum to lines that originate from higher energy levels. However, lines arising from low-energy levels are little affected by the change in temperature from 14° to 110° C, and these lines were very weak or completely absent from the laboratory spectrum, although they may be quite prominent in the solar spectrum. This is illustrated by figures 7 and 8, which show small portions of the solar and laboratory spectra for comparison, together with the calculated spectra for the corresponding temperatures. The calculated spectra are schematically shown by drawing each line as a triangle, the width corresponding to geometric slit width used in the observed spectra, and the altitude proportional to the logarithm of the calculated intensity. The solar spectrum in figure 8 was observed during a cold winter day when the water-vapor content of the atmosphere was unusually low; so the calculated intensities for 14° C of table 1 were arbitrarily divided by 5 and plotted on the logarithmic scale indicated in the figure. Figure 7 also illustrates the greater line width of the laboratory steam spectrum than that of the solar spectrum.

In a number of cases where laboratory lines are very weak, or where several lines are blended, it is believed that more accurate frequencies can be obtained from the solar spectrum. Lines that appear in both spectra, but for which the frequencies from the solar spectrum have been used because they seem more reliable, are indicated by a dagger (†) in table 1. A few lines which appear only in the solar spectrum, but which can be fairly positively identified with water vapor because their intensities change with the amount of water vapor in the atmosphere or because they are theoretically predicted, have also been included in the table. Such lines have a dash in place of a line number.

The observed intensities of the lines are given in the next four columns. The first column gives the intensities of lines observed in the solar spectrum. A question mark in this column indicates that the intensity is uncertain because of absorption by other gases in the atmosphere. The values given are for "average" conditions of humidity and altitude of the sun. The intensity scale is very approximate, but runs from 0 to 100, corresponding roughly to percentage absorption at the maximum. The next three columns give intensities as observed under various laboratory conditions; first, when water in the spectrometer alone was sufficient; next, when steam was diluted to a small fraction of its maximum value; and finally, when the full path of 800 atm-cm was used. Figures 2 to 6 may be consulted for details. The steam was diluted over a wide range of concentrations so that the intensities for the diluted water vapor should be compared only for lines in the same neighborhood. In general, the absolute intensities of lines in the solar spectrum and the laboratory spectrum of the long path length of steam are roughly the same, although the intensities of the atmospheric lines vary considerably, depending on the altitude of the sun, the humidity, and the temperature of the atmosphere.

The sixth column of table 1 gives the identification of the line; or, if several transitions overlap to give an unresolved blend, the strongest components are listed. The identification consists of a letter symbol for the vibrational transition involved, the rotational quantum numbers of the upper state, J'_τ, and those of the lower state, J''_τ. The letter symbol a refers to pure-rotation transitions within the ground vibrational level. All identified lines with frequencies below 890 cm^{-1} are of this type, and they predominate up to 1,000 cm^{-1}. Near 1,000 cm^{-1} is a region of minimum absorption by water vapor. At lower frequencies the pure-rotation lines become stronger, and at higher frequencies those of the ν_2 band rapidly increase in intensity. The symbol b identifies transitions in the ν_2 fundamental. The remaining strong lines in the laboratory spectrum belong to this band. In addition, a few weak lines have been assigned to bands in which ν_2 is the lower state: c refers to the transition $2\nu_2-\nu_2$, d to $\nu_1-\nu_2$, and e to $\nu_3-\nu_2$.

The seventh column gives the calculated frequencies derived from the term values of the corresponding rotational states. These are listed for the three lowest levels in table 2, which has been compiled partly from the present research, and partly from an extensive reinvestigation of the complete water-vapor spectrum. The term values of the upper states of bands d and e have previously been given by Benedict and Plyler [5]. A calculated frequency in table 1 is the difference between two energy levels, J'_τ and J''_τ, involved in the transition. The calculated frequencies of a few lines have been placed in parentheses because in each case one of the levels concerned has been located by means of the observed line. These assignments depend on approximate predictions of the levels from extrapolations of regularities among the reliably known levels and on the agreement between calculated and observed intensities. For the remaining lines, however, other observed transitions connect the levels in question, and the agreement between observed and calculated frequencies is a true measure of the consistency of the measurements and the interpretation of the H_2O spectrum.

The final columns of table 1 list relative values of the calculated intensities, for temperatures of 14° and 110° C. These temperatures approximately correspond to the average temperature in the solar and laboratory spectra, respectively. The tabulated numbers are, for 14° C, $v(LS)ge^{-E''/kT}\cdot 10^6$, where (LS) is the line strength, as defined and tabulated by Cross, Hainer, and King [6], g is the statistical weight, and E'' is the energy of the lower state (from table 2). v is a numerical factor for the intensity of the vibrational transitions relative to the pure-rotation band, which will be discussed presently. The factor 10^6 was arbitrarily chosen so that medium-strength lines

in the solar spectrum have intensities of the order of unity. For 110° C the factor was reduced to 10^5 to compensate for the increased Boltzmann factor.

For the pure-rotation band, it is possible to calculate intensities on an absolute basis, since all quantities in the theoretical formula

$$\int k_\nu d\nu = \frac{8\pi^3 N}{3hcQ} p^2 \nu_0 (LS) g e^{-E''/kT}$$

are known. $\int k_\nu d\nu$ is the integrated intensity of a line, N, h, c, and k are universal constants, Q is the state-sum, $\Sigma g e^{-E''/kT}$, and p is the static dipole moment, 1.86 Debye units. In order to convert our tabulated values for the pure-rotation band to the integrated intensity in units of $cm^{-2}atm^{-1}$, one must multiply by $2.19\times10^{-7}\times\nu(cm^{-1})$, at 287° K; at 383° K the factor is $1.07\times10^{-6}\times\nu(cm^{-1})$.

Not all of the transitions found in the course of this study are listed in the tables of reference [6]. The extension to $J\geq12$ requires a moderate extrapolation. Transitions in the $R_{5,\bar{5}}$ branch do not appear in their tables; according to a communication from Professor Cross, the line strength in nearly all these lines is less than 0.0001. For such lines the intensities have been estimated, and are placed in parentheses in table 1; the relative intensities at the two temperatures are significant, but the values may be in error by an order of magnitude.

The observed intensity of relatively weak lines in the pure rotation band, in both the solar and laboratory spectra, appear to be in fair agreement with the calculated absolute intensity. For example, the calculated intensity of line number one ($16_{-8}-15_{-10}$) is $\int I_\nu d\nu = 0.45\times2.19\times10^{-7}\times760 = 7.3\times10^{-5}cm^{-2}atm^{-1}$. If the atmospheric path is 5×10^3 atm-cm, the equivalent width should be 0.36 cm^{-1}, which is of the same order as given by the observed maximum absorption of 45 percent, assuming that the line has a half-width 0.10 cm^{-1} and is observed with a slit width of 0.22 cm^{-1}. For the steam path of 800 atm-cm the calculated equivalent width of the same line becomes $1.6\times1.07\times10^{-6}\times760\times800 = 1.04$ cm^{-1}, again in order of magnitude agreement with the observed maximum absorption of 68 percent for a line of half-width 0.4 cm^{-1}.

For lines in ν_2, and in the upper-state bands, the absolute value of the theoretical intensity cannot be calculated, as it depends on the empirical factor v. The following values of v were chosen by which to multiply the pure-rotation intensities, in order to obtain fair over-all agreement with the observed intensities:

Band	$b(\nu_2)$	$c(2\nu_2-\nu_2)$	$d(\nu_1-\nu_2)$	$e(\nu_3-\nu_2)$
Factor	0.005	0.01	0.0002	0.001

These result in lines of the observed order of magnitude and are not unreasonable. The ν_2 intensities, calculated in this way, appear to be somewhat weaker than the observed intensities, in the region 900 to 1,050 cm^{-1}, and somewhat stronger than the observed intensities in the region 2,000 to 2,200 cm^{-1}, by a factor of 2 or 3 in each case. These effects, which may be in part due to the greater effective slit width in the short-wave region, are similar to those encountered in other bands of H_2O, and even more strikingly in H_2S and other asymmetric-top molecules. An explanation of these effects has recently been proposed by Nielsen [7]. The anomaly in ν_2 of H_2O does not appear outstandingly large in the portions of the P and R branches near the origin, but is confined to the transitions of high J and those in which K changes by more than 1.

4. Discussion

The agreement between the observed and calculated spectra as given in table 1, and illustrated in figures 7 and 8, is quite complete, and argues well both for the accuracy of the measurements and the correctness of the interpretation. The lines not accounted for constitute less than 1 percent of the total absorption intensity. A few of the assignments to transitions of highest J, in both the pure-rotation spectrum and in ν_2, are rather uncertain. It would be desirable to obtain further accurate measurements of steam in the region 550 to 770 cm^{-1} and of superheated steam or H_2-O_2 emission spectra throughout the rest of the vibration-rotation region, for confirmation. However, all the lower energy levels, up to $J=10$, are well accounted for, in that all predicted lines appear with approximately the correct intensity and frequency, and that no strong lines remain unidentified.

An additional demonstration that the spectral analysis is quite complete and essentially correct is afforded by the arrangement of the lines into series. Table 3 presents the lines of the four prominent P branches of the ν_2 vibration-rotation band, grouped in such a way as to display the regular decrease in frequency with increasing J. A similar array may be made for the lines in the R branches, as well as for the Q branch lines, most of which, however, lie in the central region not measured in this study. Frequencies in parentheses are those of weak lines overlapped by a stronger component. It is clear, by a comparison of tables 3 and 1, that the identification of many lines of higher J cannot be expected without an increase of the path length, or, preferably, by increasing the temperature. As mentioned before, there is a distinct difference in temperature coefficient between the weaker lines of the $P_{1,\bar{1}}$, $P_{\bar{1},\bar{1}}$, and $P_{\bar{1},1}$ branches, which have relatively high transition probabilities but originate from high-energy levels, and those of the $P_{\bar{2},1}$ branch (as well as the few identified lines of the $P_{\bar{2},3}$ branch, not included in table 3), which have lower line strengths but originate from lower energy levels. This difference manifests itself in the changed relative intensities in the laboratory and solar paths.

Table 4 is a similar presentation of the lines of the low-probability branches of the pure-rotation band.

For completeness, there are included lower lines of the series as observed by other investigators [12, 13] in the farther infrared, as well as frequencies, in parentheses, of lines that have not yet been measured with high accuracy. A comparison with table 1 again shows that the suggested array accounts for most of the observed lines from 760 to 1,000 cm^{-1}, with the lines that are most enhanced in the atmosphere belonging, for the most part, to the more highly forbidden $R_{5,\bar{5}}$ and $R_{5,\bar{5}}$ series.

The energy levels of ν_2, which are now known with completeness and good precision up to $J=9$, permit an improved determination of the rotational constants for that vibrational level. The method is described elsewhere. Figure 9 presents the effective rotational constant A'_J, B'_J, and C'_J for each J, derived from the levels of table 2, plotted against $J(J+1)$. The points are seen to fall nicely on smooth curves. The intercepts give the rotational constants A, B, and C, and the limiting slopes give the centrifugal stretching constants D_A, D_B, and D_C. These are listed in table 5 and compared with the corresponding constants of the ground state. There is an appreciable curvature in the plot of A'_J, showing that centrifugal stretching terms of higher order are important at relatively low J.

The few weak lines that are not assigned may be transitions of higher J in ν_2, upper-state transitions, or lines in the isotopic molecules H_2O^{18} or HDO. The calculated vibrational shift for ν_2 of H_2O^{18} is -6.5 cm^{-1}; this shift would be increased for lines in the R branch and diminished in the P branch. Tentative assignments of some of the observed lines can be made on this basis; for example, line 285 (1414.99 cm^{-1}), which lies 4.3 cm^{-1} below the strong line 3_3-4_3, and line 353 (1764.22 cm^{-1}), which lies 8.4 cm^{-1} below the strong line 3_3-2_1, have the proper intensity ratio (1:500) and positions to be their analogues in H_2O^{18}. Other such possible lines are suggested in the table. It should be noted that, on the basis of the expected relative intensities, it would be very unlikely that many absorption lines due to HDO would appear. Although absorption due to the ν_2 band of this isotope has been postulated by Adel [8] in the 7.2 μ region of the solar spectrum, and the ν_1 fundamental has been definitely observed, resolved, and analyzed in the solar spectrum at 3.7 μ [9, 10], the intensity of the lines of the ν_2 fundamental of HDO relative to those of H_2O on our spectra would be very small. The frequencies of the ν_2 fundamental of HDO published by Barker and Sleator [11] do not show any definite coincidences with our data. There should, however, be a number of fairly strong lines at lower frequencies than their work reached, which would lie in the region of weaker H_2O absorption and might thus appear as weak lines in our spectra. For example, on the basis of the known structure of HDO, we calculate that the line 3_3-4_3 should fall near 1,250 cm^{-1}. Line 183, otherwise unaccounted for, has about the proper intensity in both laboratory and solar spectra for this transition.

It may also be of interest to point out that the completeness of the assignment, and the fact that the intensity differences in the spectra between atmospheric water vapor and nearly saturated steam can be explained in detail on the basis of temperature, is strong evidence, although of a negative sort, against the existence of $(H_2O)_2$ molecules in the saturated vapor. The association of H_2O in the liquid phase is abundantly proved by the marked lowering of frequency in the ν_3 fundamental and a somewhat smaller shift in ν_2. The existence of dimers in the vapor has often been postulated to account for changes in density, dielectric polarization, etc., near saturation. If such dimers exist as molecules with quantized vibration-rotation states, the evidence of the present study would be that their concentration, relative to H_2O monomer, must be less than 1 percent, since in the region of 1,400 cm^{-1}, where $(H_2O)_2$ should be most strongly absorbing, the unaccounted-for absorption is very small. We have mentioned[1] previously that the steam spectrum shows a somewhat greater line width than the atmospheric spectrum, but there is no appreciable frequency shift, and the amount of self-broadening is by no means abnormally large for a polar molecule.

5. References

[1] A. Adel, Astrophys. J. **94,** 451 (1941).
[2] J. U. White, J. Opt. Soc. Am. **32,** 285 (1942).
[3] H. H. Nielsen, Phys. Rev. **59,** 565 (1941).
[4] J. H. Shaw, R. M. Chapman, J. N. Howard, and M. L. Oxholm, Astrophys. J. **113,** 268 (1951).
[5] W. S. Benedict and E. K. Plyler, J. Research NBS **46,** 246 (1951) RP2194.
[6] P. C. Cross, R. M. Hainer, and G. W. King, J. Chem. Phys. **12,** 210 (1944).
[7] H. H. Nielsen, Phys. Rev. **83,** 838 (1951).
[8] A. Adel, Astrophys. J. **93,** 509 (1941).
[9] R. M. Chapman and J. H. Shaw, Phys Rev. **78,** 71 (1950).
[10] W. Benesch, J. Strong, and W. S. Benedict, Progress Report to ONR, Contract N50ri–166 (Aug. 1, 1950).
[11] E. F. Barker and W. W. Sleator, J. Chem. Phys. **3,** 660 (1935).
[12] H. M. Randall, D. M. Dennison, N. Ginsburg, and L. R. Weber, Phys. Rev. **52,** 160 (1937).
[13] L. R. Weber and H. M. Randall, Phys. Rev. **40,** 835 (1932); C. S. Rupert, J. H. Taylor, and J. Strong, private communication.

212644—52——4

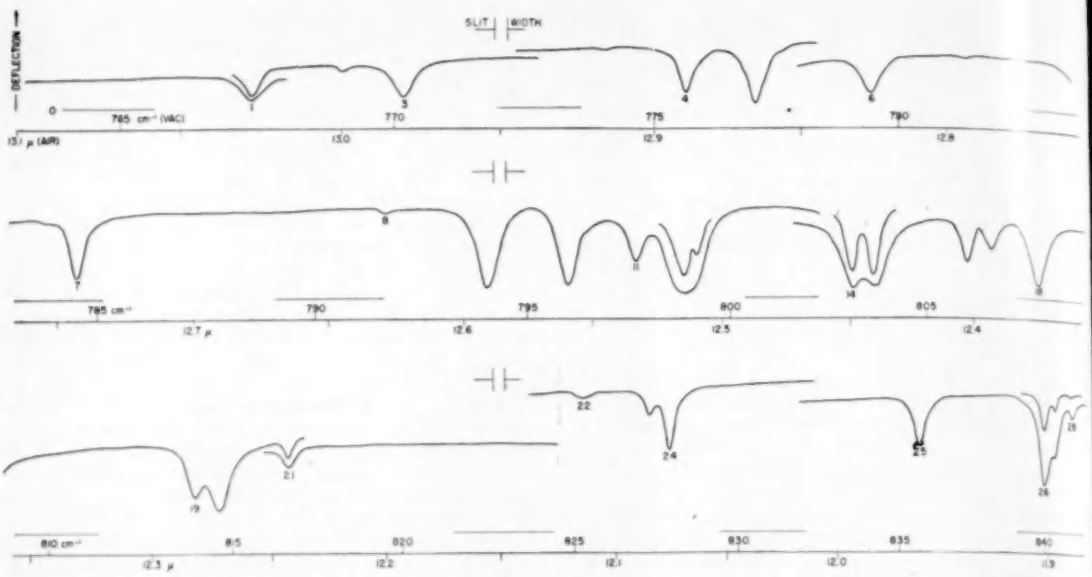

FIGURE 2. *Absorption spectrum from 11.9 to 13.1μ of an eight meter path of water vapor at 110°C and one atmosphere pressure.*

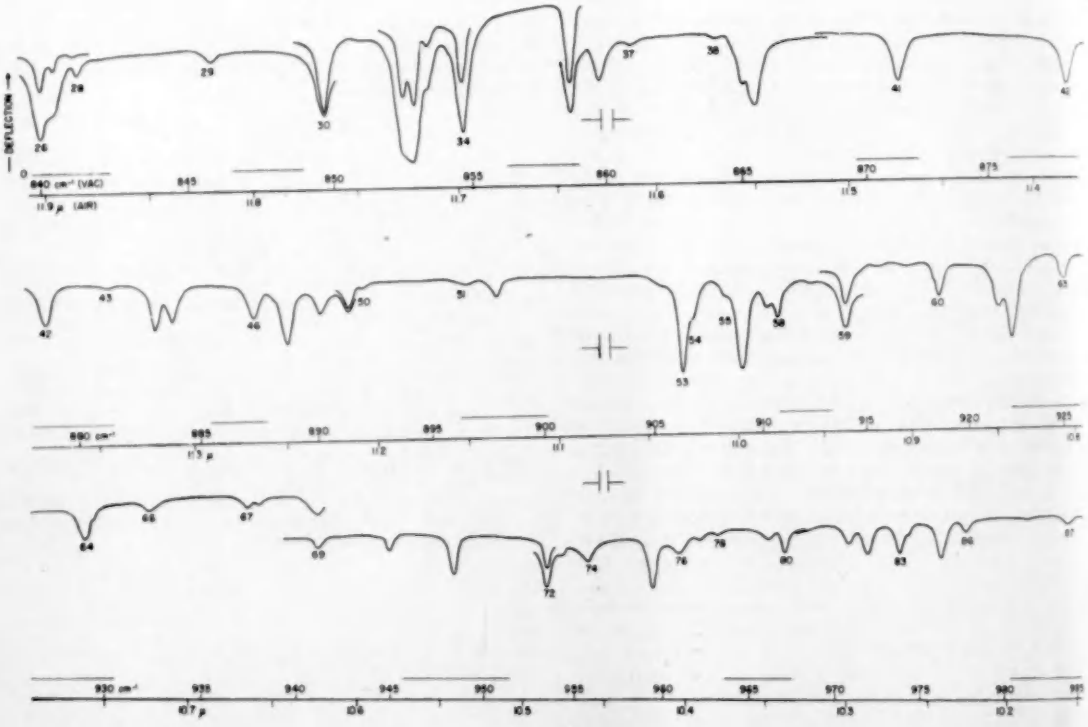

FIGURE 3. *Absorption spectrum from 10.2 to 11.9μ of an eight meter path of water vapor at 110°C and one atmosphere pressure.*

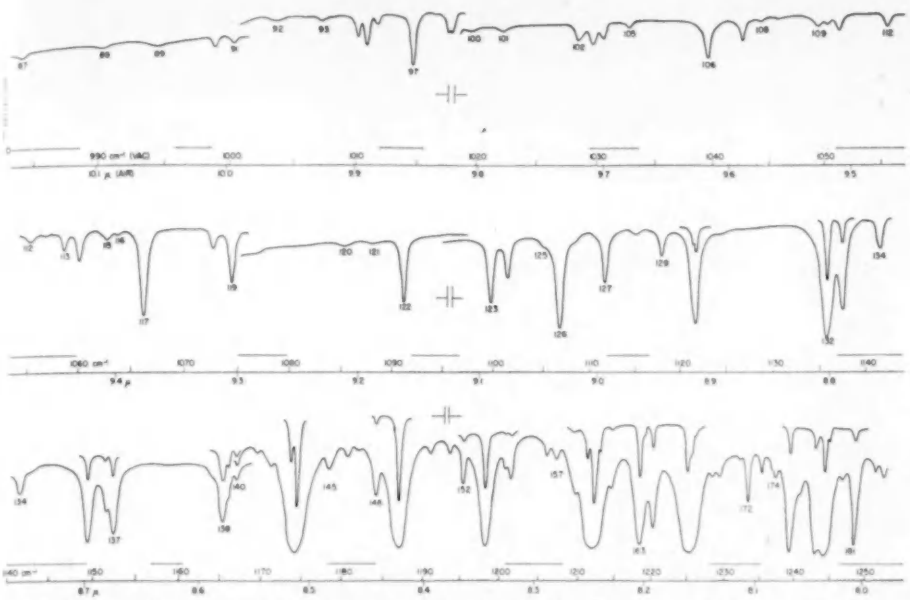

FIGURE 4. *Absorption spectrum from 10.2 to 11.9μ of an eight meter path of water vapor at 110°C and one atmosphere pressure and with small sections also at lower concentration.*

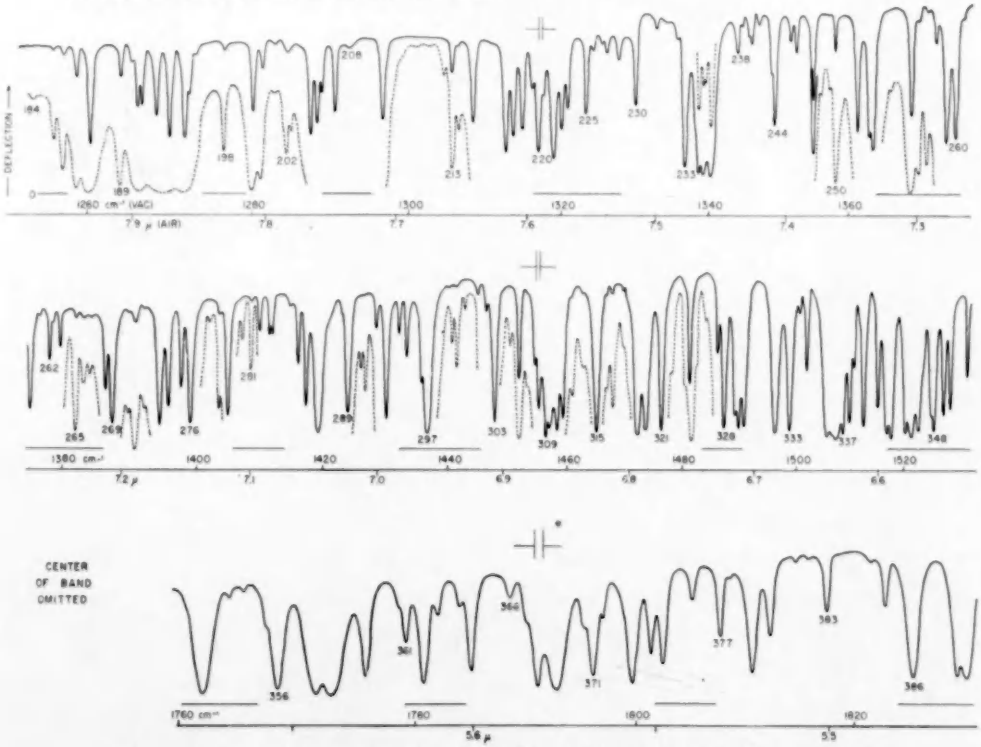

FIGURE 5. *Absorption spectrum from 5.5 to 5.7μ and from 6.6 to 8.0μ of water vapor.*

Solid line refers to water vapor in the air of the spectrometer at approximately 25°C, dotted line to an eight meter path at 110°C and various concentrations of water vapor in air.

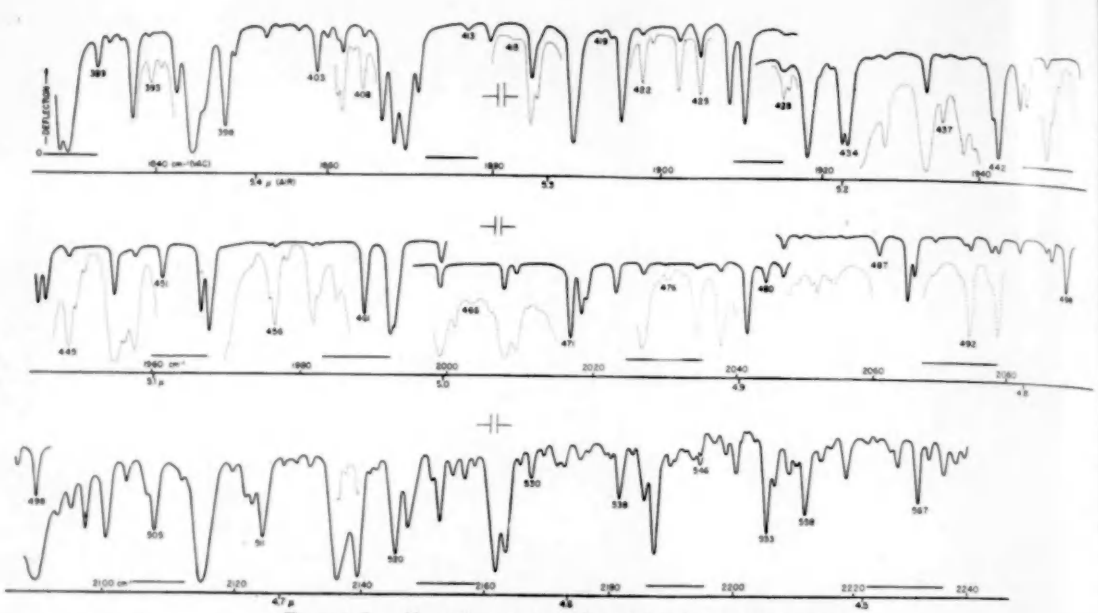

FIGURE 6. *Absorption spectrum from 4.5 to 5.5μ of water vapor.*

(A) Solid line refers to water vapor in spectrometer at approximately 25°C, dotted line to an eight meter path at 110°C and various concentrations of water vapor in air; (B) eight meter path at one atmosphere and 110°C.

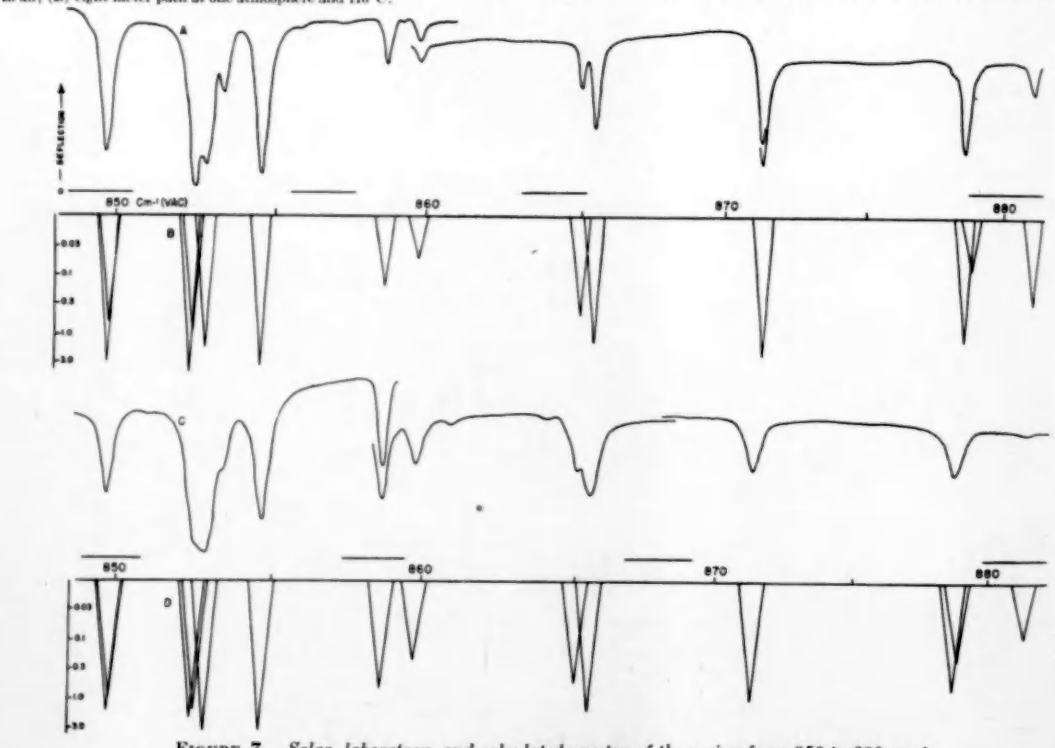

FIGURE 7. *Solar, laboratory, and calculated spectra of the region from 850 to 880 cm⁻¹.*

(A) Solar spectrum taken in August, 1950; (B) calculated spectrum at 14°C; (C) laboratory spectrum of an eight meter path of steam at one atmosphere and 110°C; (D) calculated spectrum at 110°C.

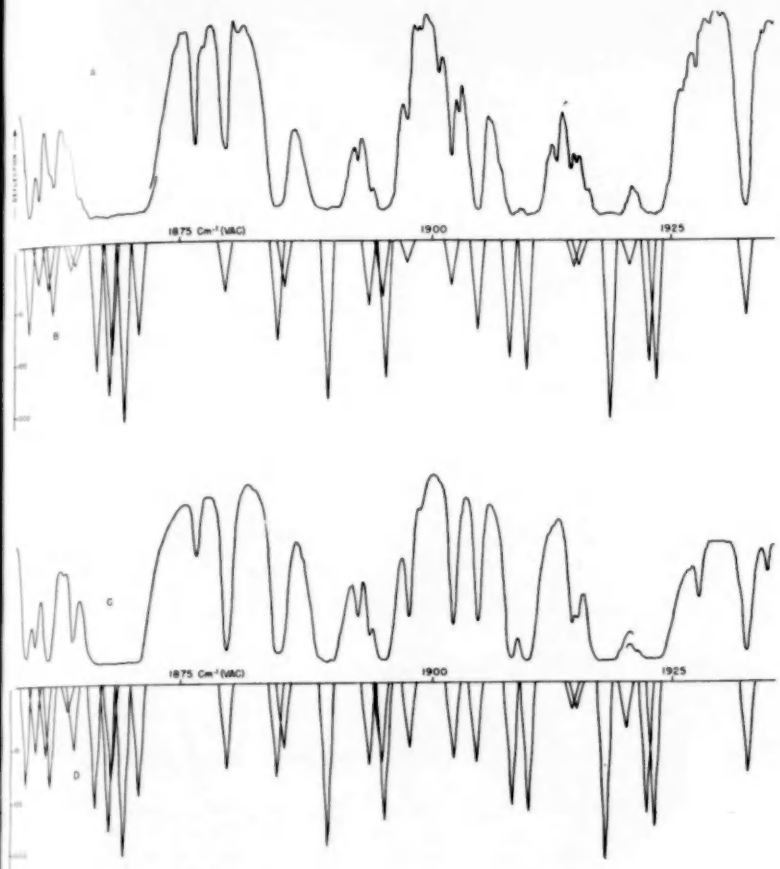

FIGURE 8. *Solar, laboratory and calculated spectra of the region from 1860 to 1925 cm⁻¹.*

(A) Solar spectrum taken in February 1951, with an air temperature of −15°C; (B) calculated spectrum at 14°C; (C) laboratory spectrum of a four meter path of steam at 110°C and nearly one atmosphere; (D) calculated spectrum at 110°C.

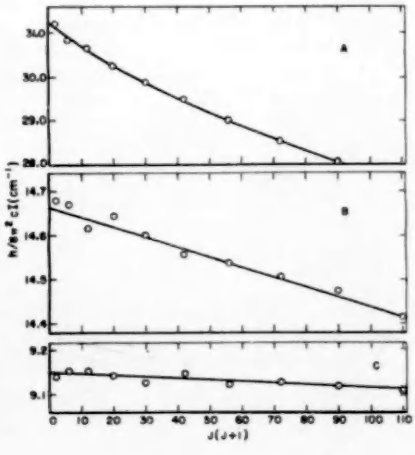

FIGURE 9. *Curves from which may be derived the inertial and centrifugal stretching constants associated with rotation about the three axes of inertia: (A) The least axis; (B) the intermediate axis; (C) the greater axis.*

TABLE 1. Absorption Spectrum of H_2O between 4.5μ and 13 μ.

Line Number	OBSERVED DATA: Wave Number cm⁻¹ (vac)	Intensity: Solar	Intensity: Laboratory: Air only	Intensity: Laboratory: 110° C (20 Atmos)	Intensity: Laboratory: 110° C (5 Atmos)	Identification $J'_\tau - J''_\tau$	CALCULATED DATA: Wave Number cm⁻¹ (vac)	Intensity: 14° C	Intensity: 110° C
1	767.37	45	0	-	68	a 16_{-8} — 15_{-10}	(67.4)	0.44	1.6
2	769.1	50?	0	-	13	a 7_5 — 6_{-5}	69.15	(0.7?)	(0.12?)
3	770.17	60?	0	-	75	a 12_2 — 11_{-4}	70.17	3.6	3.5
4	775.63	30?	0	-	73	a 12_{-2} — 11_{-8}	75.63	6.4	4.6
5	777.07	60?	0	-	94	a 10_5 — 9_1	77.09	11	7.5
6	779.36†	46	0	-	72	a 10_6 — 9_0	79.41	3.7	2.5
7	784.54	60?	0	-	73	a 11_{-3} — 10_{-9} a 16_{-7} — 15_{-11}	84.62 (84.54)	18 1.2	7.2 4.3
8[g]	791.6	-	5	-	5				
9	794.01	53?	0	-	89	a 13_{-1} — 12_{-7}	94.01	6.4	8.0
10	796.01	85	0	-	88	a 10_1 — 9_{-7}	96.08	20	8.1
11	797.65	50	0	-	56	a 11_4 — 10_0	97.66	2.3	1.9
12	798.75	99	0	73	95	a 15_{-11} — 14_{-13}	(98.75)	6.8	9.0
13	799.11	75	0	48	70	a 10_{-1} — 9_{-9} a 15_{-10} — 14_{-14}	99.16 (99.11)	25 2.2	7.7 3.0
14	803.09†	85	0	-	88	a 11_5 — 10_{-1}	03.10	6.7	5.5
15	803.60†	93	0	-	88	a 13_1 — 12_{-5}	03.61	3.1	5.2
16	806.06	30	0	-	54	a 16_{-10} — 15_{-12}	(06.06)	0.3	0.75
17	806.75	10	0	-	36				
18	808.14† 808.33†	80 90	0	-	82	a 16_{-9} — 15_{-13} a 8_5 — 7_{-3}	(08.14) 08.29	0.9 1.8	2.2 0.53
19	813.97	92	0	-	62	a 9_9 — 8_3	13.97	2.5	2.2
20	814.61	95	0	-	77	a 12_3 — 11_{-1}	14.60	3.4	4.1

See footnotes at end of table.

TABLE 1—Continued.

Line Number	OBSERVED DATA: Wave Number cm⁻¹ (vac)	Intensity: Solar	Intensity: Laboratory: Air only	Intensity: Laboratory: 110° C (8 Atmos.)	Intensity: Laboratory: 110° C (8 Atmos.)	Identification	$J'_\tau - J''_\tau$		CALCULATED DATA: Wave Number cm⁻¹ (vac)	Intensity: 14° C	Intensity: 110° C
21	816.55	10	0	-	20						
22	825.24†	85	0	-	5	a	8_4	7_{-6}	25.16	1.0?	0.4?
23	827.21	50	0	-	18	a	13_2	12_{-2}	27.31	0.42	0.73
24	827.80	95	0	-	42	a	12_4	11_{-2}	27.86	0.45	0.57
						a	9_4	8_{-4}	27.67	1.4	0.47
25	835.64	32	0	-	36	a	14_1	13_{-3}	35.64	0.30	0.78
						a	17_{-9}	16_{-11}	(35.64)	0.10	0.55
26	840.01	90	0	-	66	a	10_7	9_3	40.01	1.6	1.7
						a	10_8	9_2	40.15	0.53	0.56
27	840.36†	45	0	-	46	a	14_0	13_{-6}	(40.36)	0.24	0.50
28	841.16	5	0	-	13	a	15_0	14_{-4}	(41.16)	0.016	0.065
-	841.97†	26	0	-	0	a	7_7	6_{-3}	41.93	(0.2)	(0.04)
29	845.83	3	0	-	9						
30	849.69	78	0		56	a	11_0	10_{-8}	49.79	2.9	1.6
31	852.62	99	0	50	92	a	10_3	9_{-5}	52.51	4.3	2.0
						a	13_3	12_{-3}	52.60	0.88	1.5
32	852.91	86	0	59	96	a	16_{-11}	15_{-15}	(52.92)	1.7	3.4
33	853.41	40	0	12	40	a	14_{-2}	13_{-8}	53.41	0.59	1.0
34	854.66	92	0	40	75	a	13_{-3}	12_{-9}	54.66	3.5	3.3
35	858.65	27	0	-	49	a	17_{-11}	16_{-13}	(58.65)	0.15	0.64
36	859.78	9	0	-	29	a	17_{-10}	16_{-14}	(59.78)	0.05	0.21
37	861.0	-	0	-	4						
38	864.0	-	0	-	3						
39	865.02†	32	0	-	37	a	11_6	10_2	65.01	0.46	0.49
40	865.51†	58	0	-	54	a	11_7	10_1	65.49	1.4	1.5

TABLE 1—Continued.

Line Number	OBSERVED DATA					Identification			CALCULATED DATA		
	Wave Number cm^{-1} (vac)	Intensity					$J'_{\tau} - J''_{\tau}$		Wave Number cm^{-1} (vac)	Intensity	
		Solar	Laboratory							14° C	110° C
			Air only	110° C (8 Atmos)	110° C (8 Atmos)						
41	871.32†	78	0	-	36	a	11_{-2}	10_{-10}	71.49	2.3	0.92
42	878.61†	68	0	-	36	a	12_{-4}	11_{-10}	78.70	1.3	0.65
						a	14_{2}	13_{-4}	78.9	0.08	0.20
43	881.15†	23	0	-	2	a	8_{6}	7_{-4}	81.20	(0.3)	(0.08)
44	883.18	24	0	-	32	a	15_{-1}	14_{-7}	(83.18)	0.13	0.18
45	883.89	59	0	-	25	a	11_{2}	10_{-6}	84.01	0.95	0.57
46	887.33	72	0	-	22	a	9_{3}	8_{-7}	87.44	(1.1)	(0.27)
47	888.71	46	0	-	41	a	12_{5}	11_{1}	88.71	0.63	0.90
48	890.14	26	0	-	16	a	12_{6}	11_{0}	90.16	0.21	0.30
49	891.33	41	0	-	17	a	10_{9}	9_{5}	91.33	0.28	0.26
50	892.1†	6	0	-	4						
51	896.57†	10	0	-	4	b	12_{-12}	13_{-8}	96.53	0.006	0.009
52	897.77†	22	0	-	14	b	12_{-11}	13_{-9}	97.77	0.017	0.027
-	905.50†	10	0	-	0	b	10_{-7}	11_{-1}	05.34	0.012	0.014
53	906.32	56	0	-	69	a	17_{-13}	16_{-15}	(06.32)	0.3	0.8
54	906.8	13	0	-	30	a	15_{1}	14_{-5}	(06.6)	0.06	0.09
55	908.09†	15	0	-	12						
56	909.02	83	0	-	67	a	12_{-1}	11_{-9}	09.12	3.0	2.0
57	910.17	20	0	-	21	a	13_{4}	12_{0}	10.4	0.08	0.17
58	910.77	12	0	-	27	a	18_{-11}	17_{-15}	(10.8)	0.02	0.12
59	914.06	34	0	-	33	a	13_{5}	12_{-1}	14.06	0.24	0.50
60	918.52	37	0	-	23	a	11_{9}	10_{3}	18.52	0.25	0.31

TABLE 1—Continued.

Line Number	OBSERVED DATA: Wave Number cm^{-1} (vac)	Intensity: Solar	Intensity: Laboratory: Air only	Intensity: Laboratory: 110° B (B Atmos-ld)	Intensity: Laboratory: 110° C (B Atmos-ld)	Identification $J'_\tau - J''_\tau$	CALCULATED DATA: Wave Number cm^{-1} (vac)	Intensity: 14° C	Intensity: 110° C
61	921.48†	35	0	-	31	a 15_{-3} — 14_{-9}	(21.48)	0.29	0.70
62	922.19†	89	0	-	52	a 12_1 — 11_{-7}	22.41	1.5	1.2
63	925.05†	80	0	-	15	a 9_5 — 8_{-5}	25.12	(1.0)	(0.3)
64	929.00	22	0	-	18	a 14_3 — 13_{-1}	29.00	0.063	0.20
65	929.4	0	0	-	6				
66	932.32	1	0	-	5				
67	937.40	5	0	-	6	a 14_4 — 13_{-2}	37.2	0.020	0.06
68	938.2	2	0	-	4				
69	941.12	20	0	-	8	a 14_{-4} — 13_{-10}	(41.1)	0.29	0.36
70	944.95	13	0	-	11	b 9_{-1} — 10_3 a 12_7 — 11_3	44.90 44.96	0.022 0.22	0.029 0.35
-	946.73†	6	0	-	0	a 8_7 — 7_{-1}	46.73	0.13	0.04
71	948.35	66	0	-	27	a 12_{-3} — 11_{-11}	48.40	1.9	1.0
72	953.49	30	0	-	25	b 11_{-11} — 12_{-7}	53.49	0.069	0.078
73	954.17†	7	0	-	6	b 8_{-1} — 9_5	53.99	0.014	0.013
-	955.33†	24	0	-	0	a 10_2 — 9_{-8}	55.50	(0.3)	(0.09)
74	955.71	9	0	-	13	b 11_{-10} — 12_{-8}	55.71	0.023	0.026
75	959.33	10	0	-	36	a 18_{-13} — 17_{-17} a 9_6 — 8_{-2}	(59.33) 59.79	0.05 (0.05)	0.21 (0.02)
76	960.5† 961.1†	5 4	0	-	12	a 15_3 — 14_{-3} b 8_0 — 9_4	(60.5) 60.91	0.003 0.005	0.014 0.005
77	962.05	-	0	-	5	a 11_{11} — 10_5	62.1	0.025	0.04
78	963.0	-	0	-	3				
79	966.01	11	0	-	7	b 9_{-6} — 10_0	65.93	0.019	0.016
80	967.00	15	0	-	16	a 13_0 — 12_{-8}	(67.00)	0.20	0.22

TABLE 1—Continued.

Line Number	OBSERVED DATA					Identification			CALCULATED DATA		
	Wave Number cm^{-1} (vac)	Intensity				$J'_\tau - J''_\tau$			Wave Number cm^{-1} (vac)	Intensity	
		Solar	Laboratory							14° C	110° C
			Air only	110° C (8 Atms-M	110° C 0 Atms-M						
81	970.66	10	0	-	8	a	13_6	12_2	70.52	0.016	0.04
						a	13_7	12_1	70.75	0.047	0.12
-	971.43†	18	0	-	0	a	10_5	9_{-3}	71.53	0.20	0.10
82	971.75	12	0	-	20						
83	973.59	15	0	-	19	a	13_{-2}	12_{-10}	73.65	0.33	0.30
84	974.04†	16	0	-	7	a	10_4	9_{-6}	74.04	0.5	0.19
85	976.07	40	0	-	24	a	13_{-5}	12_{-11}	76.07	0.7	0.5
86	977.54	15	0	-	8	b	8_{-7}	9_{-1}	77.28	0.084	0.045
87	984.2	5	0	-	5	a	11_4	10_{-4}	84.15	0.14	0.10
88	990.3	6	0	-	3	a	12_9	11_5	(90.3)	0.007	0.015
89	994.4	10	0	-	4						
90	998.87	30?	0	-	10	b	8_{-3}	9_3	98.70	0.080	0.026
91	1000.35	25?	0	-	6	a	12_3	11_{-5}	00.47	0.20	0.19
92	1003.8	10?	0	-	3	a	9_7	8_{-3}	03.85	(0.40)	(0.14)
93	1007.3	15?	0	-	4	b	11_{-5}	12_{-1}	07.08	0.017	0.035
94	1010.12	15?	0	-	16	b	10_{-10}	11_{-6}	09.96	0.11	0.085
95	1010.86	15?	0	-	22	b	11_{-9}	12_{-5}	11.06	0.10	0.143
96	1011.64	10?	0	-	7						
97	1014.56	50?	0	-	38	b	10_{-9}	11_{-7}	14.38	0.318	0.265
98	1017.6	20?	0	-	15	b	8_{-5}	9_1	17.79	0.202	0.128
99	1017.9	30?	0	-	17	a	14_{-1}	13_{-9}	(17.9)	0.16	0.22
100	1019.5	5?	0	-	2	b	10_{-4}	11_0	19.52	0.013	0.018

TABLE 1—Continued.

Line Number	OBSERVED DATA						IDENTIFICATION			CALCULATED DATA		
	Wave Number cm^{-1} (vac)	Intensity					$J'_\tau - J''_\tau$			Wave Number cm^{-1} (vac)	Intensity	
		Solar	Laboratory								14° C	110° C
			Air only	110° C (8 Atmo-M)		110° C 8 Atmo-M						
101	1022.0	5?	0	-	4		a	13_2	12_{-6}	21.55	0.053	0.078
102	1028.47	30?	0	-	13		b	7_{-2}	8_4	28.47	0.043	0.024
							a	11_3	10_{-7}	28.45	0.5	0.25
103	1029.69	20?	0	-	17		b	9_{-3}	10_1	29.58	0.084	0.082
							a	11_1	10_{-9}	29.87	1.14	0.45
104	1030.58	10?	0	-	13		b	11_{-8}	12_{-6}	30.0	0.033	0.048
105	1032.76	20?	0	-	5							
106	1039.53	?	0	-	30		b	8_{-2}	9_2	39.31	0.043	0.034
							b	11_{-7}	12_{-3}	39.35	0.075	0.128
107	1042.57	15?	0	-	17		a	14_{-3}	13_{-11}	(42.5)	0.22	0.28
108	1044.4	?	0	-	3							
109	1049.39	?	0	-	7		b	7_{-6}	8_0	49.39	0.13	0.052
110	1050.22	?	0	-	6							
111	1051.28	?	0	-	11		b	7_{-1}	8_3	51.28	0.176	0.096
112	1055.56	20?	0	-	8		b	6_{-1}	7_5	55.21	0.164	0.075
113	1058.69	?	0	-	13		b	12_{-7}	13_{-5}	58.57	0.028	0.065
114	1060.14	?	0	-	23		b	10_{-8}	11_{-4}	60.06	0.146	0.146
115	1062.61	?	0	-	8		b	7_{-4}	8_2	62.50	0.164	0.075
116	1063.6	?	0	-	3							
117	1066.20	85?	0	-	70		b	9_{-9}	10_{-5}	66.14	1.17	0.71
							b	6_0	7_4	66.17	0.057	0.025
118	1072.69	?	0	-	15		b	10_{-6}	11_{-2}	72.52	0.084	0.10
119	1074.46	70?	0	-	41		b	9_{-8}	10_{-6}	74.31	0.415	0.25
120	1085.4	?	0	-	3		b	5_1	6_5	85.37	0.096	0.035

TABLE 1 — Continued.

Line Number	OBSERVED DATA: Wave Number cm⁻¹ (vac)	Intensity: Solar	Laboratory: Air only	Laboratory: 110° C (8 Atmo-M)	Laboratory: 110° C (8 Atmo-M)	Identification $J'_{\tau} - J''_{\tau}$			CALCULATED DATA: Wave Number cm⁻¹ (vac)	Intensity: 14° C	Intensity: 110° C
121	1088.1	?	0	-	2						
122	1091.24	82	0	-	55	b	10_{-7}	11_{-5}	91.21	0.575	0.54
123	1099.74	72	0	-	54	b	9_{-5}	10_{-1}	99.04	0.665	0.55
124	1101.47	76	0	-	34	b	6_{-3}	7_{3}	01.42	0.85	0.32
125	1105.3	5?	0	-	8						
126	1106.76	83	0	-	78	b	9_{-7}	10_{-3}	06.73	1.60	1.15
127	1111.59	82	0	-	41	b	6_{-5}	7_{1}	11.50	1.21	0.41
128	1114.8	?	0	-	4	c	7_{-5}	8_{-1}	14.30	0.010	0.03
129	1117.71	23?	0	-	19	b	11_{-6}	12_{-4}	17.60	0.063	0.098
130	1120.9	84	0	14	76	b	8_{-4}	9_{0}	20.76	0.45	0.29
131	1121.24	89	0	21		b	8_{-8}	9_{-4}	21.24	1.37	0.62
132	1135.80	98	0	44	86	b	8_{-7}	9_{-5}	35.80	1.78	0.80
133	1137.46	85	0	16	65	b	7_{-3}	8_{1}	37.19	1.63	0.78
134	1141.64	22?	0	-	23	b	12_{-5}	13_{-3}	41.59	0.034	0.088
135	1149.48	77	0	22	78	b	8_{-6}	9_{-2}	49.39	1.82	0.98
136	1151.59	70	0	5	47	b	6_{-2}	7_{2}	51.55	0.66	0.25
137	1152.44	77	0	19	72	b	9_{-6}	10_{-4}	52.42	0.91	0.63
138	1165.27†	87	0	29	59	b	5_{-4}	6_{2}	65.10	0.86	0.22
139	1165.4†	83	0	15	35	b	5_{-1}	6_{3}	65.40	1.56	0.48
	1165.9	73				b	4_{-1}	5_{5}	65.84	0.59	0.145
140	1167.04	?	0	5	16	c	8_{-5}	9_{-3}	66.8	0.009	0.032
						c	5_{-3}	6_{1}	67.1	0.014	0.030

TABLE 1—Continued.

Line Number	OBSERVED DATA: Wave Number cm^{-1} (vac)	Intensity: Solar	Intensity: Laboratory: Air only	Intensity: Laboratory: 110° C (8 Atmos.)	Intensity: Laboratory: 110° C (8 Atmos.)	Identification $J'_{\tau'} - J''_{\tau''}$	CALCULATED DATA: Wave Number cm^{-1} (vac)	Intensity: 14° C	Intensity: 110° C
141	1169.4	?	0	-	4				
142	1171.4	?	0	-	11	b 9_{-8} — 9_{-2}	71.47	0.043	0.021
143	1173.76	99	0	33	99	b 10_{-5} — 11_{-3}	73.74	1.11	1.09
144	1174.54		0	68		b 7_{-7} — 8_{-3}	74.54	12.6	4.4
145	1178.55	15?	0	-	15				
146	1180.75	55?	0	-	9	b 4_0 — 5_4	80.94	0.29	0.06
147	1182.2	?	0	-	3				
148	1184.14	?	0	6	44	b 12_{-3} — 13_{-1}	83.95	0.068	0.206
149	1187.00	99	0	70	98	b 11_{-4} — 12_{-2} b 7_{-5} — 8_{-1}	86.65 87.11	0.105 11.4	0.189 4.7
150	1191.16	35?	0	-	9				
151	1193.67	28?	0	-	9				
152	1195.41	?	0	6	27	b 12_{-1} — 13_1	95.28	0.046	0.196
153	1198.22	98	0	48	95	b 7_{-6} — 8_{-4}	98.18	5.2	1.78
154	1200.80	?	0	2	17				
155	1201.55	?	0	4	30	b 12_1 — 13_3 b 12_2 — 13_2	01.58 01.8	0.021	0.099
156	1206.07† 1206.37†	52? 30?	0	-	13				
157	1207.35	?	0	-	13	c 5_{-5} — 6_{-1}	07.5	0.048	0.082
158	1209.79	?	0	3	46	c 6_{-5} — 7_{-3} b 12_3 — 13_5	09.6 09.7	0.036 0.007	0.072 0.047
159	1211.29	99	0	23	99	b 4_{-3} — 5_3	11.29	3.4	0.73
160	1212.28	99	0	60		b 8_{-5} — 9_{-3}	12.23	12.8	6.4

TABLE 1— Continued.

Line Number	OBSERVED DATA: Wave Number cm⁻¹ (vac)	Intensity: Solar	Laboratory: Air only	Laboratory: 110° C (8 Atmos-M)	Laboratory: 110° C (8 Atmos-M)		Identification $J'_\tau - J''_\tau$		CALCULATED DATA: Wave Number cm⁻¹ (vac)	Intensity: 14° C	Intensity: 110° C
161	1213.0	?	0	19	99	b	11_{-2}	12_0	13.00	0.10	0.22
162	1214.91	?	0	3	25	b	8_{-7}	8_{-1}	15.06	0.36	0.15
163	1218.63	98	0	40	90	b	6_{-4}	7_0	18.63	6.70	2.07
164	1219.1	?	0	9		b	11_0	12_2	19.2	0.060	0.16
165	1220.43	?	0	18	70	b	11_1	12_1	20.60	0.18	0.47
166	1225.08	99	0	38		b	11_3	12_3	24.76	0.10	0.34
						b	6_{-6}	7_{-2}	25.08	11.0	3.08
						b	9_{-4}	10_{-2}	25.08	2.05	1.56
167	1225.5	99	0	25	99	b	10_{-3}	11_{-1}	25.46	1.97	2.36
168	1226.1	78?	0	9		b	11_{-1}	12_{-1}	26.06	0.355	0.74
169	1228.53	?	0	-	13						
170	1229.43	?	0	-	14	b	9_{-9}	9_{-3}	29.35	0.80	0.40
171	1232.1	?	0	-	3						
172	1233.31	?	0	-	47	b	11_5	12_5	32.88	0.041	0.18
173	1235.23	?	0	-	19						
174	1237.20	?	0	-	19	b	11_{-9}	11_{-3}	36.7	0.056	0.061
						b	6_0	6_{-6}	37.41	0.021	0.008
175	1239.25	?	0	25	98	b	10_{-1}	11_1	39.19	1.50	2.17
176	1240.6	?	0	-	35						
177	1242.90	95?	0	17	98	b	10_1	11_3	42.75	1.17	2.11
						b	10_2	11_2	43.1	0.39	0.70
178	1244.18	99	0	40	99	b	5_{-3}	6_1	44.04	24.1	6.27
179	1244.77		0	11		b	10_0	11_0	44.66	0.52	0.99
180	1246.63	?	-	0	7	b	7_{-1}	7_5	46.48	0.14	0.06

TABLE 1—Continued.

Line Number	OBSERVED DATA: Wave Number cm⁻¹ (vac)	Intensity: Solar	Laboratory: Air only	Laboratory: 110° C (8 Atm-cm)	Laboratory: 110° C (8 Atm-cm)	Identification $J'_\tau - J''_\tau$		CALCULATED DATA: Wave Number cm⁻¹ (vac)	Intensity: 14° C	Intensity: 110° C
181	1248.52	?	-	11	86	b	$10_3 \quad 11_5$	48.49	0.46	1.06
182	1251.43	?	-	-	13	b	$3_{-2} \quad 4_4$	51.46	0.74	0.14
183	1252.44	?	-	-	17					
184	1253.67	?	-	0	5	b	$7_{-6} \quad 7_0$	53.51	0.43	0.14
185	1255.95	?	-	3	40	b	$16_{-15} \quad 17_{-17}$	(56.0)	0.095	0.40
186	1257.07	?	-	6	67	b b	$10_5 \quad 11_7$ $11_{-3} \quad 12_{-3}$	57.07 57.10	0.182 0.645	0.56 1.10
187	1258.63	95	-	21	91	b	$9_{-2} \quad 10_0$	58.63	3.1	2.7
188	1260.38	99	-	67	99	b	$6_{-5} \quad 7_{-3}$	60.32	53.7	14.5
189	1264.04	?	-	22	92	b	$9_0 \quad 10_2$	63.93	2.0	2.1
190	1265.42	?	-	12		b	$4_{-2} \quad 5_2$	65.30	5.5	1.15
191	1266.11	?	-	41		b	$9_1 \quad 10_1$	66.31	6.2	6.5
192	1266.63	?	-	39		b	$9_3 \quad 10_3$	66.55	4.2	4.5
193	1268.40	99	-	49		b b b	$10_{-2} \quad 11_{-2}$ $10_7 \quad 11_9$ $7_{-4} \quad 8_{-2}$	67.83 67.93 68.28	0.90 0.06 19.2	1.02 0.26 7.1
194	1269.97	99	-	60	99	b	$8_{-3} \quad 9_{-1}$	69.72	31.1	17.0
195	1271.80	99	-	61		b	$5_{-5} \quad 6_{-1}$	71.73	73	16.3
196	1272.37	?	-	31		b	$9_5 \quad 10_5$	72.22	1.80	2.90
197	1273.1	80?	-	6		b b	$6_{-3} \quad 6_3$ $9_{-3} \quad 9_3$	72.64 73.24	0.78 0.14	0.23 0.10
198	1276.63	?	-	6	65	b	$15_{-15} \quad 16_{-15}$	76.67	0.50	1.35
199	1280.09	99	-	48	99	b	$9_{-1} \quad 10_{-1}$	80.09	10.4	8.88
200	1281.22	85?	-	20	89	b	$9_7 \quad 10_7$	80.99	1.06	2.30

TABLE 1—Continued.

Line Number	OBSERVED DATA: Wave Number cm⁻¹ (vac)	Intensity: Solar	Intensity: Laboratory: Air only	Intensity: Laboratory: 110° C (0 Atmos)	Intensity: Laboratory: 110° C (8 Atmos)	Identification: $J'_\tau - J''_\tau$			CALCULATED DATA: Wave Number cm⁻¹ (vac)	Intensity: 14° C	Intensity: 110° C
201	1282.9	?	-	3	7						
202	1284.37	?	-	10	63	b	3_{-1}	4_3	84.14	5.9	1.09
203	1284.89	?	-	0	40						
204	1287.38		-	61		b	8_{-1}	9_1	87.29	33.9	21.7
205	1288.28	99	-	55	99	b	8_1	9_3	88.18	21.4	16.5
206	1288.92		-	33		b	8_2	9_2	88.82	7.15	5.50
207	1290.59	?	-	47	98	b	8_3	9_5	90.52	14.6	18.2
208	1292.40	?	-	6	75	c	6_3	7_5	92.0	0.10	0.05
						b	9_9	10_9	92.30	0.25	0.69
209	1296.67	?	-	55	99	b	8_5	9_7	96.59	6.25	7.81
						b	8_0	9_0	96.53	12.1	7.6
210	1300.9	?	-	0	2	c	6_5	7_7	01.0	0.04	0.19
211	1302.7	?	-	0	2						
212	1304.46	?	-	0	22						
213	1305.60	?	-	23	89	b	8_7	9_9	05.49	2.48	3.09
214	1306.31	?	-	5	54						
215	1308.25	?	-	55	96	b	7_{-2}	8_0	08.18	42.0	17.4
216	1312.61	?	-	75	-	b	7_3	8_3	12.71	88	52
217	1313.64	?	-	64	-	b	4_{-4}	5_0	13.35	39	7.4
						b	7_0	8_2	13.68	36.7	17.6
218	1314.82	?	-	59	-	b	7_5	8_5	14.73	43.8	31.9
219	1316.20	?	-	32	-	b	11_{-5}	12_{-5}	16.38	1.67	2.39
220	1317.04	?	-	75	-	b	7_1	8_1	16.92	113	54

TABLE 1—Continued.

Line Number	OBSERVED DATA: Wave Number cm⁻¹ (vac)	Intensity: Solar	Laboratory: Air only	Laboratory: 110° C (8 Atmo-M)	Laboratory: 110° C (8 Atmo-M)		Identification $J'_\tau - J''_\tau$		CALCULATED DATA: Wave Number cm⁻¹ (vac)	Intensity: 14° C	Intensity: 110° C
221	1317.6		-	37	-	b	13_{-13}	14_{-13}	17.65	8.15	10.9
222	1318.97		-	77	-	b	6_{-3}	7_{-1}	18.95	211	61
						b	10_{-4}	11_{-4}	19.21	2.0	2.0
223	1320.09		-	58	-	b	5_{-4}	6_{-2}	20.13	61.4	13.3
224	1320.90		-	44	-	b	7_{7}	8_{7}	20.93	19.2	18.0
225	1323.31		-	51	-	b	9_{-3}	10_{-3}	23.29	19.5	14.2
226	1324.30		-	10	-	c	5_{1}	6_{1}	24.2	0.53	1.07
227	1325.63		-	8	-						
228	1326.14		-	14	-	b	13_{-11}	14_{-11}	26.08	1.93	3.48
						b	13_{-9}	14_{-9}	26.4	0.50	1.20
229	1327.72		-	22	-	b	9_{-7}	9_{-1}	27.70	2.50	1.37
230	1329.90		-	52	-	b	8_{-2}	9_{-2}	29.72	19.3	10.4
231	1332.70		-	8	-	b	7_{-3}	7_{3}	32.49	0.78	0.30
232	1335.55		-	14	-						
233	1336.64		-	88	-	b	6_{3}	7_{5}	36.56	239	110
234	1338.56		55	92	-	b	12_{-11}	13_{-13}	37.83	28.6	27.5
						b	6_{1}	7_{3}	38.50	308	117
235	1339.23		40	93	-	b	6_{5}	7_{7}	39.39	117.5	68.1
236	1339.55		39		-	b	6_{2}	7_{2}	39.59	103	39
237	1340.35		67	95	-	b	7_{-1}	8_{-1}	40.09	169	69
						b	6_{-1}	7_{1}	40.37	364	118
238	1344.04		-	22	-	b	12_{-9}	13_{-11}	44.0	7.4	9.5
239	1344.60		-	7	-						
240	1345.59		-	13	-	b	12_{-7}	13_{-9}	45.7	1.55	2.60

Complete Absorption

TABLE 1 – Continued.

Line Number	OBSERVED DATA: Wave Number cm^{-1} (vac)	Intensity: Solar	Laboratory: Air only	Laboratory: 110° C 10 Atmos.	Laboratory: 110° C 0 Atmos.		Identification $J'_\tau - J''_\tau$		CALCULATED DATA: Wave Number cm^{-1} (vac)	Intensity: 14° C	Intensity: 110° C
241	1345.97		-	18	-	c	4_1	5_3	46.0	1.22	2.04
242	1347.01		-	6	-	c	4_2	5_2	47.1	0.41	0.68
243	1349.0		-	34	-						
244	1349.39		-	64	-	b	3_{-3}	4_1	49.43	113	18.4
245	1351.67		-	15	-						
246	1352.41		-	21	-	b	11_{-7}	12_{-7}	52.4	5.65	6.61
247	1354.87		-	80	-	b	6_0	7_0	54.80	164	53
248	1356.0		-	13	-	c b	5_{-1} 8_{-6}	6_{-1} 8_0	55.4 56.54	0.86 2.6	1.47 1.08
249	1357.21		-	13	-						
250	1358.06		-	55	-	b	11_{-11}	12_{-11}	58.02	91	65
251	1361.09		70	-	-	b b	11_{-9} 5_5	12_{-9} 6_5	61.02 61.09	19.5 570	18.1 211
252	1362.70		70	-	-	b b	5_{-2} 5_2	6_0 6_4	62.70 62.96	215 250	50 76
253	1363.17		80	-	-	b	5_3	6_3	63.16	745	226
254	1365.9		2	-	-						
255	1368.60		57	-	-	b	5_0	6_2	68.74	347	89
256	1369.78		6	80	-	b b	12_{-12}^{11}	12_{-9} 12_{-10}	69.89 70.02	3.8 1.3	3.5 1.2
257	1370.95		4	74	-	c	3_3	4_3	70.9	3.2	4.6
258	1372.28		17	-	-	b	9_{-5}	10_{-5}	72.17	52.5	31.7
259	1373.76		76	-	-	b	5_1	6_1	73.76	1070	275
260	1375.09		70	-	-	b	4_{-3}	5_{-1}	75.13	670	107

Complete Absorption

TABLE 1—Continued.

Line Number	OBSERVED DATA: Wave Number cm⁻¹ (vac)	Intensity: Solar	Laboratory: Air only	Laboratory: 110° C (8 Atmos-H)	Laboratory: 110° C (8 Atmos-H)		Identification $J'_\tau - J''_\tau$		CALCULATED DATA: Wave Number cm⁻¹ (vac)	Intensity: 14° C	Intensity: 110° C
261	1376.3		3	-	-						
262	1378.04		35	-	-	b b	10_{-9} 10_{-8}	11_{-11} 11_{-8}	77.98 78.07	263 19.5	139 13.3
263	1378.5		6	-	-	b	7_{-5}	7_{1}	78.66	17.2	5.5
264	1379.63		25	-	-	b b	8_{-4} 10_{-7}	9_{-4} 11_{-9}	79.5 79.66	45.5 58.5	20.9 39.8
265	1382.11		7	85	-	b	10_{-5}	11_{-7}	82.10	18.0	14.9
266	1383.40		5	44	-						
267	1384.26		4	35	-	c	7_{-5}	8_{-5}	83.8	0.56	1.26
268	1386.51	Complete Absorption	56	-	-	b	7_{-3}	8_{-3}	86.24	311	110
269	1387.55		82	-	-	b	4_{3}	5_{5}	87.50	2160	548
270	1390.0		4	-	-	b	5_{-3}	5_{3}	90.46	22.7	4.9
271	1390.95		12	-	-	b b	11_{-10} 11_{-11}	11_{-8} 11_{-9}	90.78 91.07	4.5 13.4	3.1 9.3
272	1392.38		5	-	-						
273	1394.50		88	-	-	b b b	9_{-7} 4_{1} 6_{-2}	10_{-7} 5_{3} 7_{-2}	94.46 94.55 94.58	159 2305 233	77 500 65
274	1395.81		75	-	-	b	4_{2}	5_{2}	96.00	770	167
275	1397.74		55	-	-	b b	9_{-6} 9_{-9}	10_{-8} 10_{-9}	97.51 97.78	54 685	30 280
276	1399.16		82	-	-	b c	4_{-1} 7_{-7}	5_{1} 8_{-7}	99.15 00.8	2170 1.9	414 3.6
277	1402.0		0	5	-	c	7_{-6}	8_{-8}	01.9	0.63	1.2
278	1403.54		8	-	-	b	9_{-4}	10_{-6}	03.38	17	10
279	1404.98		80	-	-	b	5_{-1}	6_{-1}	05.10	1432	326
280	1407.09		1	22	-						

TABLE 1—Continued.

Line Number	OBSERVED DATA: Wave Number cm⁻¹ (vac)	Intensity: Solar	Laboratory: Air only	Laboratory: 110° C (8 Atmos.)	Laboratory: 110° C (8 Atmos.)		Identification $J'_\tau - J''_\tau$		CALCULATED DATA: Wave Number cm⁻¹ (vac)	Intensity: 14° C	Intensity: 110° C
281	1408.51		3	46	-	c	2_1	3_3	08.3	5.3	5.8
282	1409.94		24	85	-	b	8_{-6}	9_{-6}	09.91	135	43
283	1411.52		27	-	-	b	10_{-3}	11_{-5}	11.33	5.2	5.1
						b	10_{-9}	10_{-7}	11.43	42	23
284	1411.91		26	-	-	b	5_{-5}	5_1	11.91	73.5	14.0
						b	10_{-10}	10_{-8}	11.98	14	7.7
285	1414.99		5	38	-	Possibly H_2O^{18}			b	3_3	4_3
286	1416.11		41	-	-	b	8_{-5}	9_{-7}	16.09	382	149
287	1417.39		69	-	-	b	8_{-8}	9_{-8}	17.39	402	181
						b	8_{-7}	9_{-9}	17.64	1225	392
288[h]	1419.3		95	-	-	b	4_0	5_0	19.04	935	177
						b	3_3	4_3	19.55	5805	1090
289	1423.90		73	-	-	b	3_{-2}	4_0	23.90	625	94
						b	7_{-5}	8_{-5}	24.25	890	269
290	1425.83		0	19	-	c	6_{-3}	7_{-5}	26.3	0.5	0.9
291	1426.60		0	45	-	c	3_{-1}	4_{-1}	26.6	4.1	4.5
292	1428.31		21	-	-	b	8_{-3}	9_{-5}	28.24	128	58
293	1429.97		80	-	-	b	3_0	4_2	30.01	1580	258
294	1432.06		22	-	-	b	9_{-8}	9_{-6}	31.99	41	16
295	1433.31		40	-	-	b	9_{-9}	9_{-7}	33.21	123	38
						b	4_{-4}	4_2	33.49	36	5.7
296	1435.77		57	-	-	b	7_{-4}	8_{-6}	35.51	292	88
297	1436.72		93	-	-	b	7_{-7}	8_{-7}	36.54	2540	650
						b	3_1	4_1	36.67	5150	840
						b	6_{-4}	7_{-4}	36.89	585	143
						b	7_{-6}	8_{-8}	37.18	835	214
298	1440.64		2	28	-						
299	1441.42		2	45	-	b	11_{-8}	11_{-6}	41.42	3.8	3.2
300	1442.80		0	9	-						

Complete Absorption

TABLE 1—Continued.

Line Number	OBSERVED DATA: Wave Number cm⁻¹ (vac)	Intensity: Solar	Intensity: Laboratory: Air only	Intensity: Laboratory: 110° C (8 Atmo-M)	Intensity: Laboratory: 110° C (8 Atmo-M)	Identification $J'_{\tau} - J''_{\tau}$	CALCULATED DATA: Wave Number cm⁻¹ (vac)	Intensity: 14° C	Intensity: 110° C
301	1445.09		7	60	-	b 11_{-9} 11_{-7}	45.05	11.8	9.8
						b 9_{-2} 10_{-4}	45.12	4.9	3.4
302	1446.49		13	65	-	b 3_{-3} 3_{3}	46.52	60	8.2
303	1447.91		85	-	-	b 5_{-3} 6_{-3}	47.88	2955	594
304	1450.53		1	19	-	Possibly H_2O^{18} b 6_{-5} 7_{-7}			
305	1452.01		58	-	-	b 8_{-7} 8_{-5}	52.20	324	98
306	1453.4		1	-	-				
307	1454.59		44	-	-	b 8_{-8} 8_{-6}	54.64	109	33
308	1455.26		75	-	-	b 6_{-6} 7_{-6}	55.30	1600	310
309	1456.49		95	-	-	b 6_{-5} 7_{-7}	56.45	4785	995
310	1457.09		89	-	-	b 2_{1} 3_{3}	57.11	8400	1210
						b 6_{-3} 7_{-5}	57.11	1650	402
311	1458.24		89	-	-	b 2_{2} 3_{2}	58.39	2880	413
312	1459.26		84	-	-	b 4_{-2} 5_{-2}	59.30	1525	260
313	1460.76		2	68	-				
314	1462.71		2	-					
315	1464.92		92	-	-	b 2_{-1} 3_{1}	64.91	4800	635
316	1466.59		4	-	-	Possibly H_2O^{18} b 3_{-1} 4_{-1}			
317	1467.61		6	-	-	Possibly H_2O^{18} b 5_{-5} 6_{-5}			
318	1469.3		2	-	-				
319	1472.0		98	-	-	b 7_{-6} 7_{-4}	71.77	441	107
						b 3_{-1} 4_{-1}	71.92	6580	960
320	1473.44		94	-	-	b 5_{-5} 6_{-5}	73.46	7980	1410

Complete Absorption

TABLE 1—Continued.

Line Number	OBSERVED DATA: Wave Number cm⁻¹ (vac)	Intensity: Solar	Laboratory: Air only	Laboratory: 110° C (9 Atmo-m)	Laboratory: 110° C (9 Atmo-m)	Identification $J'_\tau - J''_\tau$	CALCULATED DATA: Wave Number cm⁻¹ (vac)	Intensity: 14° C	Intensity: 110° C
321	1476.29		94	-	-	b 5_{-4} 6_{-6}	76.09	2500	440
						b 7_{-7} 7_{-5}	76.48	800	190
322	1478.1		2	-	-				
323	1480.4		1	40	-				
324	1481.33		62	-	-	b 5_{-2} 6_{-4}	81.37	890	180
						b 8_{-1} 9_{-3}	81.73	36	18
325	1482.5		0	40	-				
326	1484.3		0	18	-	b 10_{-1} 11_{-3}	84.44	1.5	1.7
327	1486.27		40	-	-	b 9_{-7} 9_{-5}	86.22	140	63
328	1487.34	Complete Absorption	91	-	-	b 2_0 3_0	(87.34)	2970	390
329	1489.23		85	-	-	b 8_{-5} 8_{-3}	89.11	343	120
						b 6_{-1} 7_{-3}	89.19	456	122
330	1489.81		88	-	-	b 6_{-5} 6_{-3}	89.81	1685	340
331	1490.81		88	-	-	b 4_{-4} 5_{-4}	90.76	3890	590
332	1496.23		94	-	-	b 4_{-3} 5_{-5}	96.27	11560	1760
333	1498.79		92	-	-	b 1_0 2_2	(98.79)	3145	390
						b 6_{-6} 6_{-4}	98.86	610	120
334	1500.51		10	-	-	Possibly also H_2O^{18} b 3_{-3} 4_{-3}	00.54	29	15
						b 9_{-4} 9_{-2}			
335	1501.83		52	-	-	b 7_{-4} 7_{-2}	01.83	280	77
336 J	1506		99	-	-	b 1_1 2_1	05.57	11460	1370
						b 5_{-4} 5_{-2}	06.68	1065	180
						b 3_{-3} 4_{-3}	07.09	14670	1960
337	1508.55		97	-	-	b 4_{-1} 5_{-3}	08.49	3340	560
338	1509.79		85	-	-	b 8_{-1} 8_1	09.56	111	54
						b 6_1 6_3	09.72	365	111
						b 5_3 5_5	09.73	540	137
339	1510.56		43	-	-	b 7_5 7_7	10.58	20	12
						b 6_2 6_4	10.56	122	37

TABLE 1 – Continued.

Line Number	OBSERVED DATA: Wave Number cm⁻¹ (vac)	Intensity: Solar	Laboratory: Air only	Laboratory: 110° C (8 Atmo-M	Laboratory: 110° C 8 Atmo-M	Identification $J'_\ell - J''_\ell$			CALCULATED DATA: Wave Number cm⁻¹ (vac)	Intensity: 14° C	Intensity: 110° C
340	1512.37		90	-	-	b	7_1	7_3	12.22	159	60
						b	7^1	7_0	12.30	185	59
						b	6^{-2}_{-3}	6_{-1}	12.34	1735	396
341	1515.01		72	-	-	b	6_{-1}	6_1	14.84	980	250
342	1516.77		94	-	-	b	5_0	5_2	16.32	475	103
						b	4^0_1	4_3	16.73	1420	267
343	1517.50		96	-	-	b	3_{-2}	4_{-4}	17.59	4680	620
						b	4_2	4_4	17.95	470	88
344	1520.36		93	-	-	b	5_1	5_3	20.18	1470	320
						b	5^1_{-2}	5^3_0	20.24	1330	253
345	1521.4		95	-	-	b	4_{-3}	4_{-1}	21.25	5230	760
						b	5_{-5}	5_{-3}	21.25	3870	650
346	1522.67		92	-	-	b	2_{-2}	3_{-2}	22.66	5300	650
347	1525.1		72	-	-	b	6_0	6_2	24.86	347	88
348	1525.52		92	-	-	b	4_{-1}	4_1	25.45	4100	670
349	1527.38		79	-	-	b	7_{-5}	7_{-3}	27.48	1254	335
350	1528.66		75	-	-	b	3_0	3_2	28.62	1240	179
351	1531.71		55	-	-	b	7_{-1}	7_1	31.64	595	185

Complete Absorption

Note: Between lines 351 and 352 the absorption has not been measured, since our resolution is not improved over that published[3]. The calculated spectrum from our energy levels yields results agreeing to ± 0.2 cm^{-1} with the earlier work.

TABLE 1—Continued.

Line Number	OBSERVED DATA: Wave Number cm⁻¹ (vac)	Intensity: Solar	Intensity: Laboratory: Air only	Intensity: Laboratory: 110° C (8 Atmos.)	Intensity: Laboratory: 110° C (8 Atmos.)		Identification $J'_\tau - J''_\tau$		CALCULATED DATA: Wave Number cm⁻¹ (vac)	Intensity: 14° C	Intensity: 110° C
352	1761.88		88	-	-	b	6_{-3}	5_{-3}	61.86	6388	1070
353	1764.22		7	-	-	Possibly	H_2O^{18}		b 3_3	2_1	
354	1765.40		6	-	-	b	10_{-6}	10_{-8}	65.38	29	16
355	1767.3		20	-	-	b	9_{-2}	9_{-4}	67.06	54	25
356	1768.20		87	-	-	b	9_{-7}	9_{-9}	68.06	275	88
						b	9_{-9}	8_{-7}	68.23	2910	740
						b	9_{-8}	8_{-8}	68.41	970	250
357	1771.38		91	-	-	b	3_2	2_2	71.45	6050	725
358	1772.64		93	-	-	b	3_3	2_1	72.80	17850	2140
359	1775.64		77	-	-	b	7_{-4}	6_{-4}	75.61	1320	260
360	1778.6		22	-	-	b	10_{-3}	10_{-5}	78.57	55	33
						c	4_1	3_1	78.64	8	8
361	1779.14		49	-	-	b	8_{-4}	7_{-2}	79.2	210	59
						b	10_{-5}	10_{-7}	79.15	84	46
362	1780.70		84	-	-	b	4_0	3_{-2}	80.77	1485	181
						b	8_{-6}	7_{-4}	80.92	715	174
363	1781.96		28	-	-	b	9_{-3}	8_{-1}	82.04	80	33
364	1783.95		23	-	-	b	4_2	4_{-4}	84.08	80	11
365	1784.93		76	-	-	b	10_{-9}	9_{-9}	85.03	1810	580
366	1788.45		18	-	-	b	8_2	8_0	88.38	73	30
						b	10_{-8}	10_{-10}	88.79	34	14
367	1790.1		37	-	-	b	10_{-7}	10_{-9}	90.09	104	42
						b	11_{-7}	11_{-9}	90.0	27	18
368	1791.02		88	-	-	b	8_{-5}	7_{-5}	91.05	2210	540
369	1792.63		92	-	-	b	4_1	3_1	92.73	12050	1590
370	1795.22		41	-	-	b	6_4	6_2	95.28	235	60

Complete Absorption

TABLE 1 — Continued.

Line Number	OBSERVED DATA: Wave Number cm⁻¹ (vac)	Intensity: Solar	Laboratory: Air only	Laboratory: 110° C (8 Atmo-M)	Laboratory: 110° C (8 Atmo-M)	Identification $J'_\tau - J''_\tau$			CALCULATED DATA: Wave Number cm⁻¹ (vac)	Intensity: 14° C	Intensity: 110° C
371	1796.03		79	-	-	b	5_5	5_3	95.90	790	170
						b	6_3^5	6_1	96.19	710	180
						b	7_2	7_0	96.39	165	53
372	1796.87		30	-	-	b	8_1	8_{-1}	96.98	217	89
373	1799.63		86	-	-	b	4_2	3_0	99.84	3860	506
374	1801.36		55	-	-	b	11_{-11}	10_{-9}	01.50	760	310
375	1802.43		65	-	-	b	9_{-7}	8_{-5}	02.62	1065	320
376	1805.17		24	-	-	b	5_1	5_{-5}	05.16	181	27
377	1807.75		52	-	-	b	9_{-6}	8_{-6}	07.76	362	110
378	1808.62		3	-	-	b	11_{-9}	11_{-11}	08.6	36	18
						b	11_{-8}	11_{-10}	09.41	12	6
379	1810.63		81	-	-	b	5_0	4_0	10.71	2400	360
380	1812.22		54	-	-	b	9_{-5}	8_{-3}	12.26	342	106
381	1814.73		4	-	-						
382	1815.6		3	-	-						
383	1817.47		40	-	-	b	12_{-11}	11_{-11}	17.52	290	154
384	1821.46		7	-	-	b	10_{-4}	9_{-2}	21.50	13.1	6
385	1822.82		37	-	-	b	10_{-8}	9_{-6}	22.87	157	61
386	1825.31		87	-	-	b	6_{-1}	5_{-1}	25.10	3940	690
						b	10_{-7}	9_{-7}	25.52	478	186
387	1829.42		88	-	-	b	5_{-1}	4_{-3}	29.24	1850	250
388	1830.26		91	-	-	b	5_1	4_{-1}	30.14	6150	900
389	1833.39		22	-	-	b	13_{-13}	12_{-11}	33.39	100	72
390	1834.76		6	-	-	b	11_1	11_{-1}	34.52	4.2	5.1

Complete Absorption

TABLE 1 — Continued.

Line Number	OBSERVED DATA: Wave Number cm⁻¹ (vac)	Intensity: Solar	Laboratory: Air only	Laboratory: 110° C (8 Atmos-M)	Laboratory: 110° C (8 Atmos-M)	Identification $J'_\tau - J''_\tau$	CALCULATED DATA: Wave Number cm⁻¹ (vac)	Intensity: 14° C	Intensity: 110° C
391	1836.07		5	-	-	b $6_0 \quad 6_{-6}$ Possibly H_2O^{18} b $4_3 \quad 3_3$	35.85	27	4.9
392	1837.32		65	-	-	b $7_{-2} \quad 6_{-2}$ b $3_2 \quad 2_{-2}$	37.39 37.54	680 47	147 5
393	1839.29		4	20	-	c $4_3 \quad 3_3$	39.1	11	12
394	1840.5		0	7	-	b $10_2 \quad 10_0$	40.5	4.5	3.9
395	1842.25		37	-	-	b $11_{-9} \quad 10_{-7}$ b $10_{-6} \quad 9_{-4}$	42.10 42.23	187 52	103 25
396	1844.24		92	-	-	b $11_{-8} \quad 10_{-8}$ b $4_3 \quad 3_3$	43.44 44.20	62 16000	34 2300
397	1845.4	Absorption	52	-	-	b $6_5 \quad 6_3$ b $7_5 \quad 7_3$ b $8_3 \quad 8_1$	45.57 45.54 46.09	260 210 87	79 80 42
398	1847.82		67	-	-	b $8_{-3} \quad 7_{-3}$	47.87	945	253
399	1848.80		15	-	-	b $14_{-13} \quad 13_{-13}$	48.80	31	30
400	1852.44	Complete	8	19	-	b $5_3 \quad 5_{-3}$	52.38	64	9.5
401	1854.1		2	4	-	b $4_4 \quad 4_{-2}$	54.12	9.7	1.3
402	1856.30		4	11	-	b $6_2 \quad 6_{-4}$	56.40	28.4	5.7
403	1858.52		32	70	-	b $9_{-4} \quad 8_{-4}$	58.48	145	50
404	1859.73		8	40	-	b $11_{-5} \quad 10_{-3}$	59.69	16.6	12
405	1860.96		10	39	-	b $12_{-10} \quad 11_{-8}$	60.96	22.1	15
406	1861.51		18	52	-	b $12_{-9} \quad 11_{-9}$	61.51	66.6	55
407	1863.1		0	4	-	c $5_3 \quad 4_1$	63.6	4.5	5.7
408	1864.07		7	34	-	b $15_{-15} \quad 14_{-13}$	64.06	8.8	12
409	1866.39		66	-	-	b $6_0 \quad 5_{-2}$	66.44	825	140
410	1867.94		82	-	-	b $5_2 \quad 4_2$ b $4_1 \quad 3_{-3}$	67.81 68.12	2400 388	390 47

TABLE 1—Continued.

Line Number	OBSERVED DATA: Wave Number cm⁻¹ (vac)	Intensity: Solar	Laboratory: Air only	Laboratory: 110° C (8 Atmos.)	Laboratory: 110° C (8 Atmos.)	Identification $J'_\tau - J''_\tau$		CALCULATED DATA: Wave Number cm⁻¹ (vac)	Intensity: 14° C	Intensity: 110° C
411	1869.25		90	-	-	b 5_3	4_1	69.34	7220	1180
412	1870.78		45	-	-	b 10_{-5}	9_{-5}	70.91	179	80
413	1876.67		5	11	-	b 7_{-1}	7_7	76.59	25.0	5.2
414	1879.43		12	50	-	b 13_{-11}	12_{-9}	79.40	28.2	26
415	1882.3		0	2	-					
416	1884.63		36	62	-	b 6_{-2}	5_{-4}	84.64	243	37
417	1885.28		9	42	-	b 11_{-6}	10_{-6}	85.36	22	13
418	1889.59		87	95	-	b 6_1	5_1	89.60	3715	709
419	1892.63		2	17	-	b 12_{-8}	11_{-6}	(92.63)	7.1	5.8
420	1893.87		7	25	-	b 7_7	7_5	93.63	52	23
421	1895.27		65	85	-	b 8_5	8_3	94.99	37	21
						b 6_2	5_0	95.27	1230	230
						b 9_5	9_3	95.19	18	14
422	1897.57	40	5	32	-	b 14_{-11}	3_{-11}	(97.57)	8.1	10.4
423	1898.81	10	0	6	-					
424	1901.87	75	10	40	-	b 12_{-7}	11_{-7}	01.86	22	18
425	1904.50	99	23	43	-	b 5_0	4_{-4}	04.40	159	21
426	1908.12		53	82	-	b 7_0	6_0	08.12	555	128
427	1910.09		68	87	-	b 7_{-1}	6_{-3}	09.95	925	186
428	1914.70	99	3	25	-	Possibly H_2O^{18}	b 7_1 6_{-1}			
429	1915.30		1	15	-	d 6_{-5}	7_{-7}	15.16	0.07	0.10
430	1918.08		82	-	-	b 5_5	4_3	18.08	7660	1440

Complete Absorption

TABLE 1 – Continued.

Line Number	OBSERVED DATA: Wave Number cm⁻¹ (vac)	Intensity: Solar	Laboratory: Air only	Laboratory: 110° C (8 Atmos.)	Laboratory: 110° C (8 Atmos.)	Identification $J'_\tau - J''_\tau$			CALCULATED DATA: Wave Number cm⁻¹ (vac)	Intensity: 14° C	Intensity: 110° C
431	1919.3		4	-	-						
432	1920.7	99	3	-	-	b	9_{-1}	9_{-7}	20.29	9.2	4.6
433	1922.42		54	-	-	b	8_{-1}	7_{-1}	22.39	665	193
434	1923.14		63	-	-	b	7_{1}	6_{-1}	23.14	1490	340
435	1927.82	30	3	-	-						
436	1933.09	97	14	-	-	b	9_{-2}	8_{-2}	33.23	86	32
437	1935.24	15	0	20	-						
438	1937.87	40	0	40	-	b	8_{2}	8_{-4}	37.17	2.8	1.1
439	1939.2	15	0	9	-	b	9_{1}	9_{-5}	39.51	4.7	2.1
440	1940.2		3	-	-	b	8_{7}	8_{5}	40.35	8.0	5.8
441	1941.73		23	-	-	b b b	10_{-3} 9_{7} 7_{3}	9_{-3} 9_{5} 7_{-3}	41.78 41.82 41.89	86 5.0 9.5	43 5 2.6
442	1942.49	99	80	-	-	b b	6_{3} 6_{4}	5_{3} 5_{2}	42.61 42.86	3026 1009	660 220
443	1945.28		42	-	-	b	7_{-3}	6_{-5}	45.14	287	51
444	1946.25		39	-	-	b	6_{-1}	5_{-5}	46.24	364	55
445	1949.15	70	9	71	-	b	11_{-4}	10_{-4}	49.28	9.2	6.2
446	1949.96	10	0	10	-	b	6_{4}	6_{-2}	50.31	2.5	0.5
447	1950.97	50	0	10	-	b	6_{1}	6_{-5}	51.15	9.5	1.7
448	1954.99	99	36	97	-	b	8_{0}	7_{-2}	55.02	202	56
449	1956.25	97	2	75	-	b	4_{3}	3_{-1}	56.24	28.3	3.5
450	1957.62	75	8	83	-	d b	4_{-3} 12_{-5}	5_{-5} 11_{-5}	56.90 57.66	0.15 8.1	0.17 7.8

TABLE 1—Continued.

Line Number	OBSERVED DATA					Identification $J'_\tau - J''_\tau$			CALCULATED DATA		
	Wave Number cm^{-1} (vac)	Intensity							Wave Number cm^{-1} (vac)	Intensity	
		Solar	Laboratory							14° C	110° C
			Air only	110° C (8 Atmos)	110° C (8 Atmos)						
451	1961.19	96	26	95	-	b	8_{-2}	7_{-4}	61.25	108	25
452	1966.36	99	52	99	-	b	7_2	6_2	66.45	469	120
453	1967.49	99	66	99	-	b	7_3	6_1	67.54	1390	357
454	1970.0	10	0	52	-	b	11_{-1}	11_{-7}	69.35	0.8	0.6
455	1975.43	5	2	32	-	e e	5_0 8_{-8}	6_{-1} 9_{-9}	72.75 75.84	0.2 0.1	0.3 0.3
456	1976.19	83	3	50	-	b	5_2	4_{-2}	76.19	29	4
457	1977.6	14	0	8	-	Possibly H_2O^{18}			b	6_5	5_5
458	1981.32	40	2	50	-	e	6_{-4}	7_{-5}	80.83	0.25	0.45
459	1982.1	15	1	27	-						
460	1984.61	33	0	25	-	b b	9_9 9_{-3}	9_7 9_{-9}	84.40 84.62	1.0 2.2	1.3 0.7
461	1988.53	99	56	99	-	b b	4_4 8_1	3_{-2} 7_1	87.33 88.53	4.3 570	0.5 184
462	1992.06	99	71	99	-	b	6_5	5_5	92.14	2640	670
463	1992.6	99	66	99	-	b b b	8_2 9_{-1} 7_{-2}	7_0 8_{-3} 6_{-6}	92.50 93.31 93.35	211 183 65	68 65 11
-	-	-	0	-	-	e	7_{-6}	8_{-7}	95.08	0.26	0.5
464	1998.94	94	17	85	-	b	6_1	5_{-3}	98.94	144	24
465	2000.90	10	0	20	-						
466	2003.20	8	0	10	-	d d	2_{-1} 1_{-1}	3_{-3} 2_{-1}	02.96 03.29	0.18 0.20	0.16 0.17
-	-	0	-	0	-	e	5_{-2}	6_{-3}	04.14	0.31	0.4
467	2005.8	27	0	12	-	c	6_5	5_5	04.8	1.3	2.7
468	2007.66	95	26	92	-	b	9_0	8_0	07.77	67.5	28
469	2009.30	93	9	85	-	b	6_{-4}	7_{-6}	09.47	37.8	7.9
470	2012.3	3	0	8	-	Possibly H_2O^{18} e	40	5_{-1}	b 7_5 12.29	6_3 0.53	0.7

TABLE 1 — Continued.

Line Number	OBSERVED DATA: Wave Number cm⁻¹ (vac)	Intensity: Solar	Laboratory: Air only	Laboratory: 110° C (8 Atmos)	Laboratory: 110° C (8 Atmos)	Identification $J'_\ell - J''_\ell$			CALCULATED DATA: Wave Number cm⁻¹ (vac)	Intensity: 14° C	Intensity: 110° C
471	2016.78		73	-	-	b	7_5	6_3	16.76	1235	377
472	2018.30	99	50	-	-	b	9_1	8_{-1}	18.77	202	83
473	2018.92		34	-	-	b	9_{-3}	8_{-5}	19.18	93	28
474	2022.95	86	30	95	-	b	10_{-1}	9_{-1}	23.09	62.5	34
475	2026.58	90	10	84	-	b b	7_0 5_3	6_{-4} 4_{-3}	26.79 27.00	41.3 23.6	8.3 3.1
476	2030.03	16	0	10	-						
477	2034.03	52	0	4	68	b b e	11_{-2} 8_1 5_{-4}	10_{-2} 8_{-5} 6_{-5}	34.35 34.12 34.13	5.8 0.87 0.63	4.4 0.26 0.82
478	2037.54	75	5	8	80	b	10_{-2}	9_{-4}	37.54	15.3	7.0
479	2041.35	93	31	70	95	b b b	12_{-3} 8_3 8_4	11_{-3} 7_3 7_2	41.35 41.39 41.60	4.2 384 128	4.6 146 48
480	2043.97	93	9	18	86	b	8_{-3}	7_{-7}	44.00	102	21
481	2046.58	70	4	13	80	b	10_0	9_{-2}	46.64	20.8	11
482	2048.7	?	0	0	7	e	3_0	4_{-1}	48.66	0.71	0.76
483	2050.8	?	0	0	11	b	8_4	8_{-2}	51.08	0.37	0.12
484	2051.49	?	0	0	18	e	3_{-1}	4_{-2}	51.33	0.31	0.32
485	2053.06	?	0	0	12						
486	2053.96	?	0	0	16	e e	4_{-4} 4_{-3}	5_{-5} 5_{-4}	53.84 54.47	0.96 0.31	1.06 0.34
487	2060.55	?	8	16	80	b	8_{-1}	7_{-5}	60.55	92	22.2
488	2064.90	?	29	50	-	b b	7_7 9_2	6_5 8_2	64.87 65.02	690 46.7	255 22.4
489	2065.83	?	13	30	-	b	9_3	8_1	65.91	141	67.5
490	2068.74	?	0	3	8*	e CO	$^2{}_2$	$^3{}_1$ P(18)	67.98 68.85	0.60	0.58

TABLE 1—Continued.

Line Number	OBSERVED DATA: Wave Number cm⁻¹ (vac)	Intensity: Solar	Laboratory: Air only	Laboratory: 110° C (8 Atmos-M)	Laboratory: 110° C (8 Atmos-M)	Identification $J'_{\tau} - J''_{\tau}$	CALCULATED DATA: Wave Number cm⁻¹ (vac)	Intensity: 10° C	Intensity: 110° C
491	2072.9	?	0	6	12*	b 6_6 6_0 b 6_2 P(17) 5_{-4} CO	72.70 72.68 73.27	0.17 6.1	0.04 0.92
492	2074.22	?	0	10	58	e 3_{-2} 4_{-3} b 9_{-5} 8_{-7}	73.80 74.26	1.24 45.1	1.21 11.5
493[6]	2077.3	?	0	8	14*	e 2_0 P(16) 3_{-1} CO	76.83 77.65	1.12	1.02
494	2078.61	?	0	11	60	b 11_{-1} 10_{-3}	78.67	15.6	11.1
495	2081.98	?	0	10	34*	CO P(15) b 10_{-4} 9_{-6}	82.00 82.02	8.95	3.40
496	2086.52	?	0	8	17*	CO P(14) b 11_{-3} 10_{-5}	86.32 86.52	10.6	6.4
497	2087.54	?	5	13	61	b 10_1 9_1	87.54	45.4	28.7
498	2090.20	?	16	38	86	b 8_5 7_5 b 10_2 9_0	90.19 90.2	286 15.1	130 9.5
499	2093.36	?	-	-	17	e 2_{-2} 3_{-3} e 2_{-1} 3_{-2}	93.02 93.73	1.64 0.53	1.40 0.46
500	2095.29	?	-	-	23*	b 8_3 8_{-3} e 4_4 4_3	95.14 95.28	0.90 0.72	0.31 1.01
501	2097.43	48	-	-	48	b 9_{-4} 8_{-8}	97.48	14.1	3.53
502	2100.46	50	-	-	61	b 9_{-2} 8_{-6}	00.46	13.9	4.20
503	2103.31	?	-	-	17*	e 1_1 P(10) 2_0 CO	03.13 03.27	0.31	0.25
-	2105.93†	20	-	-	-	b 5_5 4_{-1}	05.86	5.35	0.77
504	2106.45†	40	-	-	29	b 6_3 5_{-1}	06.45	14.4	2.52
505	2107.47	?	-	10	55	b 11_0 10_0	07.9	4.25	3.61
506	2111.59	?	-	-	13*	d 2_1 P(8) 2_{-1} CO	11.51 11.54	0.12	0.10
507	2114.86	80?	-	44	99	d 3_{-3} 2_{-1} e 1_0 2_{-1} b 11_1 10_{-1} b 9_5 8_3 d 2_{-1} 1_{-1}	14.28 14.45 14.50 15.18 16.47	0.24 1.01 12.6 107.5 0.29	0.20 0.82 10.7 62.5 0.22

TABLE 1 — Continued.

Line Number	OBSERVED DATA: Wave Number cm⁻¹ (vac)	Intensity: Solar	Laboratory: Air only	Laboratory: 110° C (8 Atmos.)	Laboratory: 110° C (8 Atmos.)	Identification $J'_\tau - J''_\tau$	CALCULATED DATA: Wave Number cm⁻¹ (vac)	Intensity: 14° C	Intensity: 110° C
508	2119.48	?	-	-	7*	{e 4_1 4_2 / CO P(6)}	19.07 19.68	0.18	0.22
509	2121.54	20	-	-	28	{b 7_2 6_{-2} e 4_2 4_1}	21.48 21.73	6.5 0.53	1.37 0.48
510	2122.58	2	-	-	25	{e 3_2 3_3 e 3_3 3_2 e 3_{-2} 3_{-1}}	22.31 22.67 23.13	1.14 0.38 0.25	1.23 0.41 0.22
511	2124.27	30?	-	-	62	b 12_{-1} 11_{-1}	24.39	3.15	3.81
-	2125.00†	10	-	-	-	b 7_1 6_{-5}	24.87	13.7	2.36
512	2127.57	?	-	-	5*	CO P(4)	27.68		
513	2129.54	39	-	-	5				
514	2131.58	?	-	-	10*	{d 3_{-2} 2_{-2} / CO P(3)}	31.58 31.63	0.10	0.08
515	2136.06	63?	9	31	96	b 8_7 7_7	36.20	135.5	76.8
516	2137.12	55	0	-	75	{b 6_4 5_{-2} b 8_1 7_{-3}}	36.86 37.35	3.5 18.3	0.60 4.83
-	2138.25†	15	2	0	?	b 10_{-6} 9_{-8}	38.38	5.6	1.88
517	2139.30	?	4	30	95	b 10_3 9_3	39.37	25.7	19.8
518	2141.3	?	0	-	2				
519	2142.4	8	0	-	2	e 2_1 2_2	41.94	0.52	0.47
520	2145.41	52	0	12	77	{e 2_2 2_1 b 10_{-3} 9_{-7}}	44.63 45.64	1.57 20.3	1.40 7.8
521	2147.38	?	0	9	55	{d 4_{-3} 3_{-3} b 11_{-5} 10_{-7}}	45.68 47.42	0.27 7.8	0.24 3.9
522	2151.24	?	0	-	20	{d 2_1 1_1 e 1_0 1_1}	48.10 51.04	0.08 0.39	0.06 0.31
523	2152.58	45	0	-	50	b 10_{-5} 9_{-9}	52.75	16.3	5.15
524	2154.68	?	0	-	12*	{d 5_{-5} 4_{-3} / CO R(2)}	54.60 54.60	0.25	0.25

TABLE 1—Continued.

Line Number	OBSERVED DATA: Wave Number cm⁻¹ (vac)	Intensity: Solar	Intensity: Laboratory: Air only	Intensity: Laboratory: 110° C (8 Atmo-M)	Intensity: Laboratory: 110° C (8 Atmo-M)	Identification $J'_\tau - J''_\tau$	CALCULATED DATA: Wave Number cm⁻¹ (vac)	Intensity: 14° C	Intensity: 110° C
525	2156.60	22	0	- 15	b	$9_0 \quad 8_{-4}$	56.56	5.3	1.8
526	2158.26	?	0	- 6*	e CO	$4_0 \quad 4_{-1}$ R(3)	58.22 58.30	0.33	0.36
527	2161.75	?	0	- 84	b	$9_7 \quad 8_5$	61.88	51	36
528	2162.90† 2163.46†	10 15	0	- 69	b b	$11_2 \quad 10_2$ $11_3 \quad 10_1$	62.90 63.46	2.48 7.44	2.58 7.73
529	2165.50	?	0	- 8*	CO b	R(5) $12_{-3} \quad 12_{-9}$	65.60 65.68	0.05	0.05
530	2167.35	?	0	- 20	b	$13_{-1} \quad 12_{-3}$	(67.35)	0.60	1.06
531	2169.17	?	0	- 6*	CO	R(6)	69.20		
532	2171.31	15?	0	- 15	b	$7_3 \quad 6_{-3}$	71.38	10.7	2.12
533	2172.43	?	0	- 16*	e d CO	$2_0 \quad 2_{-1}$ $6_{-6} \quad 5_{-4}$ R(7)	72.06 72.35 72.76	0.60 0.07	0.49 0.08
534	2175.09	10?	0	- 11	d	$6_{-5} \quad 5_{-5}$	75.14	0.20	0.22
535	2176.45	?	0	- 7*	CO	R(8)	76.28		
536	2178.99	?	0	- 8	d	$4_{-1} \quad 3_{-1}$	78.91	0.17	0.16
537	2179.87	?	0	- 10*	CO	R(9)	79.77		
538	2181.41	?	0	- 40	b	$10_{-1} \quad 9_{-5}$	81.61	8.84	3.98
539	2183.33	?	0	- 6*	CO	R(10)	83.22		
540	2185.41	?	0	- 38	b b	$8_0 \quad 7_{-6}$ $12_1 \quad 11_1$	85.24 85.37	2.0 1.9	0.42 2.75
541	2187.05	?	0	- 28*	b b	$12_5^2 \quad 11_5^0$ $10_5^2 \quad 9_5^0$	87.0 87.04	0.65 16.6	0.92 15.8
542	2189.69	?	0	- 11	d	$7_{-7} \quad 6_{-5}$	89.52	0.13	0.16
543	2190.4	?	0	- 8*	CO d	R(12) $7_{-6} \quad 6_{-6}$	90.02 90.7	0.04	0.05
544	2191.83	?	0	- 2	d	$3_2 \quad 2_2$	91.34	0.086	0.07

TABLE 1—Continued.

Line Number	OBSERVED DATA: Wave Number cm⁻¹ (vac)	Intensity: Solar	Intensity: Laboratory: Air only	Intensity: Laboratory: 110° C (0 Atmos.)	Intensity: Laboratory: 110° C (0 Atmos.)	Identification: $J'_\tau - J''_\tau$	CALCULATED DATA: Wave Number cm⁻¹ (vac)	Intensity: 14° C	Intensity: 110° C
545	2193.36	?	0	-	9*	{d 3_3 2_1 R(13) / CO}	92.66 / 93.36	0.25	0.22
546	2194.50	?	0	-	13	b 11_{-4} 10_{-8}	94.37	2.25	1.11
547	2196.69	?	0	-	5*	CO R(14)	96.66		
548	2198.63	?	0	-	11	e 2_{-1} 1_0	98.42	0.40	0.31
549	2200.29	?	0	-	25*	b 11_{-7} 10_{-9}	00.4	5.5	2.23
550	2201.2	?	0	-	4				
551	2202.0	?	0	-	2				
552	2203.23	?	0	-	4*	CO R(16)	03.16		
553	2205.19	?	0	-	60	b 9_9 8_7	05.30	19.3	18.1
554	2206.48	?	0	-	25	e 2_{-2} 1_{-1}	06.53	1.74	1.31
555	2208.83	?	0	-	16	{e 2_0 1_1 / b 11_{-6} 10_{-10}}	08.65 / 08.96	1.12 / 1.88	0.86 / 0.75
556	2209.9	?	0	-	5	b 13_1 12_{-1}	(09.9)	0.42	0.87
557	2210.4	?	0	-	5	b 8_2 7_{-4}	10.76	2.38	0.58
558	2211.50	?	0	-	40	{b 11_5 10_3 / b 11_{-2} 10_{-6}}	11.50 / 12.65	4.83 / 1.30	6.27 / 0.79
559	2214.0	?	0	-	8	e 3_0 2_1	14.09	0.80	0.70
560	2214.3	?	0	-	8				
561	2215.80	?	0	-	5				
562	2218.48	?	0	-	26	e 3_{-2} 2_{-1}	18.36	2.00	1.73
563	2221.87	?	0	-	4	d 9_{-9} 8_{-7}	21.96	0.10	0.18
564	2223.61	?	0	-	4				

TABLE 1 — Continued.

Line Number	OBSERVED DATA: Wave Number cm⁻¹ (vac)	Intensity: Solar	Laboratory: Air only	Laboratory: 110° C (8 Atmos.)	Laboratory: 110° C (8 Atmos.)	Identification $J'_\tau - J''_\tau$			CALCULATED DATA: Wave Number cm⁻¹ (vac)	Intensity: 14° C	Intensity: 110° C
565	2225.84	?	0	-	8	b	6_5	5_1	25.45	1.55	0.29
						e	3_{-3}	2_{-2}	25.87	0.72	0.57
566	2227.30	?	0	-	16	d	4_4	3_2	27.09	0.07	0.08
						d	4_3	3_3	27.45	0.22	0.24
						b	6_3	5_{-5}	27.59	0.06	0.07
567	2231.01	?	0	-	40	b	10_7	9_7	31.01	7.10	9.0
568	2232.93	?	0	-	10	e	3_{-1}	2_0	33.13	0.55	0.45
569	2235.62	?	0	-	25	b	12_3	11_3	35.62	1.30	2.30
570	2237.76	?	0	-	10	e	4_{-3}	3_{-2}	37.64	0.66	0.58
571	2239.30	?	0	-	8						

†, Frequency obtained from solar spectrum; ε, probably due to CO_2; h, this line looks like an unresolved doublet; j, obviously consists of several unresolved components; *, intensity variable, due to CO contaminant.

TABLE 2. Energy Levels of H_2O (cm^{-1}).

J_τ	$V_1V_2V_3$ 000	010	020	J_τ	$V_1V_2V_3$ 000	010	020
0	0.00	1594.59	3151.53	4_{-4}	222.04	1817.35	3375.3
1_{-1}	23.79	1618.41	3175.4	4_{-3}	224.83	1821.63	3381.9
1_0	37.13	1634.94	3196.2	4_{-2}	275.48	1875.42	3438.6
1_1	42.37	1640.48	3202.0	4_{-1}	300.38	1907.94	3482.0
				4_0	315.73	1923.04	3495.85
2_{-2}	70.06	1664.93	3222.06	4_1	382.49	2004.89	3597.80
2_{-1}	79.48	1677.07	3237.77	4_2	383.86	2006.12	3598.8
2_0	95.17	1693.62	3255.26	4_3	488.16	2129.60	3746.8
2_1	134.91	1742.51	3316.0	4_4	488.17	2129.60	3746.8
2_2	136.15	1743.64	3317.0				
				5_{-5}	325.36	1920.70	3479.1
3_{-3}	136.77	1731.92	3289.27	5_{-4}	326.59	1922.80	3482.5
3_{-2}	142.27	1739.63	3300.1	5_{-3}	399.45	2000.80	3565.5
3_{-1}	173.36	1772.30	3334.55	5_{-2}	416.12	2024.24	3598.6
3_0	206.28	1813.87	3387.8	5_{-1}	446.50	2054.07	3627.0
3_1	212.16	1819.16	3392.90	5_0	504.00	2126.44	3719.2
3_2	285.25	1907.60	3500.4	5_1	508.79	2130.52	3722.55
3_3	285.40	1907.71	3500.5	5_2	610.12	2251.67	3868.3
				5_3	610.34	2251.83	3868.5
				$5_{4,5}$	742.10	2406.24	4052.8

TABLE 2 - Continued.

J_τ	$V_1V_2V_3$		
	000	010	020
6_{-6}	446.71	2041.73	3600.4
6_{-5}	447.24	2042.73	3602.0
6_{-4}	542.87	2146.39	3713.1
6_{-3}	552.92	2161.31	3736.2
6_{-2}	602.67	2211.23	3784.3
6_{-1}	648.97	2271.60	3864.8
6_0	661.54	2282.56	3873.55
6_1	756.76	2398.39	4015.1
6_2	757.70	2399.27	4015.8
6_3	888.67	2552.95	4197.4
6_4	888.71	2552.98	4197.4
$6_{5,6}$	1045.15	2734.24	?4411.0
7_{-7}	586.28	2180.68	3738.6
7_{-6}	586.43	2181.27	3739.5
7_{-5}	704.20	2309.89	3879.05
7_{-4}	709.50	2318.48	3894.5
7_{-3}	782.41	2392.38	3967.4
7_{-2}	816.65	2440.06	4038.7
7_{-1}	842.36	2462.87	4053.0
7_0	927.76	2569.66	?4187.8
7_1	931.23	2572.11	4190.8
7_2	1059.68	2724.15	
7_3	1059.89	2724.30	
$7_{4,5}$	1216.39	2905.43	
$7_{6,7}$	1394.85	3110.02	
8_{-8}	744.09	2337.61	3894.4
8_{-7}	744.14	2337.84	3894.8
8_{-6}	882.97	2490.42	4063.9
8_{-5}	885.64	2495.25	4071.6
8_{-4}	983.09	2595.9	
8_{-3}	1006.14	2630.28	4224.8
8_{-2}	1050.20	2670.75	
8_{-1}	1122.78	2764.75	4383.9
8_0	1131.88	2771.67	
8_1	1255.19	2919.76	
8_2	1255.98	2920.26	
$8_{3,4}$	1411.59	3101.28	
$8_{5,6}$	1590.70	3306.58	
$8_{7,8}$	1789.09	3531.05	
9_{-9}	920.20	2512.37	4068.8
9_{-8}	920.22	2512.50	
9_{-7}	1079.16	2688.26	4266.7
9_{-6}	1080.51	2690.73	
9_{-5}	1202.04	2818.40	
9_{-4}	1216.37	2841.57	

J_τ	$V_1V_2V_3$		
	000	010	020
9_{-3}	1283.02	2904.82	
9_{-2}	1341.03	2983.43	
9_{-1}	1360.56	2999.45	
9_0	1475.14	3139.65	
9_1	1477.46	3141.55	
9_2	1631.44	3321.0	
9_3	1631.58	3321.10	
$9_{4,5}$	1810.76	3526.77	
$9_{6,7}$	2009.99	3752.58	
$9_{8,9}$	2225.56	3994.39	
10_{-10}	1114.59	2705.20	4260.7
10_{-9}	1114.59	2705.23	
10_{-8}	1293.22	2903.38	
10_{-7}	1293.80	2904.68	
10_{-6}	1438.19	3058.60	
10_{-5}	1446.23	3072.95	
10_{-4}	1538.31	3162.53	
10_{-3}	1581.53	3224.80	
10_{-2}	1616.49	3253.91	
10_{-1}	1719.36	3383.65	
10_0	1724.80	3387.67	
10_1	1875.24	3565.00	
10_2	1875.72	3565.3	
$10_{3,4}$	2054.55	3770.95	
$10_{5,6}$	2254.55	3997.80	
$10_{7,8}$	2471.59	4241.0	
$10_{9,10}$	2702.09		
$11_{-11,-10}$	1327.25	2916.09	4470.1
11_{-9}	1525.02	3135.9	
11_{-8}	1525.31	3136.66	
11_{-7}	1690.85	3315.0	
11_{-6}	1695.24	3323.55	
11_{-5}	1813.47	3441.22	
11_{-4}	1843.32	3487.59	
11_{-3}	1899.21	3532.75	
11_{-2}	1986.08	3650.84	
11_{-1}	1999.34	?3660.20	
11_0	2143.01	3832.7	
11_1	2144.46	3833.86	
11_2	2322.20	4038.62	
11_3	2322.25	4038.70	
$11_{4,5}$	2522.46	4266.05	
$11_{6,7}$	2740.73		
$11_{8,9}$	2973.07		
$11_{10,11}$	3216.6		

TABLE 2 - Continued.

J_τ	$V_1V_2V_3$		
	000	010	020
$12_{-12,-11}$	1558.07	3144.77	
12_{-10}	1774.75	3386.27	
12_{-9}	1774.88	3386.53	
12_{-8}	1960.38	3587.87	
12_{-7}	1962.60	3592.71	
12_{-6}	2106.7		
12_{-5}	2124.84	3771.13	
12_{-4}	2205.95		
12_{-3}	2275.65	3940.56	
12_{-2}	2300.94		
12_{-1}	2434.14	4123.73	
12_0	2437.84		
12_1	2613.26	4329.83	
12_2	2613.49	4330.0	
$12_{3,4}$	2813.94	4557.87	
$12_{5,6}$	3033.17		
$12_{7,8}$	3267.2		
$12_{9,10}$	3512.8		
$12_{11,12}$	3767.1		
$13_{-13,-12}$	1806.94	3391.46	
13_{-11}	2042.5	3654.28	
13_{-10}	2042.5		
13_{-9}	2247.0	3877.9	
13_{-8}	2248.24		
13_{-7}	2415.95		
13_{-6}	2426.0		
13_{-5}	2534.14		
13_{-4}	2586.5		
13_{-3}	2629.54		
13_{-2}	2748.4		
13_{-1}	2756.61	4443.0	
13_0	2927.38		
13_1	2928.45	4644.0	
$13_{2,3}$	3128.25		
$13_{4,5}$	3348.2		
$13_{6,7}$	3584.0		
$14_{-14,-13}$	2073.81	3655.74	
$14_{-12,-11}$	2328.2	3940.1	
14_{-10}	2551.0		
14_{-9}	2551.5		
14_{-8}	2740.5		
14_{-7}	2745.5		
14_{-6}	2883.5		
14_{-5}	2919.5		
14_{-4}	2983.6		
14_{-3}	3085.0		

J_τ	$V_1V_2V_3$		
	000	010	020
14_{-2}	3101.65		
14_{-1}	3264.2		
14_0	3266.36		
14_1	3465.18		
14_2	3465.4		
$14_{3,4}$	3485.6		
$15_{-15,-14}$	2358.58	3937.87	
$15_{-13,-12}$	2631.6		
15_{-11}	2872.56		
15_{-10}	2872.9		
15_{-9}	3081.2		
15_{-8}	3084.2		
15_{-7}	3252.0		
15_{-6}	3277.0		
15_{-5}	3365.0		
15_{-4}	3446.0		
15_{-3}	3473.0		
15_{-2}	3624.0		
15_{-1}	3628.7		
15_0	3824.8		
15_1	3826.1		
$15_{2,3}$	4045.8		
$16_{-16,-15}$	2661.2	4237.5	
$16_{-14,-13}$	2953.0		
$16_{-12,-11}$	3211.5		
16_{-10}	3437.7		
16_{-9}	3439.7		
16_{-8}	3640.3		
16_{-7}	3657.1		
$17_{-17,-16}$	2931.5	4554.6	
$17_{-15,-14}$	3291.0		
$17_{-13,-12}$	3567.5		
17_{-11}	3811.7		
17_{-10}	3812.8		
17_{-9}	4047.1		
17_{-8}	4057.3		
$18_{-18,-17}$	3319.4		
$18_{-16,-15}$	3648.0		
$18_{-14,-13}$	3940.8		
$18_{-12,-11}$	4201.8		

TABLE 3. *Series regularities in the $P_{1,\bar{1}}$, $P_{\bar{1},\bar{1}}$, $P_{\bar{1},1}$, and $P_{\bar{1}1}$ branches of ν_2*

Branch	$(J+\tau)'$	$J'=0$	1	2	3	4	5	6	7	8	9	10	11	12	13	14	15
$\bar{3},1$	6	.....	.....	.....	.....	.....	1085.4	(1066.2)	1051.28	(1039.53)	(1029.69)	1019.5	1007.3				
$3,\bar{1}$	4	.....	.....	.....	.....	1180.75	1165.4	1151.59	1137.46	1120.9	1099.74	1072.69	1039.53				
$\bar{3},1$	2	.....	.....	.....	1284.37	1265.42	1244.18	1218.63	1187.00	1149.48	1106.76	1060.14	1010.86	961.09			
$3,\bar{1}$	0	.....	.....	(1379.6)	1349.39	(1313.64)	1271.80	1225.08	1174.54	1121.24	1066.20	1010.12	953.49	896.65			
$\bar{1},1$	1	.....	1498.79	1464.92	(1423.9)	1375.09	1320.09	1260.38	1198.22	1135.80	1074.46	1014.56	955.71	897.77			
$1,\bar{1}$	0	(1557.5)	1538.8	1522.67	1507	1490.81	1473.44	1455.26	(1436.7)	1417.39	1397.74	1378.04	1358.06	(1338.5)	1317.6	(1296.7)	1276.63
$\bar{1},1$	1	.....	1564.7	1540.1	1517.50	1496.23	1476.29	1456.49	(1436.7)	1417.39	1397.74	1378.04	1358.06	(1338.5)	1317.6	(1296.7)	1276.63
$1,\bar{1}$	2	.....	1505.8	1487.34	1472.0	1459.26	1447.91	(1436.7)	1423.90	1409.94	(1394.5)	(1378.0)	(1361.1)	.....	1326.14		
$\bar{1},1$	3	.....	.....	(1569.4)	(1538.8)	1504.55	1481.33	(1457.0)	1435.77	1416.11	(1397.7)	1379.63	(1362.7)	1344.04			
$1,\bar{1}$	3	.....	.....	1457.09	1429.97	1399.16	1362.70	1318.97	1268.40	1212.28	1152.44	1091.24	1030.58	(970.66)			
$\bar{1},1$	4	.....	.....	1458.24	1436.72	(1419.3)	1404.98	(1394.5)	1386.51	1379.63	1372.28	(1363.2)	1352.41	(1340)	(1326.14)		
$1,\bar{1}$	5	.....	.....	.....	1591.9	1558.5	(1522.7)	1489.23	(1457.1)	1428.31	1403.54	1382.11	(1362.7)	1345.51			
$\bar{1},1$	5	.....	.....	.....	1419.3	1394.50	1368.60	1340.35	1308.25	1269.97	(1225.0)	1173.76	1117.71	1058.69			
$1,\bar{1}$	6	.....	.....	.....	1419.3	1395.81	1373.76	1354.87	(1340.3)	1329.90	1323.31	(1319.0)	1316.20				
$\bar{1},1$	7	.....	.....	.....	.....	1387.55	1363.17	1338.56	1313.64	1287.38	1258.63	1225.5	(1187.0)	1141.64			
$1,\bar{1}$	8	.....	.....	.....	.....	1387.55	1363.17	1339.55	1317.04	1296.67	1280.09	(1268.4)	1257.07				
$\bar{1},1$	9	.....	.....	.....	.....	.....	1361.09	1336.64	1312.61	1288.28	1264.04	1239.25	1213.0	1184.14			
$1,\bar{1}$	10	.....	.....	.....	.....	.....	1361.09	1336.64	1312.61	1288.92	1266.11	1244.77	1226.1				
$\bar{1},1$	11	.....	.....	.....	.....	.....	.....	1339.23	1314.82	1290.59	1266.63	1242.90	1219.1	1195.41			
$1,\bar{1}$	12	.....	.....	.....	.....	.....	.....	1339.23	1314.82	1290.59	1266.63	1242.90	1220.43				
$\bar{1},1$	13	}															
$1,\bar{1}$	14	}	.....	.....	.....	.....	.....	.....	.....	1320.90	(1296.67)	1272.37	1248.52	(1225.08)	1201.55		
$\bar{1},1$	15	}															
$1,\bar{1}$	16	}	.....	.....	.....	.....	.....	.....	.....	1305.60	1281.22	(1257.1)	1233.31	1209.79			
$\bar{1},1$	17	}															
$1,\bar{1}$	18	}	.....	.....	.....	.....	.....	.....	.....	.....	1292.40	(1268.4)					

TABLE 4. *Lines in the $R_{2,\bar{1}}$, $R_{2,\bar{3}}$, $R_{3,2}$, and $R_{3,\bar{3}}$ branches, pure rotation*

Branch	$(J+\tau)''$	$J''=6$	7	8	9	10	11	12	13	14	15	16	17
$3,\bar{1}$	0	370.16	419.98	472.54	526.08	580.7	635.3	(690.3)	(744.1)	799.11	852.91	906.32	959
$3,\bar{3}$	1	484.05	545.55	(616.4)	(696.7)	784.54	878.61	976.07					
$3,\bar{1}$	2	385.06	418.57	(457.9)	502.31	550.18	599.82	(650.5)	(703.0)	(756)	808.14	859.78	910
$3,\bar{3}$	3	506.96	546.50	592.0	(644.7)	(705.5)	775.63	854.66	941.12				
$3,\bar{1}$	4	(457.0)	(472.5)	492.08	517.00	547.89	574.74	(625.3)	(672.5)	(726)	(784.54)	840.36	
$3,\bar{3}$	5	566.9	594.5	625.25	(659.2)	(696.6)	(742.6)	794.01	853.41	921.48			
$3,\bar{1}$	6	554.62	569.2	(580.7)	(592.0)	605.0	620.7	(641.4)	(669.6)	(707)			
$3,\bar{3}$	7	(638.1)	(663.0)	(688.0)	(713.5)	(740.7)	770.17	803.60	841.16	883.18			
$3,\bar{1}$	8	(637.2)	(656.4)	(678.9)	(694.0)	(705.2)	(713.0)	(721.5)	(730.8)	(741)			
$3,\bar{3}$	9	.....	(729.4)	(754.8)	779.36	803.09	827.80	(852.62)	878.9	906.8			
$3,\bar{1}$	10	.....	(729.2)	(754.0)	777.07	797.65	814.61	827.21	835.64	(841.1)			
$3,\bar{3}$	11	.....	.....	813.97	840.01	865.51	890.14	914.06	937.40	960.77			
$3,\bar{1}$	12	.....	.....	813.97	840.01	865.02	888.71	910.17	929.00				
$3,\bar{3}$	13	}											
$3,\bar{1}$	14	}	.....	.....	891.33	918.52	944.95	970.66					
$3,\bar{3}$	15	}											
$3,\bar{1}$	16	}	.....	.....	.....	962.05	990.3						
$5,\bar{3}$	0	(613.0)	(668.9)	(731.0)	798.75	871.36	948.35	(1028.5)					
$5,\bar{5}$	2	(673.5)	(707.4)	(748.5)	796.01	849.69	909.02	973.59	1042.57				
$5,\bar{3}$	4	792.2	808.33	827.80	852.62	883.89	922.19	967.00	1017.9				
$5,\bar{5}$	6	.....	946.73	959.78	971.43	984.2	1000.35	1022.0					
$5,\bar{5}$	1	769.1	825.24	887.33	955.32	1029.69							
$5,\bar{5}$	3	841.97	881.15	925.05	974.04	1028.47	1088.1						

TABLE 5. *Rotational constants for ν_2 of H_2O*

$v_1v_2v_3$	Constant					
	A	B	C	D_A	D_B	D_C
	cm^{-1}	cm^{-1}	cm^{-1}	$10^{-4}cm^{-1}$	$10^{-4}cm^{-1}$	$10^{-4}cm^{-1}$
010	31.12	14.66	9.15	56.7	2.6	0.4
000	27.877	14.512	9.285	33.7	2.39	.25

WASHINGTON, November 9, 1951.

rnal of Research of the National Bureau of Standards Vol. 49, No. 2, August 1952 Research Paper 2348

On Calculating the Zeros of Polynomials by the Method of Lucas

Herbert E. Salzer

When $f(x)$ is a polynomial of degree n and x_i, $i=0, 1, \ldots, n$, are any $n+1$ points at which $f(x_i)\neq 0$, the zeros of $f(x)$ are known to be identical with the zeros of [1] $\Sigma a_i/(x-x_i)$, where $a_i=f(x_i)/\Pi'(x_i-x_j)$. Lucas proposed this principle for use in an electric analogue device for finding zeros. The present note evaluates this principle in digital computation for both real and complex zeros when the coefficients of $f(x)$ are given exactly (integral or rational) so that the zeros of $f(x)$ are identical with the zeros of $\Sigma A_i/(x-i)$, A_i integral. The chief advantages are (1) the saving of labor in tabulating $\Sigma A_i/(x-i)$ instead of $f(x)$ in the neighborhood of the zero, especially for complex zeros, and (2) somewhat less work in the inverse interpolation for the zero. Three examples in locating a real root, and one example in locating a complex root were worked out in support of these findings.

In three separate notes F. Lucas[2] describes an ectric analogue device for calculating the roots of uations (also mentioned by J. S. Frame).[3] Al- ough the principle is familiar, as far as the writer ows it has not been investigated from the stand- int of digital computation. The present note is tended to call attention to its advantages in finding e roots of polynomial equations with exact coef- ients when one has a first approximation as a arting point.

If $f(x)$ denotes a polynomial of degree n, and x_i, $=0,1, \ldots, n$, denotes any $n+1$ points where $(x_i)\neq 0$, from

$$f(x)=\sum \frac{\Pi'(x-x_j)}{\Pi'(x_i-x_j)} f(x_i)$$

$$=\Pi(x-x_j)\sum \frac{f(x_i)}{\Pi'(x_i-x_j)(x-x_i)},$$

here follows the well-known result (which is the asis of Lucas's method) that the zeros of $f(x)$ are dentical with the zeros of

$$\sum \frac{a_i}{x-x_i}, \text{ where } a_i=\frac{f(x_i)}{\Pi'(x_i-x_j)}.$$

In problems where the coefficients of $f(x)$ are ational, the choice of $x_i=i$ is very convenient. By ultiplying through, one obtains the equation in the orm $\Sigma A_i/(x-i)=0$, A_i integral, which saves a con- iderable number of multiplication operations, espe- ially when getting all or even several of the zeros of he same $f(x)$.

By choosing $x_i=x_0+ih$, for any x_0 and h for which $(x_i)\neq 0$, Lucas's principle can be formulated also as ollows:

The zeros of $f(x)$, a polynomial of the nth degree, re identical with the zeros of $\Delta^m\{f(t)/(x-t)\}$, m any integer $\geq n$, where the $f(t)/(x-t)$ is tabulated for any $m+1$ equally spaced values of t.

Of course, in obtaining $\Delta^m\{f(t)/(x-t)\}$, t is the variable, with x as the parameter, and the resulting expression is then regarded as a function of x. (The proof is left for the reader.)

This principle of Lucas, namely, calculating the zeros of $f(x)$ by tabulating $\Sigma a_i/(x-x_i)$ or $\Sigma A_i/(x-x)_i$, instead of $f(x)$ itself, in the neighborhood of a zero, was tried out in several different examples where the zeros had already been obtained from the tabulation of $f(x)$ itself. In all examples, the use of Lucas's method showed a very great saving of computational labor. The two main advantages were (1) much less work in calculating $A_i/(x-x_i)$ instead of the separate terms of $f(x)$, especially those of high degree,[4] and (2) somewhat less work in the inverse interpolation from the tabulated $\Sigma A_i/(x-x_i)$ instead of the tabulated $f(x)$ near the zero, which was apparent from the tendency of Δ^m/Δ to be less in the former case.[5]

In connection with (1), in adding the separate terms of $\Sigma A_i/(x-x_i)$ considerably more significant figures were lost than in the summation of the separate terms of $f(x)$; but that disadvantage is slight because of the ease in getting any number of places in $A_i/(x-x_i)$ by performing continued division on an ordinary 10-bank desk calculator (the $x-x_i$ is almost certainly an exact number having fewer than 10 significant figures), and the total work in tabulating the $\Sigma A_i/(x-x_i)$ is still much less than that in tabulating the $f(x)$. But if the x_i's are not exact, or the coefficients in $f(x)$ are approximate, this principle of Lucas is severely limited in applicability, even to the point of not yielding a single significant figure. Thus, if in the example below, one were to introduce a relative error of 10^{-10} in those exact coefficients of $f(X)$, it is apparent that the $h(X)$ could not be obtained to even one significant figure. However, the choices of $x_i=i$ or $x_i=i-[n/2]$ seem most suitable for many problems. For example, in the case of the classical

[1] Here and elsewhere the summation is over the range 0 to n; similarly Π indicates a product over the same range, and Π' indicates such a product with the vanishing factor omitted.

[2] Lucas, Compt. rend. Acad. Sci. Paris **106**, 645-48 and 1072-74 (1888); **111**, 35-37 (1890).

[3] J. S. Frame, MTAC **1**, 337-53 (especially 347-50) (1945).

[4] There is the very well-known computational scheme for $a_nx^n+a_{n-1}x^{n-1}+a_{n-2}x^{n-2}+\ldots+a_1x+a_0$ in the form $u_n=a_nx+a_{n-1}$, $u_{n-1}=u_nx+a_{n-2}$, $\ldots$, etc., until $f(x)=u_1=u_0x+a_0$, which avoids the calculation of powers of x, but which may be less convenient for checking and the retention of significant figures.

[5] The rate of convergence of most inverse interpolation series depends upon the rapidity with which the Δ^m/Δ fall off.

orthogonal polynomials where the coefficients are given exactly (for example, Hermite, Laguerre, Chebyshev, Legendre, etc.) the $A_i/(x-x_i)$ can be easily had to any required number of places.

As an illustration, consider the calculation of the zero of the polynomial

$$f(X)=X^6-156X^5+8580X^4-205920X^3 +2162160X^2-8648640X+8648640,$$

which is near 67.28. Here $f(X)$ was chosen to be $H_{13}(x)/(2x)$, where $X=4x^2$ and $H_{13}(x)$ is the Hermite polynomial of order 13. Choosing $X_i=i$, one has

$f(0)=$ 86 48640	$f(4)=-24$ 89408
$f(1)=$ 19 64665	$f(5)=-13$ 89935
$f(2)=-15$ 15008	$f(6)=$ 69120
$f(3)=-27$ 39879	

The numbers $\Pi'(X_i-X_j)$ have no more than th digits. After obtaining the a_i in their lowest ter one sees that the zeros of $f(X)$ are identical with t zeros of

$$g(X)\equiv\frac{12012}{X}-\frac{392933}{24(X-1)}-\frac{94688}{3(X-2)}+\frac{304431}{4(X-3)} -\frac{155588}{3(X-4)}+\frac{277987}{24(X-5)}+\frac{96}{X-6},$$

which, in turn, are identical with the zeros of

$$24g(X)\equiv h(X)\equiv\frac{288288}{X}-\frac{392933}{X-1}-\frac{757504}{X-2} +\frac{1826586}{X-3}-\frac{1244704}{X-4}+\frac{277987}{X-5}+\frac{2304}{X-6}$$

An approximate value of the zero is $X=67.2838$, a $h(X)$ was calculated for $X=67.2838(0.0001)67.284$ The separate terms of $h(X)$ are given here to show t loss in significant figures upon summation:

	$X=67.2838$	$X=67.2839$	$X=67.2840$	$X=67.2841$
$288288/X$ =	4284. 65093 07916 61588 7	4284. 65056 27646 43547 7	4284. 64419 47565 54307 1	4284. 63782 67673 93782 5
$-392933/(X-1)$ =	−5928. 03973 21819 20771 0	−5928. 03078 87737 44453 8	−5928. 02184 53925 53255 7	−5928. 01290 20383 47054 6
$-757504/(X-2)$ =	−11603. 24613 45693 72493 6	−11603. 22836 10507 33795 0	−11603. 21058 75865 44942 1	−11603. 19281 41768 05684 7
$1826586/(X-3)$ =	28414. 40611 78710 65404 0	28414. 36191 64363 08313 6	28414. 31771 51290 70373 2	28414. 27351 39793 51037 0
$-1244704/(X-4)$ =	−19668. 60397 13165 13862 9	−19668. 57289 13673 14593 4	−19668. 54181 15163 39043 0	−19668. 51073 17635 86746 1
$277987/(X-5)$ =	4463. 23120 93995 54940 5	4463. 22404 34526 41854 5	4463. 21687 75287 36323 1	4463. 20971 16278 47235 5
$2304/(X-6)$ =	37. 59557 99085 56584 3	37. 59551 85619 71415 0	37. 59545 72155 86450 0	37. 59539 58694 01688 2
$h(X)$ =	−0. 00000 00969 68520 0	+0. 00000 00237 72288 6	+0. 00000 01445 13214 6	+0. 00000 02652 54257 8

That only three values of $h(X)$ at intervals of 0.0001 are required in order to find the zero $\overline{X}$ to the maximum attainable accuracy, follows from these differences:

X	$h(X)$	Δ	Δ^2
67. 2838	−0. (6)09696 85200	+0. (6)12074 08086	+0. (12)1174
67. 2839	+. (6)02377 22886	. (6)12074 09260	. (12)1172
67. 2840	. (6)14451 32146	. (6)12074 10432	----------
67. 2841	. (6)26525 42578	----------	----------

When these differences were compared with the corresponding differences in $f(X)$, it was noted that Δ^2/Δ for $h(X)$ was only (1/25) of Δ^2/Δ for $f(X)$, from which one can infer that the inverse interpolation is better for the function $h(X)$. The zero $\overline{X}=67.2839+0.0001p$ was found from the three-point formula[6] $p=r-r^2s$, where

$$r=-2h(67.2839)/\{h(67.2840)-h(67.2838)\}$$
$$s=\Delta^2/\{h(67.2840)-h(67.2838)\}.$$

Thus

$$h(67.2840)-h(67.2838)=0.(6)24148\,17346,$$
$$r=-0.(7)47544\ 5772/0.(6)24148\,17346 =-0.19688\ 6846,$$
$$s=0.(12)1174/0.(6)24148=0.(6)486,$$
$$r^2=0.03876,\ r^2s=0.(7)1884,$$
$$p=-0.19688\ 6865;\ \overline{X}=67.28388\ 03113\ 135,$$

which happens to be correct to 13 decimals.

This method was tested upon the calculation o two different roots of the same tenth-degree polyno mial in X (the example was to find both the smalles and largest zero of $H_{20}(x)$), the result being that th relative saving of labor was even greater than tha for $H_{13}(x)$. In fact, as the degree of the polynomi increases, the proportion of work saved also increase

Finally, this method was applied to the comput tion of a complex root of a tenth-degree polynomia from a rough first approximation. There th relative saving of labor was even greater than tha for the examples involving real roots, due in par ticular to the avoidance of the calculation of hig powers of complex numbers. Even when th computation is for complex roots, the choice o $x_i=i$ or $x_i=i-[n/2]$ is still suitable, so that if th coefficients of $f(x)$ are real, the calculation involve the sum of fractions with only real numerators.

WASHINGTON, July 24, 1951.

[6] H. E. Salzer, Bul. Am. Math. Soc. **50**, No. 8, 513-16 (1944).

Journal of Research of the National Bureau of Standards Vol. 49, No. 3, September 1952 Research Paper 2349

Effect of Moisture on Compressibility of Natural High Polymers

C. E. Weir

Studies are reported of the effect of sorbed moisture on compressibilities of leather, cellulose, wool, and silk fibroin. The general behavior of all materials is similar. For low moisture contents, compressibility is essentially independent of moisture content. For high moisture contents, compressibility increases markedly. It is suggested that these data are consistent with the concept that moisture exists in hydrogen bonded form at low and as liquid water at high moisture contents. Empirical compression equations are: for dry wool, $-\Delta V/V_0=1.37\times10^{-5}\ (P-2000)-6.79\times10^{-10}\ (P-2000)^2+1.55\times10^{-14}\ (P-2000)^3$; for dry silk fibroin $-\Delta V/V_0=1.24\times10^{-5}\ (P-2000)-7.00\times10^{-10}\ (P-2000)^2+2.68\times10^{-14}\ (P-2000)^3$, where P is expressed in atmospheres.

1. Introduction

In a previous investigation [21] it was observed that the compressibility of leather at high pressures was apparently independent of small amounts of moisture contained in the leather. The present report describes the results of studies of the effect of moisture content on the compressibilities of leather and other similar hygroscopic fibrous materials over a wide range of moisture contents. These data confirm the previous qualitative observation and show that for low-moisture contents the compressibility is essentially independent of moisture content. For high-moisture contents the compressibility rises markedly.

2. Experimental Method

The apparatus and techniques used in conducting these experiments have been described in detail [21]. Briefly, the sample is immersed in a light petroleum distillate contained in the bore of the pressure vessel and a leak-proof piston is forced into the bore. The position of the piston is measured every 1,000 atm., the pressure being generated by compression of the distillate. Pressure is determined by means of a manganin pressure gage mounted inside the vessel and immersed in the distillate. Direct comparison of the piston displacements in this experiment with those obtained in a similar experiment, in which the specimen is replaced by a steel bar having a volume approximately equal to that of the specimen, permits calculation of the compression of the specimen in terms of that of steel [3].

3. Preparation of Specimens

Measurements were made on commercial chrome upper leather, untanned hide, wool, cellulose, and silk fibroin. Leather samples consisted of a cylindrical stack of disks ½ in. in diameter and 4 in. in length. Each sample contained at least 25 individual leather disks held together by means of a fine wire threaded through each disk. Wool, cellulose, and silk fibroin were compressed into disks ½ in. in diameter and strung together in a similar manner to form a cylinder approximately 4 in. in length. These disks were formed in a cylindrical mold, using a maximum pressure of approximately 50,000 psi.

Commercial chrome upper leather was degreased exhaustively with chloroform and washed with water prior to test. Unhaired, untanned calfskin was degreased with acetone, diethyl ether, and ethyl alcohol after a thorough washing in water.

Wool specimens were made from a native wool designated as "Domestic Fine Top, WC–4", which was supplied by the Textile Research Institute. This sample originated at the Sheep Experiment Station of the United States Department of Agriculture at Dubois, Idaho. Dichlorobenzene had been used as a moth repellent in the container in which the sample was shipped and the sample was therefore extracted with diethyl ether and ethyl alcohol prior to use.

Cellulose was of cotton origin and was designated as "Lockette 140" of 93 percent maturity. This sample was supplied by the Southern Regional Research Labaratory of the United States Department of Agriculture.

Silk specimens were obtained from raw silk of uncertain origin. The specimens were degummed by the usual process and washed thoroughly with water prior to test.

Initial measurements were made on specimens dried by exhaustive evacuation at room temperature for not less than 24 hr. After ascertaining the dry weight, the test specimen was impregnated with the distillate in vacuo and the compressibility measured. Impregnation was conducted under a pressure of approximately 100 mm of mercury. The volume of the test specimen was determined following compression measurements by weighing the specimen in the distillate.

Following the initial measurement, the distillate was removed in vacuo at room temperature, the dry specimen was permitted to adsorb the desired quan-

tity of moisture (determined by weight) by exposure to moist vapor and the above procedure was repeated. It is to be noted that all measurements on a given material were conducted on the same specimen. All measurements were carried out in a temperature controlled room in which the temperature was 20.5° ±0.5° C.

The following observations on the experimental procedure are to be noted:

1. Evacuation for 24 hr does not remove all traces of moisture from such hygroscopic materials. However, the amount of moisture retained is small and for the purposes of these experiments is considered to have negligible effect on any conclusions to be drawn from the data. The specimens are therefore referred to as "dry".

2. Density measurements were made following compression to insure penetration of the voids by a light petroleum distillate. There is no indication from these or other measurements [22] of an irreversible increase in real density caused by the high hydrostatic pressure. The agreement between real densities determined here and those determined by other methods confirms this conclusion. The reproducibility of the compression data and the rapidity of attainment of pressure equilibrium are taken as indicative of purely elastic effects in time scales of the order involved in these experiments.

3. Reevacuation of distillate-impregnated specimens did not remove all of the distillate, an approximately constant amount of 200 mg of presumably trapped material being retained. Moisture contents were therefore referred to the weight of the initial dry specimen before exposure to the distillate. For this reason moisture contents are subject to some uncertainty and are reported only to the nearest percent.

4. Exposure to moisture containing air was generally carried out for 24 hr. Complete distribution equilibrium is unlikely in such a period, but these data are not likely to be sensitive to a nonequilibrium distribution [23].

4. Results and Discussion

The results of compression measurements for various moisture contents are given in table 1 and are shown graphically in figure 1 for chrome leather and cellulose. Compression values, $-\Delta V/V_0$, are computed on the basis of the original (1 atm) volume of the sample but are reckoned from the experimental reference pressure of 2,000 atm. Compressions at 1,000 atm, therefore, appear as negative values that are subject to somewhat larger experimental errors than the other values. These errors, as well as the uncertainty introduced by the assumed compression occurring between 1 and 2,000 atm, have been considered previously [21, 22].

TABLE 1. *Compression of natural fibrous polymers containing various amounts of moisture*

	Chrome leather					Untanned hide				
Pressure	Dry V_0=7.367 cm³ ρ=1.401 g/cm³ $-\Delta V/V_0$	6 percent H_2O V_0=7.988 cm³ ρ=1.404 g/cm³ $-\Delta V/V_0$	13 percent H_2O V_0=8.542 cm³ ρ=1.389 g/cm³ $-\Delta V/V_0$	20 percent H_2O V_0=9.334 cm³ ρ=1.364 g/cm³ $-\Delta V/V_0$	38 percent H_2O V_0=10.882 cm³ ρ=1.315 g/cm³ $-\Delta V/V_0$	Dry V_0=7.125 cm³ ρ=1.330 g/cm³ $-\Delta V/V_0$	5 percent H_2O V_0=7.648 cm³ ρ=1.334 g/cm³ $-\Delta V/V_0$	17 percent H_2O V_0=8.469 cm³ ρ=1.317 g/cm³ $-\Delta V/V_0$	30 percent H_2O V_0=9.613 cm³ ρ=1.285 g/cm³ $-\Delta V/V_0$	37 percent H_2O V_0=10.382 cm³ ρ=1.262 g/cm³ $-\Delta V/V_0$
atm										
10,000	0.0641	0.0666	0.0664	0.0717	0.0784	0.0672	0.0694	0.0694	0.0785	0.0790
9,000	.0599	.0622	.0614	.0654	.0721	.0615	.0631	.0632	.0719	.0716
8,000	.0535	.0533	.0548	.0579	.0643	.0544	.0557	.0557	.0641	.0638
7,000	.0465	.0460	.0476	.0500	.0555	.0473	.0480	.0481	.0578	.0556
6,000	.0396	.0390	.0396	.0429	.0465	.0406	.0411	.0410	.0477	.0469
5,000	.0317	.0307	.0312	.0337	.0372	.0319	.0321	.0320	.0385	.0369
4,000	.0218	.0210	.0222	.0230	.0260	.0218	.0224	.0217	.0275	.0258
3,000	.0121	.0111	.0114	.0121	.0141	.0114	.0121	.0116	.0157	.0134
2,000	.0000	.0000	.0000	.0000	.0000	.0000	.0000	.0000	.0000	.0000
1,000	−.0209	−.0126	−.0124	−.0139	−.0174	−.0122	−.0140	−.0130	−.0120	−.0151

	Cellulose			Wool		Raw silk		
Pressure	Dry V_0=7.230 cm³ ρ=1.538 g/cm³ $-\Delta V/V_0$	5 percent H_2O V_0=7.639 cm³ ρ=1.534 g/cm³ $-\Delta V/V_0$	9 percent H_2O V_0=8.043 cm³ ρ=1.509 g/cm³ $-\Delta V/V_0$	Dry V_0=5.281 cm³ ρ=1.316 g/cm³ $-\Delta V/V_0$	10 percent H_2O V_0=5.862 cm³ ρ=1.316 g/cm³ $-\Delta V/V_0$	Dry V_0=9.417 cm³ ρ=1.351 g/cm³ $-\Delta V/V_0$	6 percent H_2O V_0=9.838 cm³ ρ=1.357 g/cm³ $-\Delta V/V_0$	11 percent H_2O V_0=10.438 cm³ ρ=1.348 g/cm³ $-\Delta V/V_0$
atm								
10,000	0.0536	0.0536	0.0565	0.0738	0.0733	0.0679	0.0678	0.0686
9,000	.0484	.0491	.0513	.0680	.0680	.0618	.0618	.0627
8,000	.0426	.0429	.0453	.0599	.0604	.0549	.0549	.0556
7,000	.0365	.0370	.0392	.0524	.0529	.0476	.0476	.0484
6,000	.0307	.0309	.0327	.0449	.0442	.0400	.0398	.0407
5,000	.0236	.0239	.0256	.0360	.0350	.0317	.0312	.0319
4,000	.0164	.0169	.0182	.0246	.0245	.0222	.0214	.0225
3,000	.0092	.0094	.0097	.0136	.0136	.0117	.0115	.0118
2,000	.0000	.0000	.0000	.0000	.0000	.0000	.0000	.0000
1,000	−.0093	−.0097	−.0099	−.0185	−.0143	−.0138	−.0141	−.0141

* ρ calculated as described on page 137.

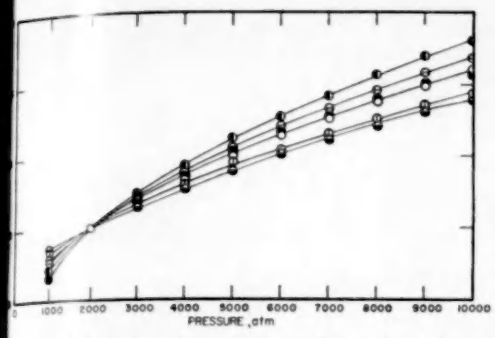

URE 1. *Effect of moisture on compression of chrome leather and cellulose.*

me leather: ●, dry, ○, 6 percent of moisture, ⊖, 20 percent of moisture, ◑ percent of moisture. Cellulose: ◒, dry and 5 percent of moisture, ⓘ, 9 per- of moisture.

Moisture contents, measured densities, and initial umes appear at the head of corresponding columns compression values in table 1. All densities were tained from weight and volume measurements cept that for wool containing moisture. A single asured density of dry wool was assumed to apply o to wool containing 10 percent moisture. Meas- ements by King [14] show that the error arising m this assumption in this moisture range is rather all. The necessity for this assumption as well as lack of data on wool at higher moisture contents se because wool specimens proved difficult to ndle. Compressed disks of wool exhibited great iliency, and the samples were generally ruptured extraction from the pressure vessel.

Density values of table 1 agree well with previously blished data on these materials [5, 7, 9, 10, 14, 17,]. However, the density maximum for chrome ther, as shown by these data, lies below 13 percent isture as compared to the data of Pomeroy and itton [17], in which the maximum is found at proximately 15 percent. The variation of density h moisture content is also somewhat less than t reported by these authors. A corresponding ximum density for untanned hide is shown by present data to lie below 17 percent of moisture. Consideration of the effect of moisture content on mpression shows that the general behavior of these terials is quite similar. Most thorough studies re performed on leather, but sufficient data were tained on other materials, except wool, to show the ilarities in behavior. It is observed that the com- ession changes relatively little at low moisture but reases markedly at high moisture contents. Inas- uch as the experimental errors involved in these periments are known to produce variations of a w digits in the third significant figure, differences ted in compression at low-moisture contents are ost probably real. These variations, however, are ther small compared to the change that occurs at gh-moisture contents. Therefore, at a given pres-

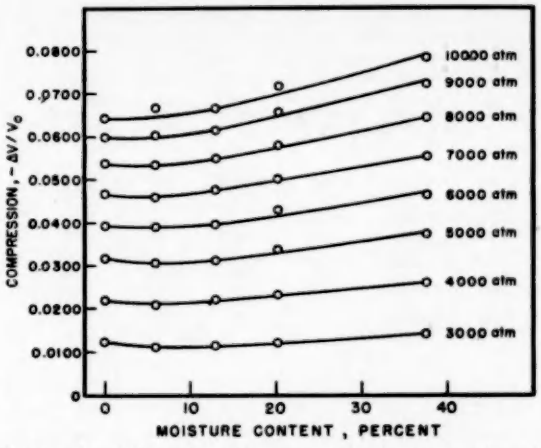

FIGURE 2. *Effect of moisture on isobaric compression of chrome leather.*

sure the compression may be considered to be essentially constant at low-moisture contents. The implications of the relative constancy in compression at low-moisture contents at a given pressure appear to be rather complex. As the moisture content increases the value of V_0 invariably increases as shown in the table. However, the change in volume, ΔV, at a given pressure appears to be just sufficient to keep the ratio constant. This result is true in the data on collagen and cellulose, two materials which are dissimilar chemically and which exhibit considerably different compressibilities. This finding shows that the added moisture on compression behaves in a manner to make it indistinguishable from an equivalent volume of the dry adsorbent. Since compressibility is dependent on the magnitude of the internal molecular forces, this near equality between compression of specimen and adsorbed moisture imples a corresponding similarity in these forces.

The variation of compression with moisture content is shown for chrome leather at several pressures in figure 2.

From these data it may be concluded that adsorbed moisture in low ranges of moisture content does not behave like liquid water. Although it is possible to calculate an effective pressure on liquid water that will produce the observed volume of moisture plus adsorbent at 1 atm, it is difficult to explain the agreement between the compressibilities of this water and the fibers over the whole pressure range, the variation of compressibilities with pressure being different for water and these fibrous polymers [1, 4, 22]. The observation that the compressibilities of moist and dry fibers essentially coincide at all pressures in the low-moisture range seems to offer a strong argument against the hypothesis that the adsorbed moisture be considered as water under high

TABLE 2. *Calculated compressions of moist chrome leather*

Pressure	6 percent of H_2O				13 percent of H_2O				38 percent of H_2O			
	Leather $V_1=0.9221$ $(-\Delta V/V_0)V_1$	Water $V_2=0.0779$ $(-\Delta V/V_0)V_2$	Total calc. $-\Delta V/V_0$	Calc. minus obs.	Leather $V_1=0.862$ $(-\Delta V/V_0)V_1$	Water $V_2=0.138$ $(-\Delta V/V_0)V_2$	Total calc. $-\Delta V/V_0$	Calc. minus obs.	Leather $V_1=0.677$ $(-\Delta V/V_0)V_1$	Water $V_2=0.323$ $(-\Delta V/V_0)V_2$	Total calc. $-\Delta V/V_0$	Calc. minus obs.
atm												
10,000	0.0591	0.0094	0.0685	0.0019	0.0553	0.0166	0.0719	0.0054	0.0434	0.0388	0.0822	0.0038
9,000	.0551	.0091	.0642	.0040	.0515	.0161	.0676	.0062	.0405	.0377	.0782	.0091
8,000	.0494	.0082	.0576	.0043	.0461	.0146	.0607	.0059	.0362	.0341	.0703	.0066
7,000	.0429	.0072	.0501	.0041	.0400	.0128	.0528	.0052	.0315	.0300	.0615	.0060
6,000	.0365	.0062	.0427	.0037	.0341	.0109	.0450	.0054	.0268	.0256	.0524	.0059
5,000	.0292	.0049	.0341	.0037	.0273	.0088	.0361	.0019	.0215	.0205	.0420	.0068
4,000	.0201	.0036	.0237	.0028	.0188	.0061	.0251	.0029	.0148	.0147	.0295	.0033
3,000	.0111	.0019	.0130	.0019	.0104	.0034	.0138	.0024	.0082	.0080	.0162	.0021
2,000	.0000	.0000	.0000	.0000	.0000	.0000	.0000	.0000	.0000	.0000	.0000	.0000
1,000	−.0190	−.0024	−.0214	−.0094	−.0178	−.0043	−.0221	−.0097	−.0141	−.0099	−.0240	−.0066

pressure [7, 9, 10, 19]. Typical results obtained by considering moist fibers as a binary mixture of water and adsorbent are shown for chrome leather in table 2 for three moisture contents.

The calculated compression contributions of leather and water are based on the respective experimentally measured volume fractions of the two components assuming no compression of the leather. The experimental volume fractions are shown at the heads of the corresponding columns. The differences between calculated and measured compressions (taken from table 1) increase much less in the high moisture range than in the low range. This implies that liquid water is present at high moisture contents as has been suggested [10, 16].

The concept that compressed water is present in these moist fibers would appear to require modification in the light of these data. Three alternatives appear possible, namely, both adsorbed moisture and adsorbent exist under an effectively high pressure; the adsorbed moisture penetrates into molecular-sized holes which are inaccessible to other liquids [9, 10]; and the adsorbed moisture enters into chemical or psuedochemical combination with the adsorbent.

The concept of effectively high pressures compressing the water has been based on the assumption that the adsorbent, being a solid, is affected by this pressure to a negligible degree. For such fibrous materials, and the high polymers which have been studied, the assumption is incorrect, the compressibilities of the two components being of the same general order of magnitude. It is doubtful if such an assumption is valid even in the case of a relatively incompressible solid since the short-range anisotropic nature of the forces might produce large local distortions. However, the consideration of the compressions of both components will not remove the difficulty of equal dependence of the compressibilities on pressure.

The concept of penetration of moisture into holes accounts for the increased density observed on adsorption of a liquid which, in bulk, is less dense than the adsorbent. The problem of pressure dependence of compressibility is not explained and data of Pomeroy and Mitton [17] obtained on leather do not exhibit the dependence of density on molecular size of the liquid to be expected from such concepts.

It is suggested, therefore, as a result of this and previous work [23] that the adsorbed moisture in the range of low moisture contents is bound by secondary valence forces. In view of the widely accepted ideas of the hydrogen bonded structure of the materials studied here, it is believed that the moisture exists largely in the hydrogen bonded form between the polymer chains and produces small changes in the original structure of the dry material. The small increase, produced by this moisture, in the enormous number of similar bonds existing in the dry material might be expected to cause the negligible effect on compression that is observed. The similarity of the new bonds with those already existing implies a similar pressure dependence of compressibility. The findings of Katz [13] that the X-ray pattern of cellulose is unchanged by moisture may be indicative as suggested [12], that the effects of the moisture are largely confined to a limited number of chains near the surface of the micelle.

It is noted that the major increase in compression occurs in the moisture content range in which the slopes of differential heat of adsorption curves are changing most rapidly [2, 8, 11, 20]. This moisture content also corresponds to that range in which the electrical properties of leather begin to change rapidly [23]. Similar electrical effects have been noted in cellulose and wool [6, 15]. The correlation of these effects substantiates the suggestion that liquid water exists at high moisture contents.

The absolute values of compressions of leather and cellulose reported here agree well with values reported earlier [21, 22]. As far as can be ascertained, compressibility data for wool and silk fibroin are being reported for the first time. In view of the similarities of the structures of these materials and leather [16], the compressions are of the order of magnitude expected, but it is surprising to note the close agreement in data obtained for these materials. It would appear that the presence of ring structures such as proline and hydroxyproline in collagen, and disulfide cross linkages in wool, produces a rath

all varia on in the nature of the intrachain forces. The com ession of dry wool and silk may be repre- ted by the following empirical equations, which re fitted to the data by the method of least squares:

ol:

$$-\Delta V/V_0 = 1.37\times10^{-5}(P-2000) - 6.79\times10^{-10}(P-2000)^2 + 1.55\times10^{-14}(P-2000)^3$$

fibroin:

$$-\Delta V/V_0 = 1.24\times10^{-5}(P-2000) - 7.00\times10^{-10}(P-2000)^2 + 2.68\times10^{-14}(P-2000)^3.$$

5. References

[1] L. H. Adams, J. Am. Chem. Soc. **53,** 3769 (1931).
[2] G. H. Argue and O. Maass, Can. J. Research **12,** 564 (1935).
[3] P. W. Bridgman, Proc. Am. Acad. Arts Sci. **74,** 11 (1940).
[4] P. W. Bridgmen, Proc. Am. Acad. Arts Sci. **76,** 71 (1948).
[5] I. D. Clarke, Ind. Eng. Chem. **23,** 62 (1931).
[6] T. W. Dakin and R. W. Auxier, Ind. Eng. Chem. **37,** 268 (1945).
[7] E. Filby and O. Maass, Can. J. Research **7,** 162 (1932).
[8] J. J. Hedges, J. Text. Inst. **T18,** 350 (1927).
[9] P. M. Heertjes, Rec. Trav. Chim. **61,** 751 (1942).
[10] P. H. Hermans, Contributions to the physics of cellulose fibers (Elsevier Publishing Co., Inc., New York, N. Y., 1946).
[11] J. R. Kanagy, J. Research NBS **44,** 31 (1950) RP2056.
[12] J. R. Katz, Trans. Faraday Soc. **29,** 279 (1933).
[13] J. R. Katz, Physik. Z. **25,** 321 (1924).
[14] A. T. King, J. Text. Inst. **T17,** 53 (1926).
[15] G. King, Trans. Faraday Soc. **43,** 601 (1947).
[16] K. H. Meyer, Natural and synthetic high polymers, 2d ed. (Interscience Publishers, Inc., New York, N. Y., 1950).
[17] C. D. Pomeroy and R. G. Mitton, J. Soc. Leather Trades Chem. **35,** 360 (1951).
[18] R. E. Porter, J. Am. Leather Chemists' Assn. **24,** 36 (1929).
[19] A. J. Stamm and M. Seborg, J. Phys. Chem. **39,** 133 (1935).
[20] A. J. Stam and M. Seborg, J. Phys. Chem. **39,** 121 (1935).
[21] C. E. Weir, J. Research NBS **45,** 468 (1950) RP2160.
[22] C. E. Weir, J. Research NBS **46,** 207 (1951) RP2192.
[23] C. E. Weir, J. Research NBS **48,** 349 (1952) RP2322.

WASHINGTON, April 9, 1952.